On the optimal control of the circular restricted three body problem

Bilel Daoud

Année 2011

THÈSE

présentée pour obtenir le titre de

DOCTEUR DE L'UNIVERSITÉ DE BOURGOGNE

École Doctorale : Carnot
Spécialité : Mathématiques Appliquées

par

Bilel Daoud

CONTRIBUTION AU CONTRÔLE OPTIMAL DU PROBLÈME CIRCULAIRE RESTREINT DES TROIS CORPS

Soutenue publiquement le 7 Novembre 2011 devant le jury composé de :

MM.	F. Bernelli	*Rapporteurs*
	D. Scheeres	
	H. Zidani	
MM.	B. Bonnard	*Examinateurs*
	R. Epenoy	
	J.–B. Pomet	
MM.	J.–B. Caillau	*Directeurs de thèse*
	J. Gergaud	

Contents

Introduction

The fuel and time-optimal control of space vehicles is a foundational topic in astrodynamics and control. This fact arises naturally from the necessity to bring all materials and propellant on-board space faring vehicles. Thus there is always an imperative to minimize propellant usage, as this either enables a mission to continue for a longer period of time or, often more crucially, allows for the launch of a less massive spacecraft from the Earth. Thus, even with the advent of highly efficient low-thrust propulsion devices, such as that used in the recent SMART-1 mission, the question of how little propellant mass is needed for a specific mission remains important.

The fundamental theory of optimal control, specially as applied to thrusting space vehicles, has been established since the 1960s in the form of the necessary conditions that an optimal control law will satisfy. This theory is quite remarkable and surprisingly simple to pose. Despite the ease with which it is stated, the solution of specific optimal control problems is quite difficult and continues to be an active area of research. The fundamental problems that arise in these solutions are several but are mainly rooted in the need to solve a two-point boundary value problem (TPBVP) for the optimal control to be found. Whereas the automatic solution of initial value problems in ordinary differential equations is well posed and highly advanced, the solution of (TPBVP)s involving ordinary differential equations is not so well developed.

The thesis carries out research that directly addresses this aspect of the problem. The motivating example is the SMART-1 mission. The goal is to design an optimal low-thrust transfer from an Earth orbit into orbit about the Moon. While a practical control law for this mission was found using direct methods, the full solution of this problem for the actual thrust constraints for that mission using the more rigorous indirect method is still lacking. The indirect solution of this problem has important theoretical implications as it can be directly checked as to whether it is a local optimum (through the identification of conjugant solutions) and in that its solutions defines the true mathematical form that extremal solutions to this problem must solve.

This problem is addressed here through the use of homotopy methods to continue solutions from "easier" versions of the problem towards parameter values for the system that are more in line with real values and which are also more difficult to solve. The homotopic methods are generally able to advance the problem over a significant range of parameter values, and thus begin to expose the mathematical solution to this optimal control problem.

Previous studies on the Earth-Moon transfers are based on dynamical system approaches relying on the fine knowledge of the CRTBP trajectories. In fact the approach given in [24] and [25] consists in patching two CRTBP, the

Sun-Earth system and the Earth-Moon system. The main idea is to use the invariant manifold [18] of both systems, an invariant manifold is a ballistic path (consumption free) that brings the spacecraft from and towards periodic orbits around the system equilibrium points, the transfer design being the following: Take an invariant manifold of the Sun-Earth system from the vicinity of the Earth until an intersection with an invariant manifold of the Earth-Moon system, then realize the switch between the two manifolds by a maneuver on the spacecraft, and finally take the invariant manifold until the capture [33] by the Moon. Another approach consists in dividing the transfer into two parts as in [26, 28, 27]: The first part is a two-body transfer from a low orbit around the Earth towards an invariant manifold of the system Earth-Moon (in this part, the influence of the Moon is taken into account) and the second part consists in taking the invariant manifold towards a lunar coverage orbit (a periodic orbit around the equilibrium points of the system near to the Moon). In [2], another mission design of Earth-Moon transfer is provided. It includes decomposition of the trajectory into subsequences involving two-body transfer arcs. Indeed, the transfer is divided into three phases. First phase consists in two-body transfer around the Earth, in which the Moon and the Sun influences as well as the Earth's oblateness are taken into account. The second phase is a free coast one, with no thrust. The third part consists of two body transfer around the Moon, in which the influences of the Earth and the Sun are taken into account. The command of the spacecraft engine is computed thanks to an optimal control algorithm based on a direct shooting method. An other approach is used in [3]. It consists in using Lyapunov functions to stabilize the targeted orbits. The goal of the method is to build a feedback control. The transfer is divided into four phases. In the first three phases an orbit around the Earth is targeted until the capture by the Moon, then the final phase is an orbital transfer around the Moon. The method uses the CRTBP to model the Earth-Moon system and the orbital elements to build the Lyapunov functions.

In our study, in contrast with the previous given missions design, we address the question of optimal control of the circular restricted three-body problem, no fine knowledge of the three-body trajectories is needed and no a priori decomposition of the trajectory into subsequence arcs is assumed. Our goal is to compute optimal steering of the spacecraft engine for transfers into the Earth-Moon system modeled by the CRTBP for the following optimization criteria: Minimization of final time, energy, and fuel consumption. In contrast with [2], the single shooting method is used. It is part of the indirect methods, and is based on Pontryagin's Maximum Principle PMP [30]. We recall that direct method, on the other hand, normally involve the partial or total discretization of the problem, and uses various approaches to solve the resulting optimization problem. Direct methods are thus supposed to be robust but the disadvantage is that the solution is of low precision and an optimization problem of huge size depending on the discretization stepsize used. This makes these methods ill-suited to some particular cases over as the minimum fuel consumption problem, which presents a bang-bang control structure with a huge number of commutations as the spacecraft maximum thrust decreases. Returning to the indirect methods, single shooting consists in finding a zero of the shooting function associated with the original problem. There is no discretization, even if the method still involves an integration of the system in some way. It is a fast and high precision method but often requires a good initial guess, as it consists of apply-

ing a Newton solver to the shooting function. The convergence radius may be quite small, depending on the problem. This is particularly true for problem involving commutations as it is often necessary to have a good knowledge of the optimal control structure. Our work focuses on building different continuation strategies to obtain a suitable initial point to solve optimal control problems for the different considered criteria.

The organization of this document is as follows. In the first chapter, we provide the equations of motion in the CRTBP, we recall then some properties of the CRTBP related to the system energy and finally we give the proof of the controllability of the CRTBP. The second chapter is devoted to the minimization of the final time transfer. In chapter 3, we focus on the minimization of fuel consumption. In chapter 4, we apply the numerical technics developed in the two previous chapters on a real mission case: The SMART-1 mission.

Chapter 1

Circular Restricted Three-Body Problem

1.1 Problem definition

We define our problem as follows [36]: Two bodies revolve around their center of mass in circular orbits under the influence of their mutual gravitational attraction and a third body (attracted by the previous two without influencing their motion) moves in the plane defined by the two revolving bodies. The Circular Restricted Three-Body Problem CRTBP is to describe the motion of this third body.

The two revolving bodies are called the primaries (or the primary and the secondary, a nomenclature popular in stellar dynamics but which we will not pursue). The masses m_1 and m_2 of these bodies are arbitrary but the bodies have such internal mass distributions that they may be considered point masses. Concerning the third body mass m the approximate statement is accepted, that m is much smaller than either m_1 or m_2. This is intuitively correct since m does not influence the circular motion of m_1 and m_2 around their mass center.

The CRTBP is an approximation of the classic three-body problem which is defined as follows: Three particles with arbitrary masses attract each other according to the Newtonian law of gravitation; They are free to move in space and initially move in any given manner; finding their subsequent motion. The difference between this and the restricted problem is, first of all that in the latter the masses of only two particles are arbitrary; the third mass is much smaller than the other two. The general problem allows any set of initial conditions for the three particles involved; the restricted problem requires circular orbits for the primaries.

There are many cases of applications: Sun-Earth-Moon, Sun-Earth-space probe, Earth-Moon-spacecraft, Jupiter-Jupiter's moon-spacecraft, ... In our case we are interested in the Earth-Moon system and we investigate optimal spacecraft trajectory design in this system. The motion of the spacecraft in the fields of attraction of the Earth and the Moon is modeled on the circular restricted three-body problem since:

(i) The spacecraft mass (some hundreds of kilograms) is very small compared to the Earth's mass ($m_1 = 5.97 \times 10^{24}$ kg) and the Moon's mass ($m_2 =$

7.3×10^{22} kg). Thus the spacecraft does not affect the motion of the primaries (Earth and Moon) which is supposed to be Keplerian, and its acceleration is only due to gravitational attraction of the two primaries.

(ii) The Moon's orbit around the Earth has an eccentricity of 0.0549, close to a circular orbit. We can assume that both the Earth and the Moon form a circular motion around their mass center.

(iii) The plane of the orbits of the Earth and the Moon shifts a few minutes of arc a year (This variation is about 5 degrees with respect to the ecliptic) so noncoplanar effects of the system {Earth,Moon} are neglected.

The spacecraft motion is also supposed to be in the orbital plane containing the primaries, since any deviation manoeuvers to get out of this plane, call for large additional energies. The three dimensional case is concerned with a motion of m that does not take place in the plane of motion of m_1 and m_2. This case appears when the initial (or final) conditions of the third body (*i.e.* spacecraft) are such that the body initially is not in the plane of motion of m_1 and m_2 or when its initial velocity vector has a component which is not included in this plane.

Within the framework of Newtonian gravitational forces, if the initial position and velocity vectors of the third body are situated in the plane of motion of m_1 and m_2 then the motion of the third body will be confined to this plane since there are no forces extracting it from this plane.

The applications of an essentially three-dimensional motion of the third body are for instance, in the case of celestial mechanics: When studying orbits of some minor planets with a large inclination to the ecliptic and in the case of space mechanics: When designing missions, for initial and/or final conditions which are not in the primaries motion plane, we mention here our example of application the SMART-1 mission (*cf.* chapter 4).

Remark 1.1.1. Now we consider the system {Earth, Moon, spacecraft}. The equations written and results given in the next chapters are deemed true even if we consider two other primaries. The study of the particular example of the Earth-Moon system does not hinder the generality of the problem.

1.2 Equations of motion

Let us consider a spacecraft on the field of attraction of the Earth and the Moon. Let $\overrightarrow{T}$ be the spacecraft driving force. According to Newtons Second Law, the vector differential equation for the spacecraft's motion is written in a inertial frame I:

$$m\frac{d^2\overrightarrow{R}}{d\tau^2} = -Gm_1m\frac{\overrightarrow{R}_{13}}{R_{13}^3} - Gm_2m\frac{\overrightarrow{R}_{23}}{R_{23}^3} + \overrightarrow{T} \tag{1.1}$$

where: m_1, m_2 and m are the masses respectively of the Earth, the Moon and the spacecraft, $\overrightarrow{R}$ is the satellite vector position, $\overrightarrow{R}_{13}$ is the vector Earth-satellite and R_{13} designs its euclidian norm, $\overrightarrow{R}_{23}$ is the vector Moon-satellite and R_{23} designs its euclidian norm, G is the gravitational constant and τ is the time unit.

A standard nondimensionalization of the CRTBP is used. Since the mass of the third body is negligible, the characteristic mass, m^*, is the sum of the two primary masses *i.e.* $m^* = m_1 + m_2$. The characteristic length is the constant distance between the primaries, $l^* = R_{12}$ where $\overrightarrow{R}_{12}$ is the vector Earth-Moon. Finally, the characteristic time τ^* is defined such a way that the non dimensional gravitational constant G^* is unity. This property is accomplished through the use of Keplers third law: $\tau^* = \sqrt{\frac{l^{*3}}{Gm^*}}$. These newly defined natural units lead to the following nondimensional quantities:

$$\overrightarrow{r} = \frac{\overrightarrow{R}}{l^*}, \quad \overrightarrow{r}_{ij} = \frac{\overrightarrow{R}_{ij}}{l^*} \quad \{i,j\} \in \{1,2,3\}, \quad \mu = \frac{m_2}{m^*} \quad \text{and} \quad t = \frac{\tau}{\tau^*}.$$

Since the gear thrust is bounded, the quantity $\overrightarrow{T}$ is normalized as follows: $\overrightarrow{T} = T_{max}\overrightarrow{u}$, here T_{max} is the gear maximum thrust and $\overrightarrow{u}$ is the control vector such that $|\overrightarrow{u}| \leq 1$. $\overrightarrow{u}$ is already the motor control gear. This quantity is computed relative to the optimization criterions.

Let us divide the equation (1.1) by the mass m and use the new unities system to simplify the equation of motion:

$$\frac{d^2\overrightarrow{r}}{dt^2} = -\frac{(1-\mu)}{r_{13}^3}\overrightarrow{r}_{13} - \frac{\mu}{r_{23}^3}\overrightarrow{r}_{23} + (\frac{l^{*2}}{m^*G})\frac{T_{max}}{m}\overrightarrow{u} \tag{1.2}$$

We note $\varepsilon = (\frac{l^{*2}}{m^*G})\frac{T_{max}}{m}$. The constant $\frac{l^{*2}}{m^*G}$ is only a normalization constant to take into account in numerical computation and it will no longer be mentioned in this thesis. However the maximal thrust $T_{\max}$ and the spacecraft mass m are two important parameters in the transfer problem, more attention will be paid to them later. ε is the ratio $\frac{T_{max}}{m}$ in the dimensionless system of units.

We intend to write the equation (1.2) in a rotating frame R, the angular velocity is the angular velocity of the rotation of the two primaries around their center of mass, the coordinates' origin. The two primaries being fixed in this frame, they lie on the abscissa axis: The Earth's coordinates are $(-\mu, 0, 0)$ and the Moon's coordinates are $(1-\mu, 0, 0)$. Let (x, y, z) be the spacecraft coordinates in the rotating frame R. Let us express $(\frac{d^2\overrightarrow{r}}{dt^2})_I$ as a function of x, y and z.

$$(\frac{d^2\overrightarrow{r}}{dt^2})_I = (\frac{d^2\overrightarrow{r}}{dt^2})_R + 2\overrightarrow{\omega} \times (\frac{d\overrightarrow{r}}{dt})_R + \overrightarrow{\omega} \times \overrightarrow{\omega} \times \overrightarrow{r} \tag{1.3}$$

where $\overrightarrow{\omega}$ is the angular velocity of the rotating frame R with respect to the inertial frame I, then $\overrightarrow{\omega} = \overrightarrow{z}$ in the new units system. The second derivative $(\frac{d^2\overrightarrow{r}}{dt^2})_R$ in equation (1.3) can also be expanded kinematically in terms of the nondimensional rotating frame, indeed:

$$\overrightarrow{r} = x\overrightarrow{x} + y\overrightarrow{y} + z\overrightarrow{z}$$

$$(\frac{d\overrightarrow{r}}{dt})_R = \dot{x}\overrightarrow{x} + \dot{y}\overrightarrow{y} + \dot{z}\overrightarrow{z}$$

$$(\frac{d^2\overrightarrow{r}}{dt^2})_R = \ddot{x}\overrightarrow{x} + \ddot{y}\overrightarrow{y} + \ddot{z}\overrightarrow{z}$$

Let us return to the equation (1.3), we obtain:

$$(\frac{d^2\overrightarrow{r}}{dt^2})_I = (\ddot{x} - 2\dot{y} - x)\overrightarrow{x} + (\ddot{y} + 2\dot{x} - y)\overrightarrow{y} + \ddot{z}\overrightarrow{z} \tag{1.4}$$

In addition we have:

$$\overrightarrow{r}_{13} = (x + \mu)\overrightarrow{x} + y\overrightarrow{y} + z\overrightarrow{z} \tag{1.5}$$

$$\overrightarrow{r}_{23} = (x - 1 + \mu)\overrightarrow{x} + y\overrightarrow{y} + z\overrightarrow{z} \tag{1.6}$$

Combining the equations (1.2), (1.4), (1.5) and (1.6) leads to a second order-controlled differential system of dimension three:

$$\begin{cases} \ddot{x} = 2\dot{y} + x - \frac{1-\mu}{r_{13}^3}(x + \mu) - \frac{\mu}{r_{23}^3}(x - 1 + \mu) + \varepsilon u_1 \\ \ddot{y} = -2\dot{x} + y - \frac{1-\mu}{r_{13}^3}y - \frac{\mu}{r_{23}^3}y + \varepsilon u_2 \\ \ddot{z} = -\frac{1-\mu}{r_{13}^3}z - \frac{\mu}{r_{23}^3}z + \varepsilon u_3 \end{cases} \tag{1.7}$$

where (u_1, u_2, u_3) are the control $\overrightarrow{u}$ coordinates in the rotating frame R.
This system is also written more compactly by introducing the potential function $V_\mu(x, y, z) = -\frac{1-\mu}{r_{13}} - \frac{\mu}{r_{23}} - \frac{1}{2}(x^2 + y^2)$, reducing the equations system to:

$$\begin{cases} \ddot{x} - 2\dot{y} + V_{\mu_x} = \varepsilon u_1 \\ \ddot{y} + 2\dot{x} + V_{\mu_y} = \varepsilon u_2 \\ \ddot{z} + V_{\mu_z} = \varepsilon u_3 \end{cases}$$

where $V_{\mu_x} = \frac{\partial V_\mu}{\partial x}$, $V_{\mu_y} = \frac{\partial V_\mu}{\partial y}$ et $V_{\mu_z} = \frac{\partial V_\mu}{\partial z}$.

Remark 1.2.1. The differential system equations (1.7) are particularly useful in numerical computation due to the inherent nondimensional scaling of the system of units.

Let us write the differential system (1.7) in an other coordinates system (q, p), where $q = \begin{bmatrix} x \\ y \\ z \end{bmatrix}$ and $p = \begin{bmatrix} \dot{x} - y \\ \dot{y} + x \\ \dot{z} \end{bmatrix}$. The potential function is then $V_\mu(q) = -\frac{1-\mu}{r_1} - \frac{\mu}{r_2} - \frac{q_1^2+q_2^2}{2}$ with $r_1^2 = (q_1 + \mu)^2 + q_2^2 + q_3^2$ and $r_2^2 = (q_1 - 1 + \mu)^2 + q_2^2 + q_3^2$.
Let $J_\mu(q, p)$ be the energy of the system (kinetic and potential energies), *i.e.* $J_\mu(q, p) = \frac{|\dot{q}|^2}{2} + V_\mu(q) = \frac{|p|^2}{2} + p_1q_2 - p_2q_1 - \frac{1-\mu}{r_1} - \frac{\mu}{r_2}$. One observes that:

$$\dot{q} = \frac{\partial J_\mu}{\partial p}, \quad \dot{p} = -\frac{\partial J_\mu}{\partial q} + \varepsilon u.$$

When $\varepsilon = 0$ (uncontrolled or free system), we are dealing with an Hamiltonian system. Thus the controlled CRTBP is a perturbation of an Hamiltonian system (the uncontrolled CRTBP itself) by a small parameter ε.

In addition the system itself is parametrized by an intrinsic parameter: The mass ratio μ. In fact the limit case $\mu = 0$ is a two body-problem for instance Earth-spacecraft. In the Earth-Moon system case; $\mu = 0.012153 << 1$, one

can assume that our system is a two bodies problem disrupted by the small parameter μ, from here derives the idea of the two-three body continuation used to solve minimum time transfers.

Thus, as a conclusion, the controlled CRTBP is a system depending on two parameters μ: the mass ratio $m_2/(m_1 + m_2)$ defining the mass distribution between the primaries and ε: The bound on the acceleration of the spacecraft is the ratio of its maximum thrust by its instantaneous mass.

Remark 1.2.2. Notice that both the Lagrangian and the Hamiltonian form of the equations in rotating coordinates (x, y, z) provide a time independent system. Viewed as a dynamical system, it is a dynamical system in a six-dimensional phase space, viewed as either $(x, y, z, \dot{x}, \dot{y}, \dot{z})$ or $(q_1, q_2, q_3, p_1, p_2, p_3)$ space, subset of $\mathbf{R}^6$ which exclude the singularities at the position of the primaries.

1.3 Jacobi integral and Hill's regions

1.3.1 Jacobi integral

Let us consider the uncontrolled CRTBP *i.e.* $\varepsilon = 0$ and write the equation of motion using the (q, p) coordinates:

$$\dot{q} = \frac{\partial J_\mu}{\partial p}, \quad \dot{p} = -\frac{\partial J_\mu}{\partial q}.$$

Since the previous equations of motion of the CRTBP are Hamiltonian and independent of time they have an energy integral of motion:

$$E(x, y, z, \dot{x}, \dot{y}, \dot{z}) = \frac{\dot{x}^2 + \dot{y}^2 + \dot{z}^2}{2} + V_\mu(x, y, z) \tag{1.8}$$

Physically, the measurement of the particle's position and velocity in either the inertial or rotating frames determines the value of the energy associated with the particle's motion.

The celestial mechanics and dynamical astronomy communities use $-2E$, which is called the Jacobi integral and is written as thus:

$$C(x, y, z, \dot{x}, \dot{y}, \dot{z}) = -2E(x, y, z, \dot{x}, \dot{y}, \dot{z}) = -(\dot{x}^2 + \dot{y}^2 + \dot{z}^2) - 2V_\mu(x, y, z)$$

Usually the existence of the Jacobi integral is derived directly from the equation of motion. The calculation is straightforward:

$$\begin{aligned}\frac{\mathrm{d}}{\mathrm{d}t}(\dot{x}^2 + \dot{y}^2 + \dot{z}^2) &= 2(\dot{x}\ddot{x} + \dot{y}\ddot{y} + \dot{z}\ddot{z}) \\ &= 2(\dot{x}(2\dot{y} - V_{\mu_x}) + \dot{y}(-2\dot{y} - V_{\mu_y}) + \dot{z}(-V_{\mu_y})) \\ &= 2\frac{\mathrm{d}}{\mathrm{d}t}(-V_\mu)\end{aligned}$$

therefore we require

$$\frac{\mathrm{d}}{\mathrm{d}t}C = \frac{\mathrm{d}}{\mathrm{d}t}(-(\dot{x}^2 + \dot{y}^2 + \dot{z}^2) - 2V_\mu) = 0.$$

In general, there are not other integrals constraining the motion of the article, making the CRTBP a non-integrable problem.

1.3.2 Hill's regions

In the two body Kepler problem, one may divide the phase space into two major categories, based on the value of the Keplerian energy, $E = -\frac{1}{2a}$, where a is the semimajor axis of the particle's orbit around the central massive body (for instance Earth-spacecraft system). The following two cases divide the phase space into two major categories of possible motion for the particle:

(i) $E < 0$: Negative Keplerian energies correspond to bound motion of the particle around the single massive body *i.e.* elliptical orbits.

(ii) $E > 0$: Positive Keplerian energies correspond to unbound motion *i.e.* hyperbolic orbits coming from and going to infinity.

The critical case of zero energy orbits between these two are the unbound parabolic orbits. If we restrict ourselves to the planar Kepler problem, we have a four-dimensional phase space, which we can view as an open set in $\mathbf{R}^4$: Two position coordinates and their two corresponding velocities. for each value e the equation $E = e$ describes a three-dimensional set in the four-dimensional phase space, termed the energy surface corresponding to the energy e. The phase space can be viewed as a many layered "onion", each layer or leaf corresponding to a value of the energy. one says that the energy surfaces foliate the phase space.

In the CRTBP, the picture is more complicated, but we can follow a similar strategy by categorizing the possible motion of a particle by energy, this time the CRTBP energy is given by the equation (1.8). Later in this section, we will concentrate on the study of the PCRTBP (P for planar) with $z = \dot{z} = 0$.

Definition 1.3.1. Energy surface. Let M be the energy manifold or energy surface given by setting the energy integral (1.8) equal to a constant e:

$$M(\mu, e) = \{(x, y, \dot{x}, \dot{y}) | E(x, y, \dot{x}, \dot{y}) = e\}. \tag{1.9}$$

for a fixed μ and energy e, one can consider the surface $M(\mu, e)$ as a three-dimensinal surface embedded in the four-dimensional phase space.

Definition 1.3.2. Hill's region. The projection of this surface onto position space in the rotating frame, the (x, y) plane, is the region of possible motion for a particle of energy e in the field of two masses with mass parameter μ. This projection is presented by:

$$\{(x, y) | V_\mu(x, y) \leq e\}, \tag{1.10}$$

known historically as the Hill's region. Its boundary is known as the zero velocity curve and plays an important role in placing bounds on the motion of the particle.

Definition 1.3.3. The zero velocity curves or the boundaries of the Hill's region are the locus of the points in the (x, y) plane where the kinetic and hence the velocity $v = \sqrt{\dot{x}^2 + \dot{y}^2}$ vanishes *i.e.* $\frac{1}{2}v^2(x, y) = e - V_\mu(x, y) = 0$.

From (1.10) it is clear that the particle is only able to move on the side of this curve for which the kinetic energy is positive. The other side of the curve,

where the kinetic energy is negative and motion is not possible, is known as the forbidden realm.

Recall that the energy E is given by $E(x, y, \dot{x}, \dot{y}) = \frac{\dot{x}^2+\dot{y}^2}{2} + V_\mu(x, y)$. Fixing the energy function to be a constant *i.e.* $E(x, y, \dot{x}, \dot{y}) = e$ is like fixing a height in the plot of the effective potential $V_\mu(x, y)$ surface. Consider this surface and note the following features:

- Near either m_1 or m_2, there is a potential well.
- Far away from either m_1 or m_2, the term that corresponds to the centrifugal force dominates $V_\mu(x, y)$ *i.e.* $\frac{|\frac{1}{2}(x^2+y^2)|}{|\frac{1-\mu}{r_1}+\frac{\mu}{r_2}|} << 1$ and then there is another potential well.
- By multivariable calculus, one finds that there are five critical points where the slope is zero: Three saddle points along the x axis and two symmetric points o the x axis. As will be covered in the next section, these points are the (x, y) locations of the equilibrium points for a particle in the rotating frame *i.e.* a particle placed here at rest with respect to m_1 and m_2 (zero initial velocity), will remain at rest for all time (zero acceleration). We label these points L_i , $i = 1, \ldots, 5$, as in figure (1.2) (*cf.* [36]).
- Let E_i be the energy of a particle at rest at L_i , then $E_5 = E_4 > E_3 > E_1 > E_2$. Thus, L_2 is the location of the lowest energy equilibrium point and L_4 and L_5 are the highest energy equilibrium points. Since the energy is measured in a rotating frame, we cannot determine the stability properties of all the equilibrium points according to their energy order.

For a given μ there are five basic configurations for the Hills region, corresponding to five intervals of energy value e in (1.9). We refer to these basic configurations as energy cases, or simply cases. The cases are shown in figure (1.1). We will show how to compute the energy intervals corresponding to these cases. Contour plots of the effective potential provide the five cases of Hills region. The shaded areas in figure (1.1) are the Hills region and the white areas are the forbidden realm.

- Case 1: $e < E_2$, if the energy of the particle is below E_2, the particle can not move between the realms around m_1 and m_2.
- Case 2: $E_2 < e < E_1$, this is the case that concerns us the most; when the energy is just above E_2. A neck between the realms around m_1 and m_2 opens up, permitting the particle to move between the two realms. The L_2 point is in this neck.
- Case 3: $E_1 < e < E_3$, if the energy is just above E_1, The particle can move between the vicinity of m_1 and m_2 and the exterior realm via a neck around L_1 .
- Case 4: $E_3 < e < E_4 = E_5$, in this case the energy is above E_3 but below that of E_4 and E_5. The particle can pass directly from the vicinity of m_1 to the exterior realm via a neck around L_3 .
- Case 5: $E_4 = E_5 < e$, if the energy is above $E_4 = E_5$, the forbidden realm disappears. Case 5 is where the particle is free to move in the entire (x, y) plane.

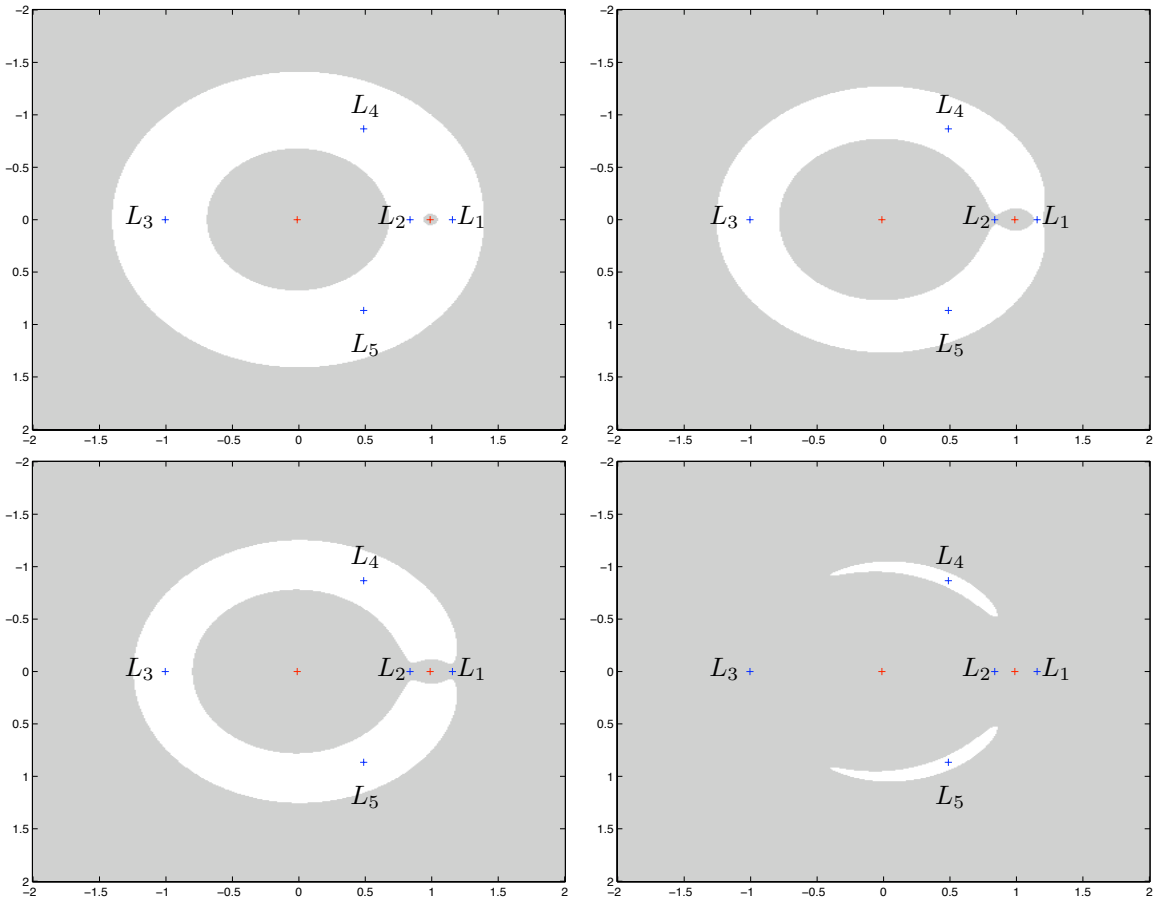

Figure 1.1: *Hill's region with respect to the energy value e for $\mu = \mu_{Earth-Moon} = 0.012153$. Case 1: Top corner left, Case 2: Top corner right, Case 3: Bottom corner left and Case 4: Bottom corner right.*

A glance at figure (1.1) reveals that beginning in case 1, there are three main realms of possible motion. Considering, for example, figure (1.1) case 1, the large region surrounding m_1 is referred to as the m_1 realm, sometimes referred to as the interior realm. The small region surrounding m_2 is the m_2 realm. The realm which lies outside both the m_1 and m_2 realms, and extends to infinity, is the exterior realm. For this case, the realms are separated. Moving up in energy to case 2, a neck around L_2 opens up between the m_1 and m_2 realms, permitting the particle to pass between the two. An additional neck opens up around L_1 when energy increases to case 3, permitting travel between all three realms.

Our main interest in this study will be case 2 for which we will prove later the controllability of the system and then we will design missions transferring a particle (*i.e.* spacedraft) from the m_1 realms (*i.e.* Earth's attraction field) to the m_2 realms (*i.e.* Moon's attraction field).

Remark 1.3.1. The critical values of e which separate these five cases are the values E_i, $i = 1, \ldots, 4$ previously mentioned, corresponding to the equilibrium points $L_i, i = 1, \ldots, 4$ can be easily calculated for small values of μ.

Remark 1.3.2. The introduction of the parameter ε in this Hamiltonian system allows to control the velocity of the third body and hence to control its energy e. Thus we get an energy time function $e(t)$ when transferring a particle from one point to another. This implies changes at the Hill's region topology with respect to time *i.e.* Hill's region dynamics. This points will be investigated later when studying the Earth-libration point L_2 transfer.

1.4 Libration points

Since the equations of motion in the restricted problem do not possess time explicitly due to the formulation in a rotating frame, the possibility exists for time invariant equilibrium locations. Such solutions are characterized by a stationary position and velocity in the synodic frame corresponding to the nonlinear system of differential equations. These particular solutions are determined by nulling the velocity and acceleration terms in the following system:

$$\begin{cases} \ddot{x} = 2\dot{y} + x - \frac{1-\mu}{r_{13}^3}(x+\mu) - \frac{\mu}{r_{23}^3}(x-1+\mu) \\ \ddot{y} = -2\dot{x} + y - \frac{1-\mu}{r_{13}^3}y - \frac{\mu}{r_{23}^3}y \\ \ddot{z} = -\frac{1-\mu}{r_{13}^3}z - \frac{\mu}{r_{23}^3}z, \end{cases}$$

resulting in the scalar equations:

$$-x_{eq} = -\frac{1-\mu}{r_{13}^3}(x_{eq}+\mu) - \frac{\mu}{r_{23}^3}(x_{eq}-1+\mu) \tag{1.11}$$

$$-y_{eq} = -\frac{1-\mu}{r_{13}^3}y_{eq} - \frac{\mu}{r_{23}^3}y_{eq} \tag{1.12}$$

$$0 = -\frac{1-\mu}{r_{13}^3}z_{eq} - \frac{\mu}{r_{23}^3}z_{eq} \tag{1.13}$$

Equation (1.13) gives $z_{eq} = 0$, then all equilibrium points are in the orbital plane of the primaries. We notice that if $r_{13} = r_{23} = 1$, the two equations (1.11) and (1.12) reduce to identity. This implies that two of the equilibrium points are located at vertices of two unique equilateral triangles. Thus, in the rotation frame, the primaries comprise two of the common vertices of both triangles, with the remaining vertex defined by $x_{eq} = \frac{1}{2} - \mu$ and $y_{eq} = \pm\frac{\sqrt{3}}{2}$. Three other equilibrium points also exist along the abscissa axis, which are known as the collinear points. The abscissa of these points are computed by forcing $y_{eq} = 0$ into the equation (1.11) (solving this equation amounts to finding the real roots of an order five polynomial).

For the Earth-Moon system, $\mu = 0.012153$, the point L_2 is situated between the Earth and the Moon, its abscissa is $x_2 \simeq 0.8369$, the abscissa of the point L_1 situated to the right of the Moon is $x_1 \simeq 1.1557$ and finally the point L_3 situated to the left of the Earth, its abscissa is $x_3 \simeq -1.0051$. These five points are also called libration points or Lagrange points. figure (1.2) shows clearly the position of these points relative to the two primaries in the CRTBP synodic frame.

Our study is focussed more on the equilibrium point L_2 because of its position between the two primairies. We want to compute precisely its abscissa x_2

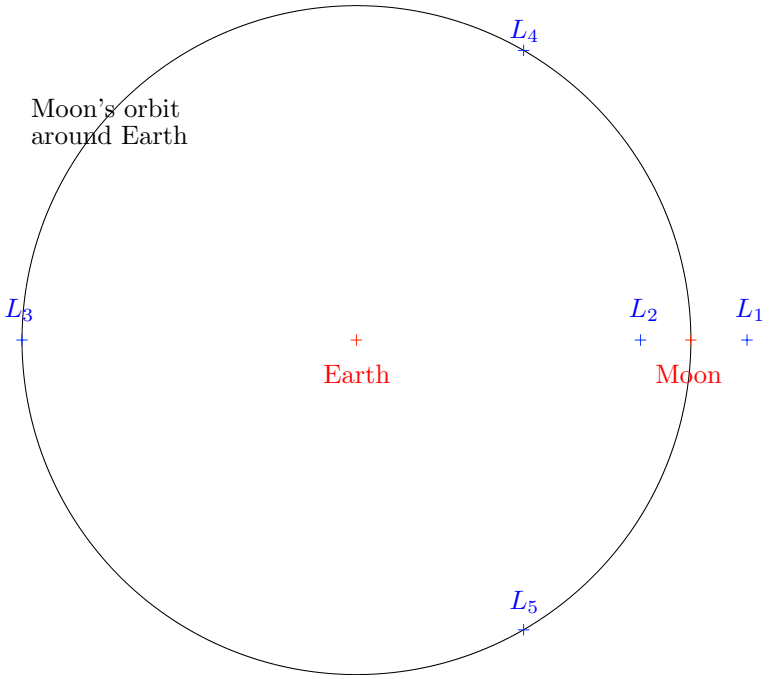

Figure 1.2: Libration Points.

[36], $-\mu \leq x_2 \leq 1-\mu$. Let us return to the equation (1.11) and substitute y_{eq} by 0 therefore:

$$x_2 = \frac{1-\mu}{(x_2+\mu)^2} - \frac{\mu}{(1-\mu-x_2)^2}$$

Let $\xi = 1-\mu-x_2$ be the distance between the Moon and the point L_2, it follows:

$$-\xi + 1 - \mu = \frac{1-\mu}{(1-\xi)^2} - \frac{\mu}{\xi^2} \tag{1.14}$$

we put the same denominator in the previous equation, this leads to an order 5 polynomial equation depending uniquely on the parameter μ:

$$\xi^5 - (3-\mu)\xi^4 + (3-2\mu)\xi^3 - \mu\xi^2 + 2\mu\xi - \mu = 0 \tag{1.15}$$

which shows the existence of at least one positive root according to Descartes' rule of signs. Numerical computation of the solution is done by a basic zero-search Newton-type algorithm, the initialization point is chosen close to the solution. Then we have a numerical approximation of ξ with high precision ($\sim 10^{-10}$) and therefore a numerical approximation to the libration point L_2 position x_2.

Another approach is to calculate series expansion of ξ. Indeed, (1.14) judicious factorization gives us:

$$\frac{\mu}{3(1-\mu)} = \frac{\xi^3(1-\xi+\xi^2/3)}{(1-\xi)^3(1+\xi+\xi^2)}$$

A series solution in powers of the quantity $\nu = [\frac{\mu}{3(1-\mu)}]^{\frac{1}{3}}$ is:

$$\xi = \nu(1 - \frac{1}{3}\nu - \frac{1}{9}\nu^2 - \frac{23}{81}\nu^3 + \frac{151}{243}\nu^4 - \frac{1}{9}\nu^5) + o(\nu^7).$$

When $\mu << 1$ (for instance Earth-Moon and Sun-Earth system cases), one is able to register:

$$\frac{\mu}{3(1-\mu)} = \frac{\mu}{3}(1 + \mu + \mu^2 + \mu^3 + \mu^4 + \cdots) \simeq \frac{\mu}{3}.$$

Then an expansion of ξ with respect to μ is:

$$\xi = (\frac{\mu}{3})^{\frac{1}{3}}(1 - \frac{1}{3}(\frac{\mu}{3})^{\frac{1}{3}} - \frac{1}{9}(\frac{\mu}{3})^{\frac{2}{3}} + \cdots)$$

Remark 1.4.1. Knowing the series expansion of ξ with respect to ν, a judicious initialization to the zero-search algorithm is simply $\nu = [\frac{\mu}{3(1-\mu)}]^{\frac{1}{3}}$.

1.5 Controllability

Let us return to the controlled CRTBP for $\varepsilon > 0$ and $\mu \in (0, 1)$ (the cases $\mu = 0$ and $\mu = 1$ corresponds to the two-body case which is not the aim of this current study) written in the space coordinates (x, y, z) *i.e.*:

$$\begin{cases} \ddot{x} = 2\dot{y} + x - \frac{1-\mu}{r_{13}^3}(x+\mu) - \frac{\mu}{r_{23}^3}(x-1+\mu) + \varepsilon u_1 \\ \ddot{y} = -2\dot{x} + y - \frac{1-\mu}{r_{13}^3}y - \frac{\mu}{r_{23}^3}y + \varepsilon u_2 \\ \ddot{z} = -\frac{1-\mu}{r_{13}^3}z - \frac{\mu}{r_{23}^3}z + \varepsilon u_3 \end{cases}$$

In the remainder of this thesis, we shall note x a vector of $\mathbf{R}^6$ such that $x = (x_1, x_2, x_3, x_4, x_5, x_6) = (x, y, z, \dot{x}, \dot{y}, \dot{z})$ *i.e.* the phase space vector relative to the third body. The previous second order differential system is reduced to first order differential system on the vector x as described below.

$$\begin{aligned} \dot{x} &= F(x, u) \\ &= F_0(x) + \varepsilon \sum_{i=1}^{3} F_i(x) u_i. \end{aligned}$$

Where:

$$F_0(x) = \begin{pmatrix} x_4 \\ x_5 \\ x_6 \\ 2x_5 + x_1 - \frac{1-\mu}{r_{13}^3}(x_1+\mu) - \frac{\mu}{r_{23}^3}(x_1-1+\mu) \\ -2x_4 + x_2 - \frac{1-\mu}{r_{13}^3}x_2 - \frac{\mu}{r_{23}^3}x_2 \\ -\frac{1-\mu}{r_{13}^3}x_3 - \frac{\mu}{r_{23}^3}x_3 \end{pmatrix},$$

$$F_1(x) = \begin{pmatrix} 0 \\ 0 \\ 0 \\ 1 \\ 0 \\ 0 \end{pmatrix}, F_2(x) = \begin{pmatrix} 0 \\ 0 \\ 0 \\ 0 \\ 1 \\ 0 \end{pmatrix}, F_3(x) = \begin{pmatrix} 0 \\ 0 \\ 0 \\ 0 \\ 0 \\ 1 \end{pmatrix}$$

and $u = \begin{pmatrix} u_1 \\ u_2 \\ u_3 \end{pmatrix} \in B_c(0,1) \subset \mathbf{R}^3$ is the control vector ($|u| \leq 1$). The system written in this way is said affine with respect to the control u and the vector field F_0 is called the system drift *i.e.* describes the system free evolution (no control term). The vector fields F_1, F_2 and F_3 introduce the control action on the system. The state vector $x \in \mathbf{R}^6$ is such that:

$r_{13} = \sqrt{(x_1+\mu)^2 + x_2^2 + x_3^2} > R_1$, R_1 is the radius of the first primary.
$r_{23} = \sqrt{(x_1-1+\mu)^2 + x_2^2 + x_3^2} > R_2$, R_2 is the radius of the second primary.
$r = \sqrt{x_1^2 + x_2^2 + x_3^2} < R_\infty$, R_∞ such that $R_\infty >> l^*$.

In fact, we define two security balls around the primaries, this is relevant since physically, the primaries represent two planets with which collision is to be avoided when designing missions. We suppose also that the transfers do not occur very far from the two primaries, this hypothesis is also relevant for two reasons: First we aim in this study to compute Earth-Moon transfers so the spacecraft is supposed to be close enough to the two planets. Secondly when the spacecraft is so far apart from the two primaries, the system is modeled on a two-body problem since the two primaries are seen by the spacecraft as one body of mass $m^* = m_1 + m_2$ situated on their barycenter. Hence the state x is in the tangent bundle of A_μ *i.e.* $x \in X_\mu = TA_\mu = A_\mu \times \mathbf{R}^3$ and $A_\mu = \{\mathbf{R}^3 \setminus \{B_c((-\mu,0,0),R_1) \cup B_c((1-\mu,0,0),R_2) \cup B_c((0,0,0),R_\infty)\}\}$. An immediate consequence is that the potential of the system $V_\mu(x_1,x_2,x_3)$ is bounded:

$$\forall \mu \in (0,1),\ 0 < -V_\mu < \underbrace{\frac{1}{2}R_\infty^2 + \frac{1-\mu}{R_1} + \frac{\mu}{R_2}}_{V_\mu^\infty} \tag{1.16}$$

This inequality is needed later to prove the recurrence of the vector field F_0 using the Poincaré recurrence theorem.

The system controllability is a natural and primordial question before beginning any transfer design. The question is simple: Consider two points on the phase space vector X_μ of dimension 6, is one sure to find a trajectory connecting these two points?

The question asked in this way seems to be simple and relevant, in fact any trajectory calculus does not make sense if we are not sure if such a trajectory really exists. The response is generally related to the intrinsic characteristics of the system itself *i.e.* related to the drift vector field F_0 properties.

For instance, in the two-body case the controllability is due to the recurrence (more precisely the periodicity which is stronger) of the drift, see [9] for more details. We take this point as directive idea for the CRTBP case. Since our goal is to design transfer from one primary to the second, the transfer can be represented in two parts: The first part orbiting around the departure primary and the second part orbiting around the arrival primary. It is known that when the spacecraft is "so" close to one primary a two-body behavior is a good approximation of the situation and the drift can be approximated to a periodic one and can be said recurrent when taking into account the low influence of the far primary. Thus intuitively the main task to prove controllability is to define the limits of the zone where the CRTBP is a recurrent system. Let us first recall the definition of a recurrent system.

Definition 1.5.1. A vector field F is said to be recurrent on a set X if for each open set of X there exist orbits that intersect the set infinitely often.

$$\forall x \in X, \forall V \in \vartheta(x), \forall T \geq 0, \exists t > T, \exp tF(x) \in V.$$

We recall that the drift F_0 has five equilibrium points L_i, $i \in \{1, \ldots, 5\}$, to each point is associated its energy E_i, $i \in \{1, \ldots, 5\}$, such that $E_2 < E_1 < E_3 < E_4 = E_5$, as detailed in the previous sections. The open subset $\{x \in X_\mu \mid E(x) < E_1\}$ has two connected components, and we denote by X_μ^1 the component containing L_2 (see Fig. (1.3)), $E(x)$ is the particle energy as defined in (1.8), $E(x) = \frac{\dot{x}_1^2+\dot{x}_2^2+\dot{x}_3^2}{2} + V_\mu(x_1, x_2, x_3)$, we recall that in the Hamiltonian form $E(x)$ is $J_\mu(q, p) = \frac{|\dot{q}|^2}{2} + V_\mu(q) = \frac{|p|^2}{2} + p_1 q_2 - p_2 q_1 - \frac{1-\mu}{r_1} - \frac{\mu}{r_2}$, with:

$$\dot{q} = \frac{\partial J_\mu}{\partial p}, \quad \dot{p} = -\frac{\partial J_\mu}{\partial q}.$$

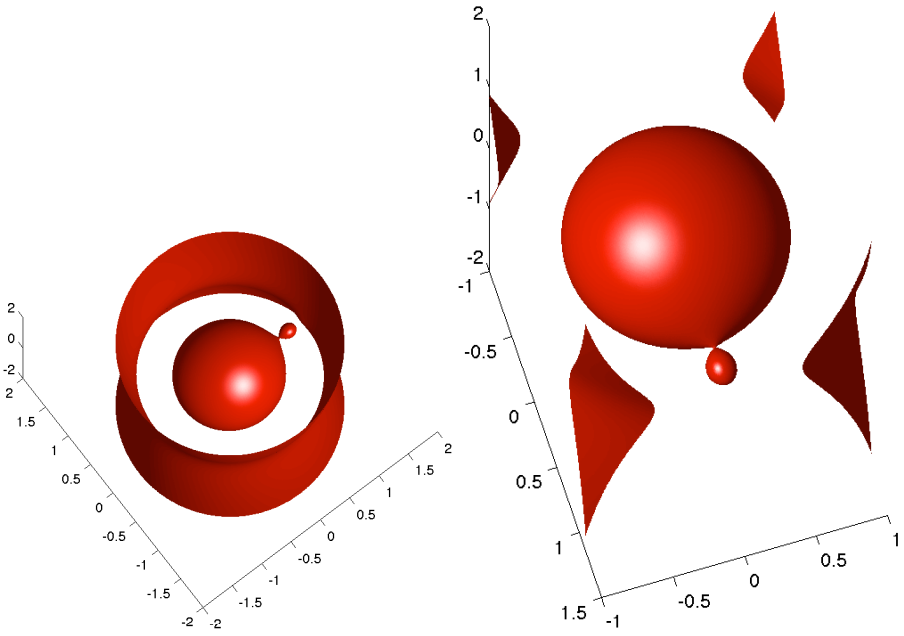

Figure 1.3: Projection of the open submanifold $\{x \in X_\mu \mid E(x) < E_1\}$ in the (q_1, q_2, q_3)-space. The boundary of the volume is an apparent surface generated by the projection. It is the *zero velocity*set.

Proposition 1.5.1. *for all $\mu \in (0, 1)$ the CRTBP drift F_0 is recurrent on X_μ^1.*

Proof. The proof is based on Poincaré recurrence theorem [29]. It is shown in the previous section that the uncontrolled CRTBP is a Hamiltonian system. We may therefore conclude that the system is recurrent, provided that the system

orbits are bounded on X_μ^1. For all $(q,p) \in X_\mu^1$,

$$0 \leq |\dot{q}|^2 < 2(E_1 - V_\mu(q)).$$

Then, we have, thanks to (1.16),

$$0 \leq (p_1 + q_2)^2 + (p_2 - q_1)^2 + p_3^2 < 2(E_1 + V_\mu^\infty)$$

In the (p_1, p_2, p_3)-space this condition defines a ball whose volume is $4\pi(2(E_1 + V_\mu^\infty))^{\frac{3}{2}}/3$ independently of q_1, q_2, q_3. Since the projection of X_μ^1 on the (q_1, q_2, q_3)-space is also finite (*cf.* figure(1.3)), it follows that X_μ^1 is of finite measure, and the recurrence theorem now stipulates as in [34] that for all initial values in X_μ^1, the particle keeps returning after arbitrarily large time intervals arbitrarily close to its initial values, both as to its position and velocity. Hence the drift F_0 is recurrent on X_μ^1. □

Proposition 1.5.2. *for any $\mu \in (0,1)$, for any positive ε, the CRTBP is controllable on X_μ^1.*

Proof. We apply the controllability theorem of recurrent systems given in [23].

- X_μ^1 is a connected set.
- The control set $U = B_c(0,1)$ is a neighbourhood of the origin.
- $\{F_0, F_1, F_2, F_3\}$ is bracket generating as, for all $x \in X_\mu$,

  $$\mathrm{Vect}_x\{F_1, F_2, F_3, [F_0, F_1], [F_0, F_2], [F_0, F_3]\}$$

  is of rank six. In fact, for $i \in \{1,2,3\}$

  $$[F_0, F_i] = F_i'(x)F_0(x) - F_0'(x)F_i(x) = -F_0'(x)F_i(x) = -\frac{\partial F_0}{\partial x_{i+3}}$$

  then

  $$[F_0, F_1](x) = -\begin{pmatrix} 1 \\ 0 \\ 0 \\ 0 \\ -2 \\ 0 \end{pmatrix}, [F_0, F_2](x) = -\begin{pmatrix} 0 \\ 1 \\ 0 \\ 2 \\ 0 \\ 0 \end{pmatrix}, [F_0, F_3](x) = -\begin{pmatrix} 0 \\ 0 \\ 1 \\ 0 \\ 0 \\ 0 \end{pmatrix}$$

  It is then obvious that $\mathrm{Vect}_x\{F_1, F_2, F_3, [F_0, F_1], [F_0, F_2], [F_0, F_3]\} = \mathbf{R}^6$
- The drift F_0 is recurrent on X_μ^1 as demonstrated in proposition (1.5.1).

The CRTBP system is then controllable on X_μ^1. □

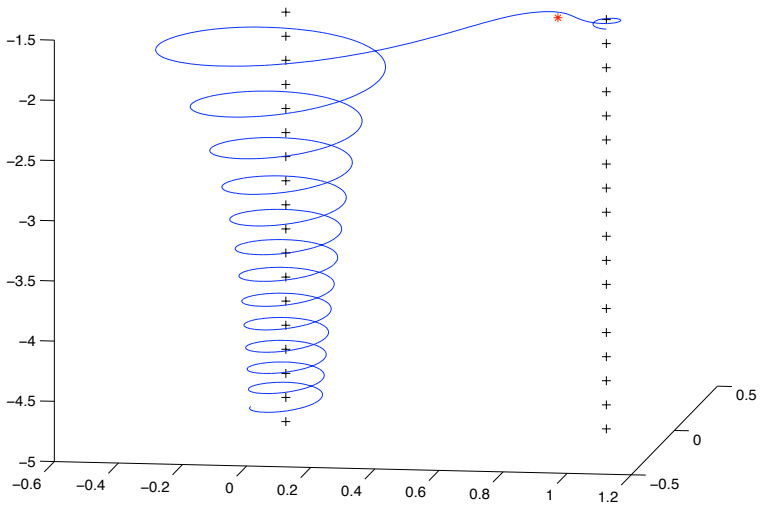

Figure 1.4: Illustration of the controllability. Trajectory relying an Earth orbit to a Moon orbit in the planar case. The picture shows the evolution of the system's energy along the transfer. The trajectory is plotted in the coordinate system (x_1, x_2, E). The cross axes indicate the Earth and the Moon. The red asterisk is the L_2 libration point *i.e.* $(x_{L_2}, 0, E_{L_2})$. The Energy of the spacecraft grows up when orbiting around the Earth. When the energy level reach the energy level of the libration point L_2, transmission to the lunar region is permitted by the mean of L_2. Once the spacecraft is captured by the Moon, the energy level decreases. Hence, to ensure connection between the Earth region and the Moon region one has to allow the spacecraft to attend the energy level of the libration point L_2. This is feasible using the control to increase the semi-major axis of the orbit around the primary.

Chapter 2

Minimum time transfer

Once the controllability of the system is proven, one is sure about the existence of trajectory connecting two points in the phase space. Let x_0 and x_f be the initial and final points. More generally, we define the initial and final sets as X_0 and X_f, these sets are submanifolds of $\mathbf{R}^6$ and describe initial and final orbits around the primaries. In this chapter and in the one which follows X_0 is a point on a circular orbit in the CRTBP plane *i.e.* (x_1, x_2) around the first primary (Earth) of radius equal to 42.165Mm, X_0 is in the primaries axis, respecting this order from left to right, we have X_0 then the Earth followed by the Moon. We aim to design optimal transfers from X_0 to two different targets X_f: The libration point L_2 and an orbit around the second primary (Moon) LO. LO is a circular orbit centered on the second primary of radius $r = 13.084$ situated in the CRTBP plane *i.e.* (x_1, x_2). Since the initial and final conditions are in the CRTBP plane, the motion of the spacecraft will be restricted to this plane, as we explained in the previous chapter, thus numerical simulations are considered in the CRTBP plane: Planar CRTBP for sake of simplicity. However, theoretical results are given in the three dimensional case. The spacecraft mass is fixed along the transfer to $m = 1500$kg; mass variation is neglected, this fact will be justified in the next chapter. We aim to compute optimal steering to realize minimum time transfers in the CRTBP from X_0 to L_2 and LO. Let us write the optimal control problem to solve:

$$(P_t) \begin{cases} \min t_f = \int_0^{t_f} \mathrm{d}t \\ \dot{x} = F(x,u) = F_0(x) + \varepsilon \sum_{i=1}^{3} F_i(x) u_i \\ |u| \leq 1 \\ x(0) \in X_0 \\ x(t_f) \in X_f \end{cases}$$

2.1 Existence of solutions

We first investigate on the existence of optimal solution of (P_t). The third body (spacecraft) dynamics is provided by:

$$\dot{x} = F(x,u)$$
$$\dot{x} = F_0(x) + \varepsilon \sum_{i=1}^{3} F_i(x) u_i.$$

Where $x \in X^1_\mu$, the set X^1_μ is an open set.

One can apply the Filippov theorem only when the state set is closed. Recall that $X^1_\mu = \{x \in \mathbf{R}^6 \,|\, E(x) < E_1,\, r_{13} > R_1,\, r_{23} > R_2\}$. We proceed as follows. Consider $\eta > 0$ and define $X^{1\eta}_\mu = \{x \in \mathbf{R}^6 \,|\, E(x) \leq E_1 - \eta,\, r_{13} \geq R_1 + \eta,\, r_{23} \geq R_2 + \eta\}$, this a closed set for all $\eta > 0$. Thus we apply the Filoppov theorem on the closed set $X^{1\eta}_\mu$. This reduction of the domain does not hinder our problem resolution since the spacecraft is far enough from the primaries (see initial and final conditions) and does not reach the libration point L_1 (point of energy E_1).

Theorem 2.1.1. *For all $\varepsilon > 0$ and $\mu \in (0,1)$, a steering u realizing the minimum time transfer exists.*

Proof.
– There is an admissible trajectory (*cf.* controllability proof in the previous chapter).

– All admissible controls have values in a compact set since, $|u| \leq 1$ so $u \in U = \mathrm{B}_c(0,1)$.

– $\forall x \in X^{1\eta}_\mu$, $F(x,U) = \{F(x,u),\ u \in U\}$ is convex set since $F(x,u)$ is an affine function of u.

– The set state $X^{1\eta}_\mu$ is closed and the set $\{(t,x,u),\, t \in [0,t_f],\, |x| \leq M, u \in U\}$ is a compact set for all $M > 0$.

– $\forall u \in U$, $\forall x \in X^{1\eta}_\mu$, $\exists C \geq 0$, $(x|F(x,u)) \leq C(|x|^2 + 1)$. Indeed,

$$\begin{aligned}(x|F(x,u)) &= (x|F_0(x)) + \varepsilon u_1 (x|F_1(x)) + \varepsilon u_2 (x|F_2(x)) + \varepsilon u_3 (x|F_3(x)) \\ &= (x|F_0(x)) + \varepsilon u_1 x_4 + \varepsilon u_2 x_5 + \varepsilon u_3 x_6 \\ &\leq (x|F_0(x)) + \varepsilon |u_1||x_4| + \varepsilon |u_2||x_5| + \varepsilon |u_3||x_6| \\ &\leq (x|F_0(x)) + 3\varepsilon |x|\end{aligned}$$

$$\begin{aligned}(x|F_0(x)) &= (2 - (\frac{1-\mu}{r_{13}^3} + \frac{\mu}{r_{23}^3}))(x_1x_4 + x_2x_5 + x_3x_6) + \mu(1-\mu)(\frac{1}{r_{23}^3} - \frac{1}{r_{13}^3})x_4 - x_6x_3 \\ &\leq |2 - (\frac{1-\mu}{r_{13}^3} + \frac{\mu}{r_{23}^3})||x_1x_4 + x_2x_5 + x_3x_6| + \mu(1-\mu)|\frac{1}{r_{23}^3} - \frac{1}{r_{13}^3}||x_4| + |x_6||x_3| \\ &\leq |2 - (\frac{1-\mu}{r_{13}^3} + \frac{\mu}{r_{23}^3})|\sqrt{x_1^2 + x_2^2 + x_3^2}\sqrt{x_4^2 + x_5^2 + x_6^2} + \mu(1-\mu)|\frac{1}{r_{23}^3} - \frac{1}{r_{13}^3}||x| + |x|^2 \\ &\leq (1 + \max(2, |2 - (\frac{1-\mu}{R_1^3} + \frac{\mu}{R_2^3})|))|x|^2 + \mu(1-\mu)\max(\frac{1}{R_1^3}, \frac{1}{R_2^3})|x|\end{aligned}$$

We therefore conclude with the Filippov theorem [15]. □

2.2 Structure of optimal controls

Now we are sure of the existence of the (P_t) solutions, let us try to find one. (P_t) is an optimal control problem. As mentioned in the introduction, our study aims to compute optimal solutions for transfers in the CRTBP frame by the means of indirect methods. Those methods are based on the Pontryagin Maximum Principle and shooting methods. First step to solve (P_t) is to apply the PMP (Pontryagin Maximum Principle) [1, 30]. Let us recall the PMP: We consider our control system in $\mathbf{R}^n$

$$\dot{x}(t) = F(x(t), u(t)) \tag{2.1}$$

where $F : \mathbf{R}^n \times \mathbf{R}^m \longrightarrow \mathbf{R}^n$ (in our case $n = 6$ and $m = 3$) is C^1 and where the control u is an essentially bounded and measurable function on an interval $[0, t_e(u)[$ of $\mathbf{R}^+$ whose values are in $U \subset \mathbf{R}^m$ ($U = B_c(0, 1)$ in our study). Let X_0 and X_f be two subsets of $\mathbf{R}^n$. We denote by $L^\infty([0, t(u)])$ the set of admissible controls u which permit to steer the system from an initial point of X_0 to a final point of X_f in a time $t(u) < t_e(u)$.

Moreover we define the cost of a control u on $[0, t]$

$$C(t, u) = \int_0^t F^0(x(s), u(s))ds,$$

where $F^0 : \mathbf{R}^n \times \mathbf{R}^m \longrightarrow \mathbf{R}^n$ is C^1, and $x(.)$ is the trajectory solution of (2.1) associated to the control u.
We consider the following optimal control problem : Determine a trajectory from X_0 to X_f which minimizes the cost. The final time can be fixed (minimum consumption transfer, next chapter) or not (our current case).
If the control $u \in L^\infty([0, t(u)])$ associated with the trajectory $x(.)$ is optimal on $[0, t_f]$, then there exists, according to the Pontryagin maximum principle, an absolutely continuous mapping $p(.) : [0, t_f] \longrightarrow \mathbf{R}^n$ called *costate vector*, and a real number $p^0 \leq 0$, with $(p(.), p^0) \neq (0, 0)$, such as for almost every $t \in [0, t_f]$,

$$\begin{cases} \dot{x} = \frac{\partial H}{\partial p}(x, p, p^0, u), \\ \dot{p} = -\frac{\partial H}{\partial x}(x, p, p^0, u), \end{cases} \tag{2.2}$$

where $H(t, x(t), p(t), p^0, u(t)) = \langle p, F(x, u)\rangle + p^0 F^0(x, u)$ is the *Hamiltonian* function, and the maximization condition

$$H(x, p, p^0, u) = \max_{v \in U} H(x, p, p^0, v) \tag{2.3}$$

is maintained almost everywhere on $[0, t_f]$.
If the final time to reach the target X_f is free, we obtain another condition at the final time t_f

$$\max_{v \in U} H(x(t_f), p(t_f), p^0, v) = 0. \tag{2.4}$$

Moreover if X_0 or X_f (or both) is a manifold of $\mathbf{R}^n$ having tangent spaces in $x(0) \in X_0$ or $x(t_f) \in X_f$ (or both), then the adjoint vector must verify respectively the first or the second condition (or both) below

$$p(0) \perp T_{x(0)}X_0 \tag{2.5}$$

$$p(t_f) \perp T_{x(t_f)}X_f. \tag{2.6}$$

Remark 2.2.1. During our study, initial conditions of the considered transfers are punctual *i.e.* X_0 is defined as a point on a given orbit, thus the condition (2.5) is inactive.

Remark 2.2.2. F and F^0 do not depend on t (for the minimum time case $F^0 : (x,u) \mapsto 1$ and for the minimum consumption case $F^0 : (x,u) \mapsto |u|$), then H does not depend on t, the system is autonomous, we have

$$\forall t \in [0, t_f] \quad \max_{v \in U} H(x(t), p(t), p^0, v) = C.$$

Definition 2.2.1. An extremal of the optimal control problem is a quadruple $(x(.), p(.), p^0, u(.))$ solution of the equations (2.2) and (2.3). If $p^0 = 0$, the extremal is said to be abnormal and if $p^0 \neq 0$ it is said to be normal.

Definition 2.2.2. The conditions (2.5) and (2.6) are called transversality conditions on the adjoint vector. The condition (2.4) is called condition of transversality on the Hamiltonian.

Definition 2.2.3. The function

$$H(x,p) = H(x,p,p^0,u(x,p)) \tag{2.7}$$

is called the *true Hamiltonian*, when the maximum condition gives the control u in terms of (x,p).

Let us resume the minimum time transfer case from X_0 to X_f, the cost function is $F^0 : (x,u) \mapsto 1$, we introduce the costate vector (p^0, p): $p = (p_1, p_2, p_3, p_4, p_5, p_6)$ and $p^0 \leq 0$. The Hamiltonian is then:

$$\begin{aligned} H(x,p,u) &= p^0 + \langle p, F(x,u) \rangle \\ &= p^0 + \langle p, F_0(x) \rangle + \varepsilon \langle p, F_1(x) \rangle u_1 + \varepsilon \langle p, F_2(x) \rangle u_2 + \varepsilon \langle p, F_3(x) \rangle u_3. \end{aligned}$$

The normal case is considered *i.e.* $p^0 \neq 0$, the costate vector is normalized by setting $p^0 = -1$. We note $H_i = \langle p, F_i(x) \rangle$ for $i \in \{0,1,2,3\}$, H is then written as below.

$$H(x,p,u) = -1 + H_0 + \varepsilon H_1 u_1 + \varepsilon H_2 u_2 + \varepsilon H_3 u_3.$$

The PMP application leads to:

$$\begin{aligned} \dot{x} &= \frac{\partial H}{\partial p}(x,p,u) \\ \dot{p} &= -\frac{\partial H}{\partial x}(x,p,u) \\ u &= argmax_{|v| \leq 1} H(x,p,v) \\ &= argmax_{|v| \leq 1} H_1 v_1 + H_2 v_2 + H_3 v_3 \end{aligned}$$

The maximization condition gives: $u = \begin{pmatrix} \frac{H_1}{\sqrt{H_1^2+H_2^2+H_3^2}} \\ \frac{H_2}{\sqrt{H_1^2+H_2^2+H_3^2}} \\ \frac{H_3}{\sqrt{H_1^2+H_2^2+H_3^2}} \end{pmatrix}$ if $(H_1, H_2, H_3) \neq (0,0,0)$ otherwise any control u such as $|u| \leq 1$ is admissible. The equation

$H_1 = H_2 = H_3 = 0$ defines a codimension 3 manifold called switching surface Σ. the true Hamiltonian is:

$$H(x,p) = -1 + H_0 + \varepsilon\sqrt{H_1^2 + H_2^2 + H_3^2}$$

The true Hamiltonian is smooth outside of Σ. An extremal $z = (x,p)$, solution of $\dot{z} = \overrightarrow{H}(z)$(*i.e.* $(\dot{x},\dot{p}) = (\frac{\partial H}{\partial p}(x,p), -\frac{\partial H}{\partial x}(x,p))$), is said to be an order zero extremal if the curve (x,p) does not intersect the manifold $H_1^2 + H_2^2 + H_3^2 = 0$. We consider an instant $\bar{t}$ where $H_1^2(\bar{t}) + H_2^2(\bar{t}) + H_3^2(\bar{t}) = 0$. Let $\psi = (H_1, H_2, H_3)$ be the switching function, the optimal control is then $u = \frac{\psi}{|\psi|}$ if $\psi \neq 0$. Let us first enunciate the two following results.

Lemma 2.2.1. *If F is a vector field on x ($z = (x,p)$, $\dot{z} = \overrightarrow{H}(z)$) and $H_F = \langle p, F\rangle$ then $\frac{d}{dt}(H_F(z(t))) = \{H, H_F\}$ where $\{.,.\}$ denotes Poisson brackets.*

Proof.

$$\begin{aligned}
\frac{d}{dt}(H_F(z(t))) &= \frac{d}{dt}{}^t pF(x) \\
&= \underbrace{{}^t pF'(x)}_{\frac{\partial H_F}{\partial x}} \underbrace{\dot{x}}_{\frac{\partial H}{\partial p}} + \underbrace{{}^t\dot{p}}_{-\frac{\partial H}{\partial x}} \underbrace{F(x)}_{\frac{\partial H_F}{\partial p}} \\
&= \sum_i \left(\frac{\partial H_F}{\partial x_i}\frac{\partial H}{\partial p_i} - \frac{\partial H}{\partial x_i}\frac{\partial H_F}{\partial p_i}\right) \\
&= \{H, H_F\}.
\end{aligned}$$

□

Lemma 2.2.2. *If F et G are two vector fields on x ($z = (x,p)$, $\dot{z} = \overrightarrow{H}(z)$) and $H_F = \langle p, F\rangle$ and $H_G = \langle p, G\rangle$ then $\{H_F, H_G\} = H_{[F,G]}$ where $[.,.]$ denotes the Lie brackets.*

Proof.

$$\begin{aligned}
\{H_F, H_G\} &= \sum_i \left(\frac{\partial H_G}{\partial x_i}\frac{\partial H_F}{\partial p_i} - \frac{\partial H_F}{\partial x_i}\frac{\partial H_G}{\partial p_i}\right) \\
&= {}^t pG'(x)F(x) - {}^t pF'(x)G(x) \\
&= {}^t p(G'(x)F(x) - F'(x)G(x)) \\
&= \langle p, [F,G]\rangle \\
&= H_{[F,G]}.
\end{aligned}$$

□

Let us resume to our study, z is absolutely continuous, thus ψ has derivatives almost everywhere: $\dot{\psi} = (\dot{H}_1, \dot{H}_2, \dot{H}_3)$. We recall that the Hamiltonian is demonstrated by $H = -1 + H_0 + \varepsilon(u_1H_1 + u_2H_2 + u_3H_3)$, $H_i = \langle p, F_i\rangle$, $i \in \{0,1,2,3\}$. By **lemma 2.2.1** we have:

$$\begin{aligned}
\dot{H}_1 &= \{H, H_1\} = \{H_0, H_1\} + u_2\{H_2, H_1\} + u_3\{H_3, H_1\} \\
\dot{H}_2 &= \{H, H_2\} = \{H_0, H_2\} + u_1\{H_1, H_2\} + u_3\{H_3, H_2\} \\
\dot{H}_3 &= \{H, H_3\} = \{H_0, H_2\} + u_1\{H_1, H_3\} + u_2\{H_2, H_3\}
\end{aligned}$$

By **lemma 2.2.2** we achieve:

– $\{H_1, H_2\} = H_{[F_1,F_2]} = \langle p, \underbrace{[F_1, F_2]}_{0} \rangle = 0$

– $\{H_1, H_3\} = H_{[F_1,F_3]} = \langle p, \underbrace{[F_1, F_3]}_{0} \rangle = 0$

– $\{H_3, H_2\} = H_{[F_3,F_2]} = \langle p, \underbrace{[F_3, F_2]}_{0} \rangle = 0$

Thus $\dot{\psi} = (\{H_0, H_1\}, \{H_0, H_2\}, \{H_0, H_3\})$. Since $\{H_0, H_1\}$, $\{H_0, H_2\}$ and $\{H_0, H_3\}$ are continuous then ψ is C^1 and $\dot{\psi}$ are defined everywhere. If $\dot{\psi} = 0$ then

$$\begin{aligned}
\{H_0, H_1\} = H_{[F_0,F_1]} = \langle p, [F_0, F_1] \rangle = 0 \Rightarrow p \perp [F_0, F_1] \\
\{H_0, H_2\} = H_{[F_0,F_2]} = \langle p, [F_0, F_2] \rangle = 0 \Rightarrow p \perp [F_0, F_2] \\
\{H_0, H_3\} = H_{[F_0,F_3]} = \langle p, [F_0, F_3] \rangle = 0 \Rightarrow p \perp [F_0, F_3]
\end{aligned}$$

$\bar{t}$ is a switching time so $\psi(\bar{t}) = (H_1(\bar{t}), H_2(\bar{t}), H_3(\bar{t})) = (0, 0, 0)$ and consequently $p \perp F_1$, $p \perp F_2$ and $p \perp F_3$. Since $\text{Vect}_x\{F_1, F_2, F_3, [F_0, F_1], [F_0, F_2], [F_0, F_3]\} = \mathbf{R}^6$ then $p(\bar{t}) = 0$ and $p \equiv 0$ since by PMP $\dot{p} = -\frac{\partial F}{\partial x} p$ thus $H = -1$ absurd (minimum time transfer $\Rightarrow H = -1$). To conclude, if $\bar{t}$ is a switching time *i.e.* $\psi(\bar{t}) = 0$ then $\dot{\psi}(\bar{t}) \neq 0$. Thus it follows:

Proposition 2.2.1. *[14] Contacts with the switching surface are of order equal to one. The curve (x, p) crosses the surface $H_1 = H_2 = H_3 = 0$ and the control u turns of an angle of π, hence the term* π-singularity*. The number of switching times is moreover finite.*

Proof. It has been already proven that when $\psi(\bar{t}) = 0$, $\dot{\psi}(\bar{t}) \neq 0$ contacts with the switching surface are of order equal to one. Since ψ is continuously differentiable, its graph has a tangent at the origin (*cf.* figure 2.1). Thus the quotient $\frac{\psi}{|\psi|} = u$ has opposite left and right limits at $\bar{t}$ so the control u turns at an angle of π.
let us suppose that there is an infinity of switching time $(t_i)_{i \in \mathbf{N}}$ where $t_i \in [0 \ \ t_f] \, \forall i \in \mathbf{N}$. Then there exists a convergent subsequence $(t_{\phi(i)})_{i \in \mathbf{N}}$ of limit $\bar{t}$. By the continuity of ψ we have $\psi(\bar{t}) = 0$. ψ is C^1 thus

$$\dot{\psi}(\bar{t}) = \lim_{i \to \infty} \frac{\psi(t_{\phi(i)}) - \psi(\bar{t})}{t_{\phi(i)} - \bar{t}} = 0 \text{ absurd}$$

therefore the switching number is finite. □

Definition 2.2.4. An extremal (x, p, u) is said to be regular if the strong Legendre condition holds along the extremal, that is, the hessian matrix $\frac{\partial^2 H}{\partial u^2}$ is definite negative along the extremal.

Proposition 2.2.2. *Order zero extremals are regular.*

Proof. Along an order zero extremal, $u \in \mathbf{S}^2$. In any chart of $\mathbf{S}^2$,

$$\frac{\partial^2 H}{\partial u^2} < 0 \ \textit{i.e.} \ \frac{\partial^2 H}{\partial u^2} \text{ is negative definite.}$$

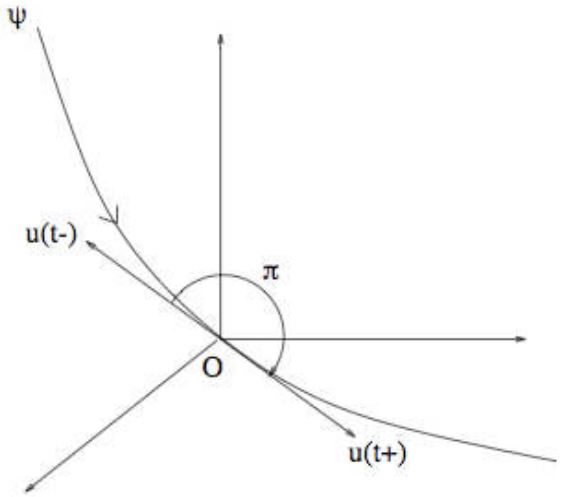

Figure 2.1: *Switch - π-singularity.*

then the strong Legendre condition is verified along the extremal.Indeed, let us for instance consider the following chart on $\mathbf{S}^2$:

$$(\varphi, \theta) \in (0, \pi) \times \mathbf{R} \mapsto (\sin\varphi\cos\theta, \sin\varphi\sin\theta, \cos\varphi)$$

Then $u = u(\varphi, \theta) = (\sin\varphi\cos\theta, \sin\varphi\sin\theta, \cos\varphi)$ and the Hamiltonian is written as a function of φ and θ:

$$H(\varphi, \theta) = -1 + H_0 + \varepsilon(\sin\varphi\cos\theta H_1 + \sin\varphi\sin\theta H_2 + \cos\varphi H_3)$$

This yields, in (φ, θ) chart:

$$\frac{\partial H}{\partial u} = \begin{pmatrix} \frac{\partial H}{\partial \varphi} \\ \frac{\partial H}{\partial \theta} \end{pmatrix} = \varepsilon \begin{pmatrix} \cos\varphi(\cos\theta H_1 + \sin\theta H_2) - \sin\varphi H_3 \\ \sin\varphi(-\sin\theta H_1 + \cos\theta H_2) \end{pmatrix}$$

and

$$\begin{aligned} \frac{\partial^2 H}{\partial u^2} &= \begin{pmatrix} \frac{\partial^2 H}{\partial \varphi^2} & \frac{\partial^2 H}{\partial \varphi \partial \theta} \\ \frac{\partial^2 H}{\partial \theta \partial \varphi} & \frac{\partial^2 H}{\partial \theta^2} \end{pmatrix} \\ &= \varepsilon \begin{pmatrix} -(\sin\varphi(\cos\theta H_1 + \sin\theta H_2) + \cos\varphi H_3) & \cos\varphi(-\sin\theta H_1 + \cos\theta H_2) \\ \cos\varphi(-\sin\theta H_1 + \cos\theta H_2) & -\sin\varphi(\cos\theta H_1 + \sin\theta H_2) \end{pmatrix}. \end{aligned}$$

An order zero extremal is considered so the control is expressed by the mean of H_1, H_2 and H_3 as below.

$$u = \begin{pmatrix} u_1 \\ u_2 \\ u_3 \end{pmatrix} = \begin{pmatrix} \frac{H_1}{\sqrt{H_1^2+H_2^2+H_3^2}} \\ \frac{H_2}{\sqrt{H_1^2+H_2^2+H_3^2}} \\ \frac{H_3}{\sqrt{H_1^2+H_2^2+H_3^2}} \end{pmatrix} = \begin{pmatrix} \sin\varphi\cos\theta \\ \sin\varphi\sin\theta \\ \cos\varphi \end{pmatrix}.$$

It follows that

$$-\sin\theta H_1 + \cos\theta H_2 = 0$$

and

$$\frac{\partial^2 H}{\partial u^2} = -\varepsilon \begin{pmatrix} \sqrt{H_1^2+H_2^2+H_3^2} & 0 \\ 0 & \frac{H_1^2+H_2^2}{\sqrt{H_1^2+H_2^2+H_3^2}} \end{pmatrix} < 0.$$

□

2.3 Two-Three body continuation

Once we have expressed the control by the mean of the state x and the costate p, one has to integrate the following differential system to evaluate the control u along the transfer.

$$\begin{cases} \dot{x} = \frac{\partial H}{\partial p}(x,p) \\ \dot{p} = -\frac{\partial H}{\partial x}(x,p) \end{cases} \tag{2.8}$$

To integrate the system (2.8), one has to know the initial values of both state x and costate p. Unfortunately, only the initial state is given in our case and the initial costate is unknown. We introduce the initial values problem:

$$(IVP) \begin{cases} \dot{x} = \frac{\partial H}{\partial p}(x,p) \\ \dot{p} = -\frac{\partial H}{\partial x}(x,p) \\ x(0) = x_0 \\ p(0) = z \end{cases} \tag{2.9}$$

The knowledge of the parameter z is the key to integrate the system (2.9) and then to calculate the control solution. The method to determine z is the following. We define the shooting function $S(z)$ which takes into account the final conditions on the state x (satellite final target *i.e.* $x(t_f) \in X_f$) and the transversality conditions (2.6) and (2.4). The resolution of the optimal control problem consists in finding zero of the function S. This method is called single shooting.

Let us resume to our minimum time problem (P_t) and let us first consider as target transfer the libration point L_2 *i.e.* $X_f = L_2$. As the final target is a punctual one the transversality condition (2.6) is inactive. However the transversality condition on the Hamiltonian (2.4) is considered, since the final time t_f is free. The corresponding shooting function is written as below.

$$S_t^{L_2} \ : \ z = (t_f, p(0)) \ \mapsto \ \begin{pmatrix} x_1(t_f) - x_{L_2}(\mu) \\ x_2(t_f) \\ x_3(t_f) \\ x_4(t_f) \\ H(t_f) \end{pmatrix}$$

Remark 2.3.1. Here the shooting function is written in the planar case. In fact, the initial and final conditions are in the CRTBP plane, spacecraft motion is restricted to this plane *i.e.* $x_3 = \dot{x}_3 = 0$ along the transfer. We recall the equation of motion in the planar case (we omit the equations relative to the

third system dimension):

$$\begin{aligned}\dot{x} &= F(x,u)\\ &= F_0(x) + \varepsilon \sum_{i=1}^{2} F_i(x) u_i.\end{aligned}$$

Where:

$$F_0(x) = \begin{pmatrix} x_3 \\ x_4 \\ 2x_4 + x_1 - \frac{1-\mu}{r_{13}^3}(x_1+\mu) - \frac{\mu}{r_{23}^3}(x_1 - 1 + \mu) \\ -2x_3 + x_2 - \frac{1-\mu}{r_{13}^3} x_2 - \frac{\mu}{r_{23}^3} x_2 \end{pmatrix},$$

$$F_1(x) = \begin{pmatrix} 0 \\ 0 \\ 1 \\ 0 \end{pmatrix}, F_2(x) = \begin{pmatrix} 0 \\ 0 \\ 0 \\ 1 \end{pmatrix}$$

and $u = \begin{pmatrix} u_1 \\ u_2 \end{pmatrix} \in B_c(0,1) \subset \mathbf{R}^2$ is the control vector ($|u| \leq 1$).

Newton-type algorithms are used to find zero of the shooting function S. These algorithms are known to be very sensitive to the initialization point. In our case, the convergence radius is quite small especially for low thrust transfers. The major difficulty is: How can one find a suitable initialization point?

Up until the moment of writing this thesis there was no known systematic method of answering this question. To address this concern, we propose here to use a homotopic method also called continuation method. The principle is: Immerse the principal problem, *i.e.* (P_t) here, in a problems family depending on a parameter $\lambda \in [\lambda_0, \lambda_f]$ *i.e.* $(P_t)_\lambda$ such as for $\lambda = \lambda_f$ we retrieve our problem and for $\lambda = \lambda_0$ we have an easier problem to solve or problem with a known solution. The continuation procedure is to follow the zeros of the problems $(P_t)_\lambda$ shooting functions from $\lambda = \lambda_0$ to $\lambda = \lambda_f$ and then a solution of our initial problem could be obtained. There are many types of continuation methods. First, we consider the discrete continuation. The principle is the following: Consider a sequence of problems $(P_{\lambda_k}), k = 1 \dots N$ such as $\lambda_1 = \lambda_0$ and $\lambda_N = \lambda_f$ and let S_{λ_k} be the corresponding shooting function,

- Step 1: A zero of S_{λ_1} is found easily.
- Step k, $k = 2, \dots, N$: The zero of $S_{\lambda_{k-1}}$ is used as an initialization to solve $S_{\lambda_k}(z) = 0$

The discretization step $h_k = \lambda_k - \lambda_{k-1}$ is adjusted as follows. If the zero of $S_{\lambda_{k-1}}$ is a suitable initialization to solve $S_{\lambda_k}(z) = 0$ then (P_{λ_k}) is solved otherwise h_k is decreased and so another homotopic step is added.

The idea is to perform a homotopy *à la Poincaré*: Connect a two-body problem to a three-body problem [11]. This idea is strengthened by the fact that the two-body is well known and already solved [9, 5, 17]. The method is: Solve the transfer in the two-body case {Earth,spacecraft} and then connect it to the three-body case {Earth,Moon,spacecraft}. The way to attain it is to

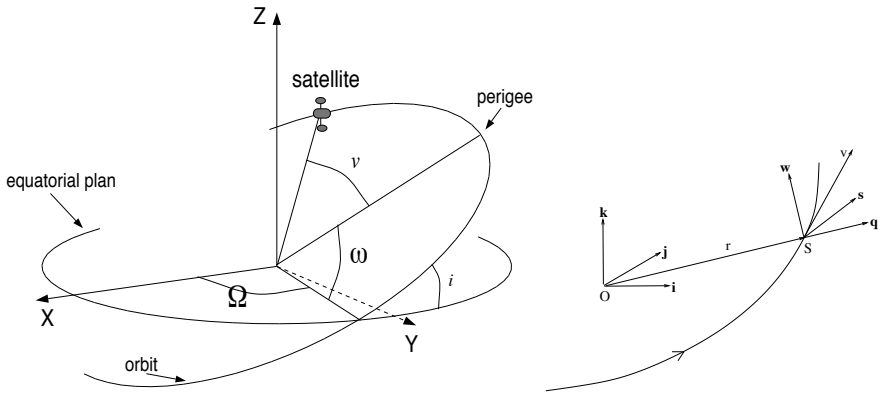

Figure 2.2: *orbital elements and ortho-radial frame.*

assume that initially, the Moon's mass is null and consider the continuation on the parameter μ: $\mu(\lambda) = \lambda\mu_{Earth-Moon}$, $\lambda \in [0, 1]$.

For $\mu = 0$ we have a two body-problem. We utilize a suitable coordinates system called modified Gauss coordinates $(P, e_x, e_y, h_x, h_y, L)$ where:

- $P = a(1 - e^2)$ is the osculating ellipse parameter, a is the semi-major axis of the ellipse and e is its eccentricity;
- $e_x = e\cos(\Omega + \omega)$, Ω is the longitude of ascending node and ω is the argument of perigee;
- $e_y = e\sin(\Omega + \omega)$;
- $h_x = \tan(i/2)\cos(\Omega)$, i is the inclination of the orbital plane relative to the equator;
- $h_y = \tan(i/2)\sin(\Omega)$;
- $L = \Omega + \omega + \nu$ is the cumulative longitude and ν is the true anomaly.

The control is expressed in a ortho-radial frame attached to the spacecraft (q, s, w), this frame is defined using the position vector of the spacecraft r and its velocity vector v as below.

$$q = \frac{r}{|r|},$$
$$s = w \wedge s,$$
$$w = \frac{r \wedge v}{|r \wedge v|}.$$

The spacecraft motion is restricted to the orbital plane of the Earth and the Moon. Therefore we also assume that the transfer occurring in the two-body case is planar and thus $i = 0$ along the transfer. This leads to $h_x = h_y = 0$ along the transfer, the coordinates are reduced then to $x = (P, e_x, e_y, L)$ and the control is expressed only using the couple (q, s).

Remark 2.3.2. Assuming that $i = 0$ means that the transfer occurs in the equatorial plane which is clearly different from the Moon-Earth orbital plane. We assume that the plane $i = 0$ is the plane of the Moon's orbit around the Earth *i.e.* we change the reference plane of inclination in the definition of the orbital elements. This is not bothersome since the Earth is considered as a material point.

The starting point is on a circular orbit around the Earth whose coordinates are $(42.165, 0, 0, \pi)$ (the parameter P unit is the Mm and the cumulative longitude is expressed as radians). The target orbit is the Moon's orbit around the Earth which is supposed to be circular as assumed by the CRTBP approximation. the target coordinates are $(384.402, 0, 0, \text{free})$. (P_t) is written in the Gauss modified coordinates as follows.

$$(P_t^G) \begin{cases} min \int_0^{t_f} dt \\ \dot{x} = f_0(x) + \varepsilon(u_1 f_1(x) + u_2 f_2(x)) \\ |u| \leq 1 \\ P(0), e_x(0), e_y(0), L(0) \text{ fixed} \\ P(t_f), e_x(t_f), e_y(t_f) \text{ Moon's orbit} \\ L(t_f) \text{ free} \end{cases}$$

where:

$$f_0(x) = \sqrt{\frac{\mu}{P}} \begin{pmatrix} 0 \\ 0 \\ 0 \\ W^2/P \end{pmatrix},$$

$$f_1(x) = \sqrt{\frac{P}{\mu}} \begin{pmatrix} 0 \\ \sin(L) \\ -\cos(L) \\ 0 \end{pmatrix},$$

$$f_2(x) = \sqrt{\frac{P}{\mu}} \begin{pmatrix} 2P/W \\ \cos(L) + (e_x + \cos(L))/W \\ \sin(L) + (e_y + \sin(L))/W \\ 0 \end{pmatrix},$$

and

$$W = 1 + e_x \cos(L) + e_y \sin(L),$$

Since (P_t^G) and (P_t) have the same form, the PMP application leads to the same control shape. The final longitude $L(t_f)$ is free, in fact the position of the Moon is known at any given time as t_f however, the number of required revolutions around the Earth to reach the Moon's orbit is unknown. Consequently, transversality condition (2.6) yields to $p_L(t_f) = 0$ (costate with respect to the state L). The corresponding shooting function is:

$$S^G \ : \ z = (t_f, p(0)) \ \mapsto \ \begin{pmatrix} P(t_f) - 384.402 \\ e_x(t_f) \\ e_y(t_f) \\ p_L(t_f) \\ H(t_f) \end{pmatrix}$$

The aim of the study is to design low thrust transfers in the CRTBP, spatial missions are undertaken using low thrust ion propulsion engines such as in the mission SMART-1 of the European Space Agency [31, 32]; A maximum thrust of 70mN for an initial mass of 350kg which corresponds to a thrust of 0.3N for 1500kg in our case. It is hard to find an initialization to solve $S^G(z) = 0$ for low thrust. The idea is to introduce a continuation on the maximal thrust $T_{\max}$. In fact, a suitable initialization is found for $T_{\max} = 60$N. Subsequently a discrete homotopy on $T_{\max}$ leads to a solution for different thrust values ranging from 60N to 85mN.

Once problem (P_t^G) is solved for different thrust values. One has now to import the initialization solution from Gauss modified coordinates to CRTBP coordinates and proceed with the homotopy on μ from 0 to $\mu_{Earth-Moon}$. For $\mu = 0$ the Moon and the libration point L_2 are the same and as μ increases as L_2 distances itself from the Moon, this distance depends on the parameter μ and is computed thanks to the equation (1.15).

The goal is to find a suitable initialization to solve $S_t^{L_2}(z) = 0$ for $\mu = \mu_{Earth-Moon} = 0.012153$. The key of the initialization is the final time transfer t_f $(z = (t_f, p(0)))$. In fact, since $\mu_{Earth-Moon}$ is quite small, the first numerical tests consist of taking an initialization, composed of $t_{f\,min}(\mu = 0)$ (solution of $S^G(z) = 0$) and arbitrary vector $p(0)$, to solve $S_t^{L_2}(z) = 0$ for $\mu = \mu_{Earth-Moon}$ therefore the shooting converges. Thus only one homotopic step is required to perform the two-three body continuation and the final time transfer is the dominating term in the initialization vector z.

This method produces solutions of (P_t) for $X_f = L_2$ and for two different maximal thrusts 10 and 1N. Unfortunately, this technic is not efficient for lower thrust (less than 1N). In order to obtain extremals for low thrust, we introduce, as in the two-body transfer, a continuation on the parameter $T_{\max}$ starting from 1N and then let the thrust down in discrete steps so as to reach the lowest thrust values. We attain a thrust value of 0.17N (acceptable compared with 0.3N required for SMART-1 mission). The homotopic step decreases as the thrust decreases, when the thrust is close to 0.2N a homotopic step of 10^{-5}N is needed to perform the continuation.

In figure 2.3, some extremal trajectories are portrayed for different maximal thrusts. Each trajectory is composed of two parts: The first is the Keplerian phase where the spacecraft is practically under only the influence of the Earth's attraction *i.e.* a two-body problem $\{Earth, spacecraft\}$ is a good approximation. Secondly the three-body aspect is highlighted and the spacecraft reachs the libration point L_2.

In table 2.3 minimum final time is provided for maximal thrust values between 1N and 0.17N. We notice that the product $T_{\max} t_{f\,\min}$ is almost a constant $(\simeq C =)$, when $T_{\max}$ is tending towards zero. This is in accordance with the two body case [13]. This is useful when performing discrete homotopy on the thrust for minimum time transfer, in fact one can initialize the final time for the step $k+1$ as follows: $t_{f\,k+1} = C_k/T_{\max k+1} = t_{f\,k} T_{\max k}/T_{\max k+1}$, this is a better initialization than considering $t_{f\,k}$.

Let us consider the extremal trajectory for $T_{\max} = 10$N. We aim to study the Hill's region evolution relative to time t along the transfer. Since $\varepsilon \neq 0$ the energy of the system is a time function depending on the acceleration of the

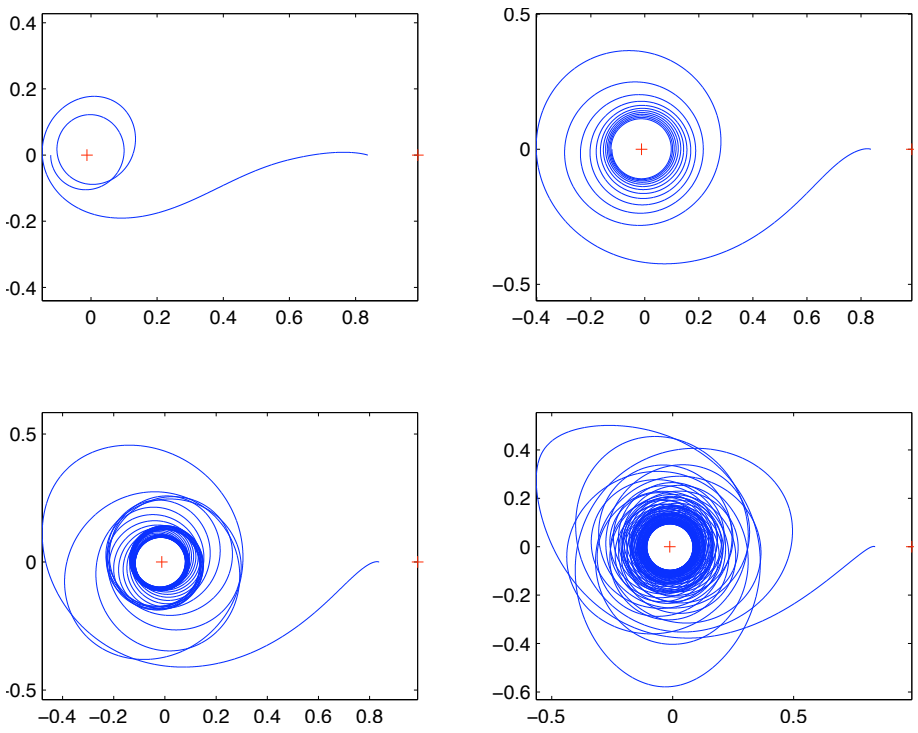

Figure 2.3: *Minimum time trajectories to* L_2 *for* 10, 1, 0.5 *and* 0.17 *Newtons, CRTBP frame.*

spacecraft gear. Recall the definition of Hill's region at an instant t:

$$\{(x_1, x_2) \in \mathbf{R}^2 | V_\mu(x_1, x_2) \leq e(t)\}.$$

We want to determine the space region accessible at time t from the point $(x_1(t), x_2(t))$ if the spacecraft is control free. In figure 2.4 the Hill's region evolution is given for three different stages along the transfer (at the beginning of the transfer t_1, at the middle t_2 and at the end t_3). For each time $t_1 < t_2 < t_3$ we associate the corresponding points on the (x_1, x_2) plane *i.e.* $P1 = P(t_1) = (x_1(t_1), x_2(t_1))$, $P2 = P(t_2) = (x_1(t_2), x_2(t_2))$ et $P3 = P(t_3) = (x_1(t_3), x_2(t_3))$. For each instant $t \in \{t_1, t_2, t_3\}$, in the same figure are portrayed: The controlled trajectory until t in red and the osculating one (control free) starting from t in blue. The point $P(t) = (x_1(t), x_2(t))$, $t \in \{t_1, t_2, t_3\}$ is marked by an aster, it is the point where the energy $e(t)$ is computed in order to compute the corresponding Hill's region. Figure 2.5 gives the integral energy J_μ evolution along the transfer.

The figure on the bottom right of the figure 2.4 is a close-up of the figure on the bottom left, at the vicinity of the arrival point *i.e.* the target L_2, the point P_3 is the final transfer point and the blue curve is the free control trajectory after the end of the transfer. One observes that the spacecraft does not remain on the point L_2 and it is no longer captured by the second primary *i.e.* the Moon. In fact, we already targeted a point of the phase space *i.e.* the state is defined by the L_2 position and a null velocity. In order to remain on the point

Table 2.1: Minimum final time (CRTBP normalized unit) for different maximal thrust values, target L_2, the product $T_{\max} t_{f\min}$ is almost constant when $T_{\max}$ tends towards zero

T_{max}(N)	$t_{f_{min}}$	$T_{\max} t_{f\min}$	$t_{f\min}$(days)
10	1.470566633802046	14.7056663380204	6.384
1	8.440118858213319	8.440118858213319	36.64
0.91	9.771072365657723	8.891675852748529	42.42
0.83	11.152247725959276	9.256365612546199	48.42
0.74	13.157672247027882	9.736677462800634	57.12
0.65	14.369930436233620	9.340454783551854	62.39
0.53	18.024798634539373	9.553143276305867	78.25
0.44	21.323275412549972	9.382241181521987	92.58
0.3	32.216276854781320	9.664883056434396	139.8
0.1789	51.504129714977552	9.214088806009483	223.6

L_2 at the end of transfer, the spacecraft must be situated exactly on the point L_2 with an identically zero velocity, since the point L_2 is an unstable equilibrium point.

However, numerical simulations give precision of 10^{-10} on the shooting function (for maximal thrust of 10N). Thus the spacecraft is not exactly on the point L_2 with null velocity. At the end of transfer there are two issues: First of all, the spacecraft is captured by the second primary as our case shows and secondly the spacecraft is returning to the attraction field of the first primary. It actually depends on the signs of the shooting function components. Let us take a closer look at the situation. Let $(\delta x_1, \delta x_2, \delta \dot{x}_1, \delta \dot{x}_2)$ be small variations of the position and the velocity at the vicinity of the point L_2, this models the numerical errors of the shooting function related to the position and the velocity. The free motion of the spacecraft on the vicinity of L_2 is given by the linearized system as below.

$$\begin{pmatrix} \delta\dot{x}_1 \\ \delta\dot{x}_2 \\ \delta\ddot{x}_1 \\ \delta\ddot{x}_2 \end{pmatrix} = \underbrace{\begin{pmatrix} 0 & 0 & 1 & 0 \\ 0 & 0 & 0 & 1 \\ -\frac{\partial^2 V}{\partial x_1^2}(x_{L_2}, 0) & 0 & 0 & 2 \\ 0 & -\frac{\partial^2 V}{\partial X_2^2}(x_{L_2}, 0) & 2 & 0 \end{pmatrix}}_{A} \cdot \begin{pmatrix} \delta x_1 \\ \delta x_2 \\ \delta \dot{x}_1 \\ \delta \dot{x}_2 \end{pmatrix}$$

The matrix A has two purely imaginary eigenvalues and two real ones: A strictly positive one and a strictly negative one. The strictly positive eigenvalue of A causes the instability of the libration point L_2. this explains the capture of the spacecraft at the end of the transfer by the Earth or by the Moon because of the precision errors on the final position and velocity.

Thanks to the discrete homotopy on the parameter μ from 0 (two-body case) to $\mu_{Earth-Moon}$, we manage to compute minimum time extremal trajectories from X_0 to L_2 for different maximal thrusts of the spacecraft gear. We investigate the impact of the parameter μ: We want to know what happens when the parameter μ increases from $\mu_{Earth-Moon}$ to 0.5 (case of equimasses planets). This permits us to have an idea for others planetary cases of the

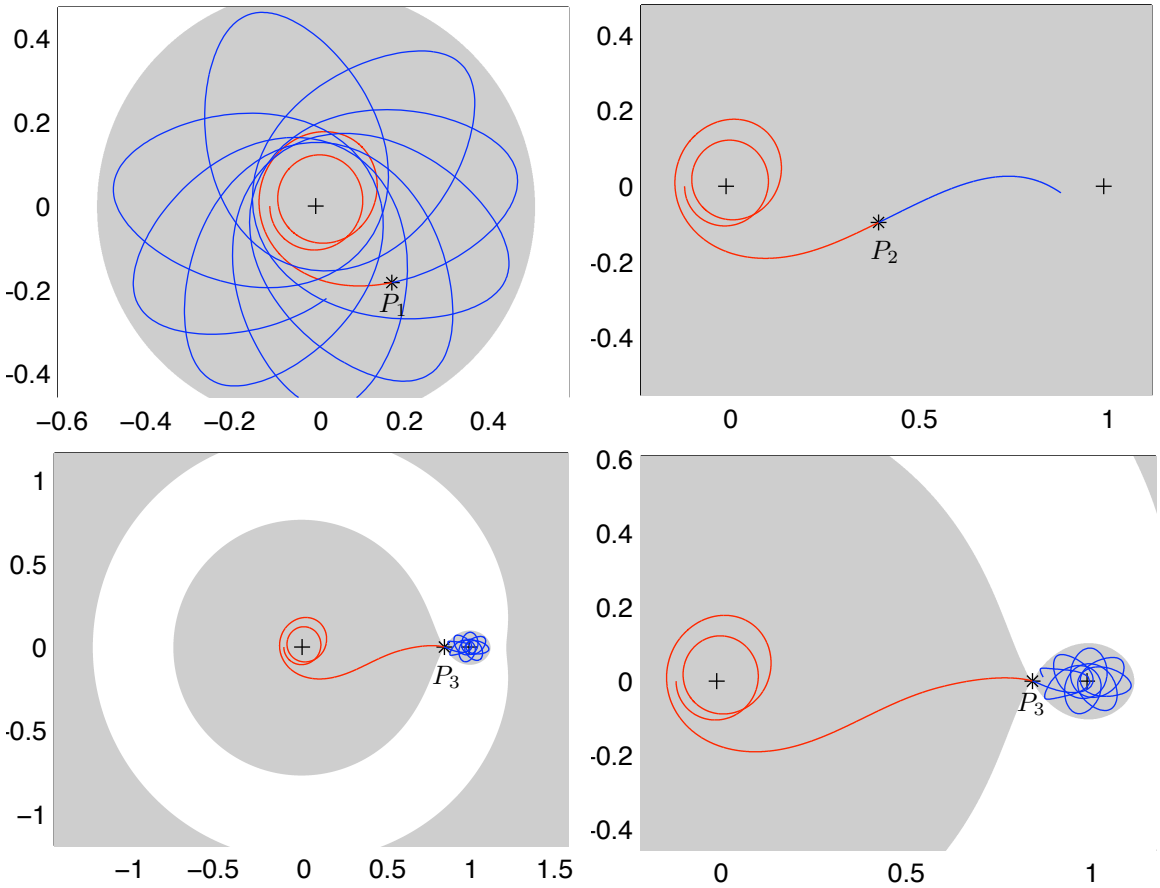

Figure 2.4: *Controlled and osculating trajectories , Hill's region evolution relative to time ($T_{\max} = 10$ Newtons), accessible region is in gray, forbidden one in white.*

CRTBP. We, subsequently, draw a discrete continuation on the parameter μ. The homotopy is performed successfully for $T_{\max} = 10$ and 1N. The discrete homotopy was unsuccessful for $T_{\max} = 0.3$N and we have not managed to go further from $\mu_{Earth-Moon}$. For instance, in figure 2.6, the minimum time optimal trajectories for different μ values between $\mu_{Earth-Moon}$ and 0.5 are provided for $T_{\max} = 1$N.

Table 2.2 resumes the discrete homotopic steps from $\mu = \mu_{Earth-Moon}$ to $\mu = 0.5$. The minimum time of the optimal transfer increases with respect to μ but a slight decrease is noticeable from $\mu = 0.45$ to $\mu = 0.5$.

2.4 Conjugate points and locus

2.4.1 Conjugate locus

The Pontryagin Maximum principle only provides a first order condition. We aim in this section to built second order conditions. We are interested in local optimality since there is no theoretical framework already developed for global optimality of such optimal control problems.

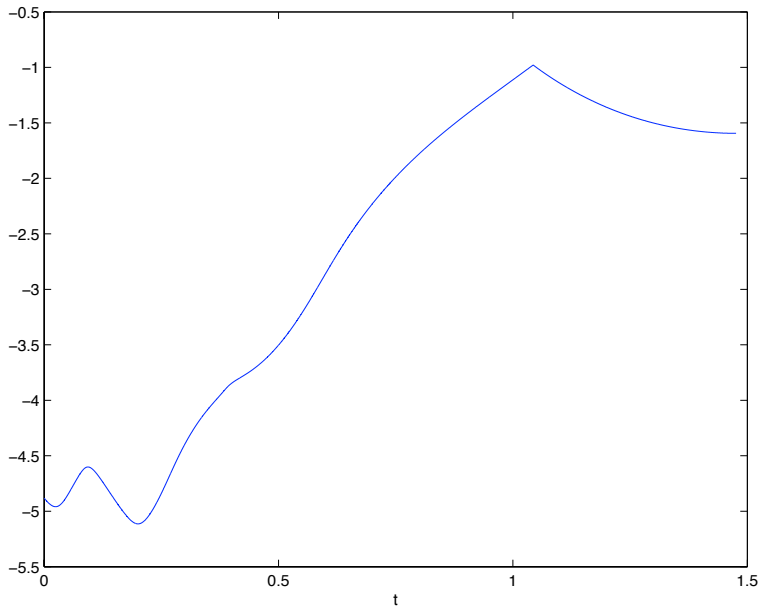

Figure 2.5: *energy integral J_μ evolution along the minimum time transfer, target L_2, $T_{\max} = 10$ Newtons.*

Let $(\bar{x}, \bar{u}, \bar{p})$ be a reference minimum time extremal. If the maximized Hamiltonian, $h(x,p) = \max_{u \in U} H(x,u,p)$, is well defined and smooth in a neighborhood of $\bar{z} = (\bar{x}, \bar{p})$, then $\bar{z}$ is an integral curve of h. If the Legendre condition holds in this neighborhood, then

$$H(x,p) = H(x, u(x,p), p) = h(x,p)$$

(the implicit function $u(x,p)$ being locally the unique zero of $\partial_u H(x,.,p)$, it is also the only maximizer of $H(x,.,p)$).

Let then $\bar{z}$ be a smooth solution of $\dot{z} = \overrightarrow{H}(z)$ where $\overrightarrow{H}(z) = (\frac{\partial H}{\partial p}, -\frac{\partial H}{\partial x})(x,p)$, defined on $[0, t_f]$, with fixed initial and final conditions *i.e.* $x(0) = x_0$ and $x(t_f) = x_f$.

Definition 2.4.1. Conjugate point [1, 7]. A point $x(t_c)$ on an extremal $z = (x,p)$ is conjugate to x_0 if there exists a Jacobi field $\delta z = (\delta x, \delta p)$, solution of the linearized system along the extremal,

$$\delta \dot{z} = \mathrm{d}\overrightarrow{H}(z(t))\delta z, \quad \overrightarrow{H} = (\partial_p H, -\partial_x H),$$

which is non-trivial (δx not $\equiv 0$) and vertical at $t = 0$ and t_c,

$$\delta x(0) = 0, \quad \delta x(t_c) = 0.$$

A control is said to be $\mathscr{C}^0$-locally optimal whenever there exists a neighborhood of the associated trajectory in $\mathscr{C}^0([0,\, t_f], \mathbf{R}^n)$ such that any other admissible trajectory in this neighborhood has a greater cost.

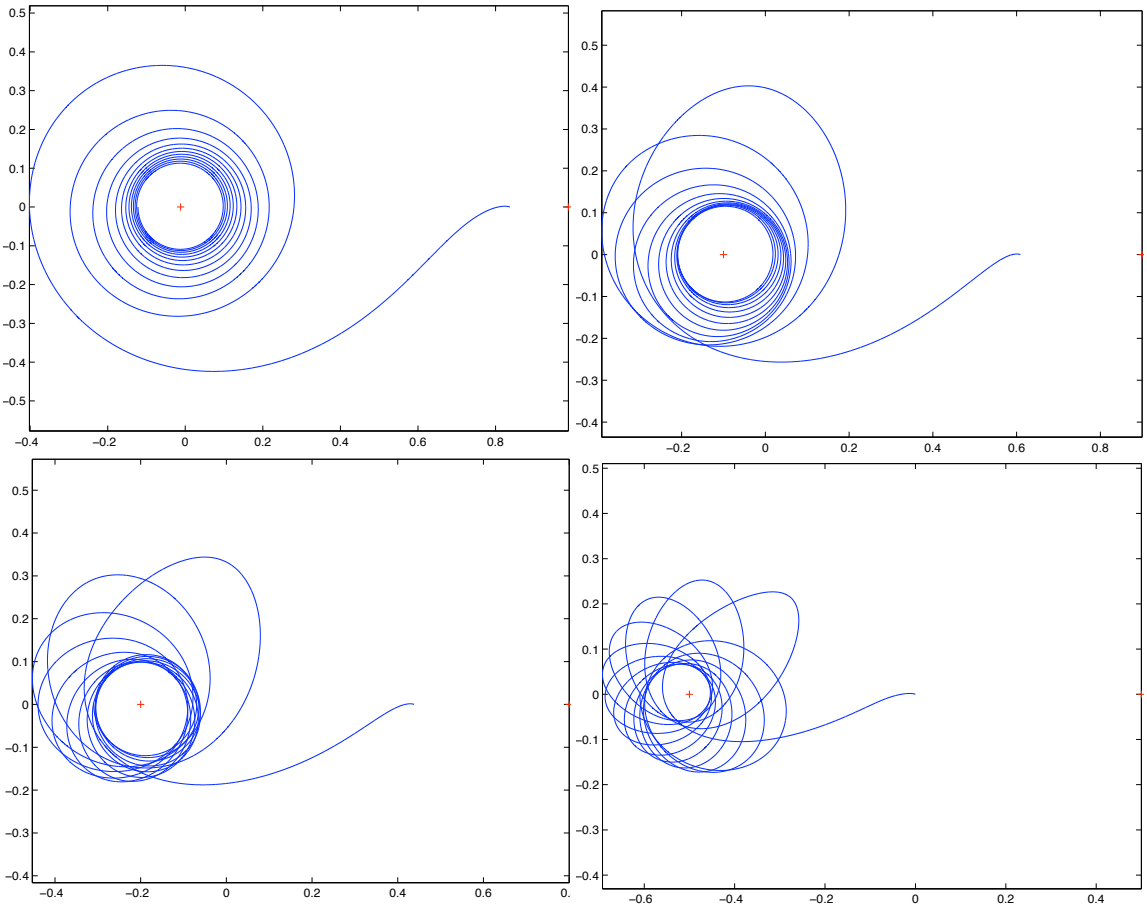

Figure 2.6: *Alteration of the quasi-keplerian phase for* μ *equal to* 0.1 *(top corner left),* 0.2 *(top corner right),* 0.3 *(bottom corner left) et* 0.5 *(bottom corner right),* $T_{max} = 1N$*, target* L_2*.*

Theorem 2.4.1. *[1, 7] For a normal regular extremal in the neighborhood of which the maximized Hamiltonian is smooth, the absence of conjugate time on* $(0, t_f]$ *is sufficient for* $\mathscr{C}^0$*-local optimality.*

The method to compute conjugate times is the following [5, 6].
In the minimum time problem the final time is free. In this case the Pontryagin maximum principle yields the additional condition $H = 0$ along the extremal. One has to take into account this condition when computing the Jacobi fields. We thus introduce the

$$W = \{p_0 \in T^*_{x_0} \,|\, H(x, p) = 0\}.$$

It is a submanifold of M of codimension one provided by:

$$\frac{\partial H}{\partial p}(x_0, p_0) = F(x_0, u(x_0, p_0)) \neq 0.$$

Consequently the domain of $\exp_{x_0}$ is a subset of W locally diffeomorphic to

Table 2.2: Minimum time transfer for different μ values, target L_2, $T_{\max} = 1$N.

μ	$t_{f_{min}}$	$t_{f_{min}}$(days)
0.012153	8.440099825863490	36.64
0.1	7.856528339755506	34.11
0.2	7.276968009437341	31.59
0.3	6.881785501415163	29.87
0.4	6.718500411887269	29.16
0.42	6.713953041575635	29.15
0.45	6.728716837504543	29.21
0.47	6.754134857622678	29.32
0.5	6.823072313018849	29.62

$\mathbf{R}^{n-1}$. Consider the $(n-1)$ dimensional vector space of Jacobi fields

$$J_i(t) = (\delta x_i(t), \delta p_i(t)),\ i = 1, \ldots, n-1,$$

vertical at 0 satisfying $\delta p_i(0) \in T_{x(0)}W$, that is satisfying

$$F(x_0, u(x_0, p_0)).\delta p_i(0) = 0.$$

Subsequently, one must compute then these Jacobi fields. Note that the derivative of the exponential mapping with respect to t is equal to the dynamics F of the system. The time t_c is conjugate time whenever

$$\det(\delta x_1(t_c), \ldots, \delta x_{n-1}(t_c), F(x(t_c), u(x(t_c), p(t_c)))) = 0$$

Indeed by assumption ${}^t p.F(x,u)$ is not equal to zero along the extremal and thus $\dot{x}(t)$ is transverse to $(\delta x_1(t), \ldots, \delta x_{n-1}(t))$. An extremal is locally optimal if the first conjugate time t_{c1} satisfies $t_{c1} > t_f$.

We test optimal locality of the computed extremals in the CRTBP frame. Consider first the extremals computed for $\mu = \mu_{Earth-Moon}$ and for different maximal thrust values *i.e.* the continuation on $T_{\max}$. Second order conditions tests are resumed in table 2.3. For all thrusts we have $t_{1c} > t_{f_{\min}}$ then the correspondent extremal are locally optimal. One notices that the ratio $t_{1c}/t_{f_{\min}}$ decreases when $T_{\max}$ tends towards 0.

We consider the extremals corresponding to the continuation on the parameter μ for the thrust $T_{\max} = 1$N. We resume the second order condition tests on table 2.4. For all considered μ values, we have $t_{1c} > t_{f_{\min}}$ thus the correspondent extremals are locally optimal. One also remarks that the ratio $t_{1c}/t_{f_{\min}}$ is almost constant with respect to μ.

2.4.2 Numerical computation

A general question could be asked: Given an initial state x_0, determine the location of the points on the phase space where an extremal beginning at x_0 loses its local optimality. In others words, this corresponds to determining all the conjugate points in the phase space relative to the initial condition x_0. The set of all conjugate points is called conjugate locus. Let us first recall that in our case

Table 2.3: First conjugate time t_{1c} for different thrusts values, $\mu = \mu_{Earth-Moon}$, target L_2.

T_{max}	$t_{f_{min}}$	t_{1c}	$t_{1c}/t_{f_{min}}$
10	1.470566633802046	2.275078393243948	1.547076032428326
1	8.440118858213319	10.640001984456987	1.260645988901317
0.91	9.771072365657723	12.045026891057153	1.232723128056207
0.83	11.152247725959276	13.500018429122381	1.210519956232514
0.74	13.157672247027882	15.595000128504694	1.185240051258106
0.65	14.369930436233620	16.900006380267907	1.176067375918169
0.53	18.024798634539373	20.700025000258922	1.148419209554621
0.44	21.323275412549972	24.125635629178436	1.131422596313656
0.3	32.216276854781320	35.295058947217477	1.095566042789927
0.1789	51.504129714977552	54.930014374272687	1.066516698335723

Table 2.4: First conjugate time t_{1c} for different μ values, $T_{\max} = 1$N, target L_2.

μ	$t_{f_{min}}$	t_{1c}	$t_{1c}/t_{f_{min}}$
0.012153	8.440099825863490	10.635048155422323	1.260061892020842
0.1	7.856528339755506	9.849000000000000	1.253607137157797
0.2	7.276968009437341	9.216352750603498	1.266509999583757
0.3	6.881785501415163	9.072009144753101	1.318263863773078
0.4	6.718500411887269	8.784035369066334	1.307439879519014
0.42	6.713953041575635	8.760003934459252	1.304746083300494
0.45	6.728716837504543	8.736045008301531	1.298322580556301
0.47	6.754134857622678	8.744025382294039	1.294618121583045
0.5	6.823072313018849	8.784011520305938	1.287398274168294

for the CRTBP transfer problems, we are not able to calculate analytically the conjugate locus. Hence, one resorts to numerical computation to figure out the disposition of the conjugate locus in the phase space. Therefore this paragraph includes the results of numerical simulations undertaken in order to clarify as much as possible the conjugate locus set. The method to compute the conjugate locus is the following: For an initial costate p_0, integrate the Hamiltonian flow and the Jacobi equation and perform the second order conditions rank tests to locate the conjugate points relative to this extremal, then repeat the same process for different p_0 values. The task is then to demonstrate the location of the conjugate points when the initial costate vector p_0 vary. p_0 may be written as follows.

$$p_0 = [|p_q| \cos\alpha \quad |p_q| \sin\alpha \quad |p_{\dot{q}}| \cos\beta \quad |p_{\dot{q}}| \sin\beta]$$

The vector p_0 is set by four parameters i.e. $|p_q|$, $|p_{\dot{q}}|$, α, and β thus p_0 describes a space of dimension 4. The minimum time condition induces $H = 0$ where H is the Hamiltonian of the system. Thus p_0 varies on a submanifold of dimension 3. Indeed, using the equation $H(t = 0) = 0$, we can write $|p_q|$ as function of the three other parameters $|p_{\dot{q}}|$, α, and β.

To view the globality of the conjugate locus we must vary both α and β

in all the interval $[0, 2\pi]$ and $|p_{\dot{q}}|$ in all $\mathbf{R}$ all of the three parameters at the same time. This is very difficult if not impossible. To make it easier we first vary only one parameter and observe the variations of the extremals and the conjugate points. Moreover the conjugate points are in a space of dimension 4, *i.e.* the phase space (position and velocity), this makes it difficult to portray the conjugate locus on a graph, thus in the following graphs in this section, we plot the conjugate points on both the position space and the velocity space. The optimal control solution of the PMP principle is $u = (p_3, p_4)/\sqrt{p_3^2 + p_4^2}$ where $p = (p_1, p_2, p_3, p_4)$ is the costate vector. Thus, the initial control is given by $u(t = 0) = (\cos\beta, \sin\beta)$. This approach leads us to vary first of all the parameter β.

We consider the initial costate $\bar{p}_0$ solution of the transfer problem from X_0 towards the libration point L_2.

$$\bar{p}_0 = [|\bar{p}_q|\cos\bar{\alpha} \quad |\bar{p}_q|\sin\bar{\alpha} \quad |\bar{p}_{\dot{q}}|\cos\bar{\beta} \quad |\bar{p}_{\dot{q}}|\sin\bar{\beta}]$$

Firstly we vary β in all the interval $[0, 2\pi]$, in fact we compute 100 extremals for different values of β in $[0, 2\pi]$. Unfortunately the computed extremals and the corresponding conjugate points do not provide us with a clear idea of the conjugate locus and the variation of the extremals and the conjugate points seems to be chaotic (no regularity). Thus, we will investigate the conjugate locus in the neighborhood of a certain value of β, the value $\bar{\beta}$ could be a convenient one.

We vary the parameter β in the neighborhood of $\bar{\beta} \simeq 0.84$ *rad i.e.* in the interval $[\bar{\beta} - \Delta\beta, \bar{\beta} + \Delta\beta]$. (We compute 101 extremals in which 50 correspond to $\beta < \bar{\beta}$, 50 are such that $\beta > \bar{\beta}$ and one corresponds to $\beta = \bar{\beta}$). We test different values of $\Delta\beta$ *cf.* figure 2.7 for instance. The blue curves are the extremals, the red points are the conjugate points and the green ones are the same cost attainable points (in our case the cost corresponds to the final time). We show the extremals in the position plan and the velocity plan, the red axes define the initial state and the black dotted axes define the final state. In the position plan, the red cross is the Earth's position and the black one is the Moon's position, in the velocity plane, the red axes define the initial velocity and the dotted axes define the final velocity (velocity at the point L_2). We note N the number of computed points for each extremal. We intend then to vary the second parameter α and study how this parameter will affect the configuration of the conjugate points previously computed. We consider the variation of β in the neighborhood of $\bar{\beta}$ then we vary α in the neighborhood of $\bar{\alpha} \simeq 0.55$ *rad*, in fact, for each value of β (101 values) we compute 21 extremals in which 10 are such that $\alpha < \bar{\alpha}$, 10 are such that $\alpha > \bar{\alpha}$ and one corresponds to $\alpha = \bar{\alpha}$, *cf.* figure 2.8. The figure contains only the conjugate points (no extremals are plotted). The last step is to vary $|p_{\dot{q}}|$. We intend to show the variation of the conjugate locus when the three parameters of the costate initial vary at the same time. When $|p_{\dot{q}}|$ decreases slightly over $|\bar{p}_{\dot{q}}|$ we obtain some numerical bugs in the integration of the extremals therefore this case is not considered. Thus we consider the variation of the conjugate locus when the value of $|p_{\dot{q}}|$ increases slightly in the neighborhood of $|\bar{p}_{\dot{q}}| \simeq 0.1$ (the variation is $\delta|p_{\dot{q}}| = 0.0005$ for every step). The figures are listed in ascending order relative to the value of $|p_{\dot{q}}|$, *cf.* figures 2.9 and 2.10 and 2.11. The conjugate points degenerate when the $|p_{\dot{q}}|$ increases until the disappearance of all conjugate points for $|\bar{p}_{\dot{q}}| + 8\delta|p_{\dot{q}}|$. In this paragraph is

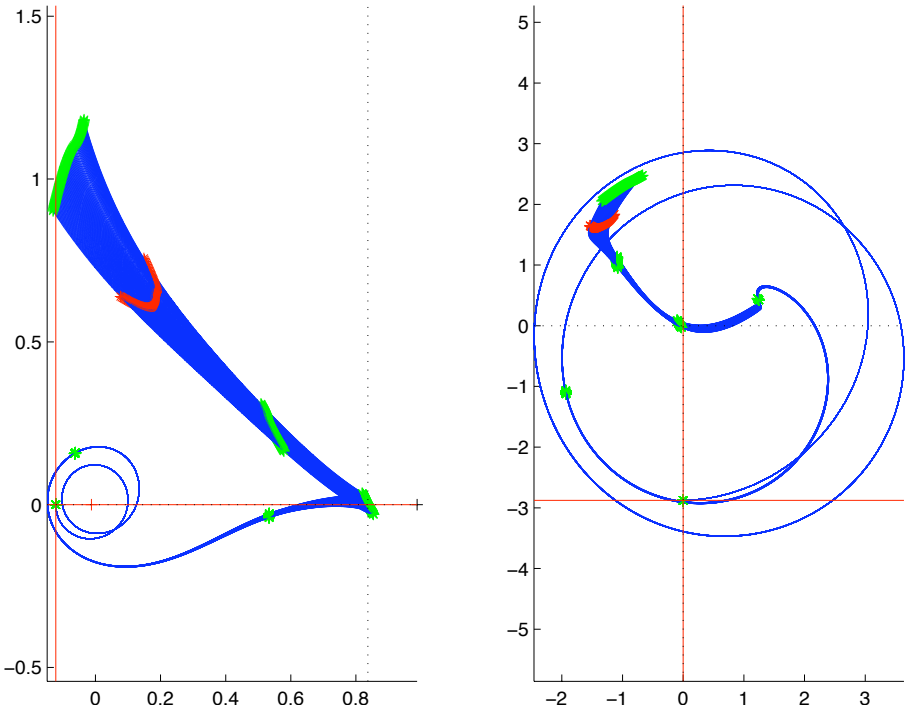

Figure 2.7: *Extremals and conjugate points. On the left is the position plane and on the right is the velocity plane, variation of* $\Delta\beta = 0.001$ *around the angle* $\beta = \bar{\beta}$*, number of computed points for each extremal is* $N = 10000$*,* $T_{\max} = 10\text{N}$

presented an overview of the conjugate locus in the phase space and its variation when the initial costate varies. The given results are fruits of a long and hard numerical computing. We think that a larger time span of numerical simulations is required in order to visualize more of the conjugate locus. Unfortunately, we have not had enough time during the PhD to investigate this point further.

2.5 Target the lunar orbit LO

In this section we are interested in computing minimum time trajectories from X_0 to $X_f = LO$. LO is described in the phase space by the following equations.

$$(x_1(t_f) - 1 + \mu)^2 + x_2^2(t_f) = r^2$$

$$x_3^2(t_f) + x_4^2(t_f) = v^2$$

$$(x_1(t_f) - 1 + \mu)x_3(t_f) + x_2(t_f)x_4(t_f) = 0$$

Where $r = 13.084\text{Mm} = 0.034$ is the circle radius and $v = \sqrt{\frac{\mu}{r}}$ is the velocity of the spacecraft on this circle. Since the final target is a manifold of $\mathbf{R}^4$, transversality condition (2.6) suggests another equation combining the final state and costate:

$$x_1(t_f)p_2(t_f) - x_2(t_f)p_1(t_f) + x_3(t_f)p_4(t_f) - x_4(t_f)p_3(t_f) = 0.$$

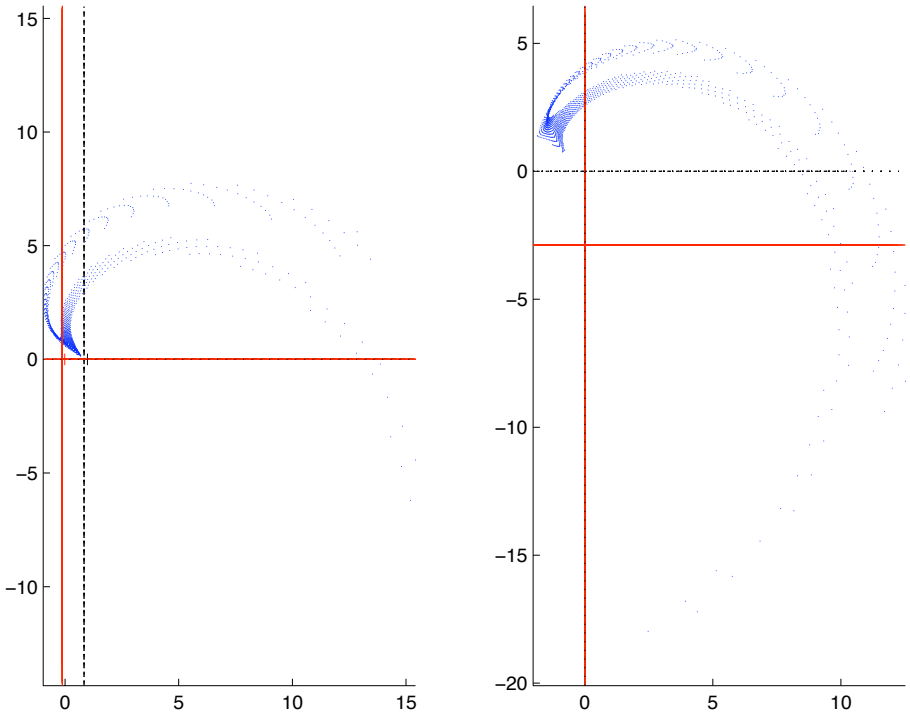

Figure 2.8: *Conjugate points. On the left is the position plane and on the right is the velocity plane,* $\beta = \bar{\beta}$, $\alpha = \bar{\alpha}$, $\Delta\beta = 0.005$, $\Delta\alpha = 0.005$, *number of computed points for each used extremal is* $N = 1000$, $T_{\max} = 10\text{N}$

The corresponding shooting function is as follows:

$$S_t^{LO} \ : \ z = (t_f, p(0)) \ \mapsto \ \left(\begin{array}{l} x_1^2(t_f) + x_2^2(t_f) - r^2 \\ x_3^2(t_f) + x_4^2(t_f) - v^2 \\ x_1(t_f)x_3(t_f) + x_2(t_f)x_4(t_f) \\ x_1(t_f)p_2(t_f) - x_2(t_f)p_1(t_f) + x_3(t_f)p_4(t_f) - x_4(t_f)p_3(t_f) \\ H(t_f) \end{array} \right).$$

Our goal is to find a suitable initialization to solve $S_t^{LO}(z) = 0$. A spontaneous idea is to use the initialization solution of $S_t^{L_2}([t_{f_{L_2}}\, p_{L_2}(0)]) = 0$. Let us consider it. We keep the same initial costate $p_{L_2}(0)$. We vary the final time t_f at the vicinity of $t_{f_{L_2}}$ until the shooting algorithm converges. This method is successful for maximal thrusts $T_{max} = 10\text{N}$ and 1N.

Once the spacecraft is on the target orbit LO, we may study the stability of the orbit LO by computing the free trajectory ($T_{\max} = 0$) after the end of the transfer. The spacecraft free motion draws a circular tube around the Moon (not a fine circle). This is due to the Earth's influence on the spacecraft. To emphasize this fact we draw upon an homotopy on the radius r of the orbit LO from its current value *i.e.* $r = 0.034$ to lower values *i.e.* the spacecraft will be closer to the Moon. We obtain extremals by discrete continuation for $r = 0.02$, 0.015 and 0.01, the maximal thrust is fixed at $T_{\max} = 10\text{N}$. Figure 2.12 shows the extremals trajectories (in blue) and the free trajectories after the end of the transfer (in green).

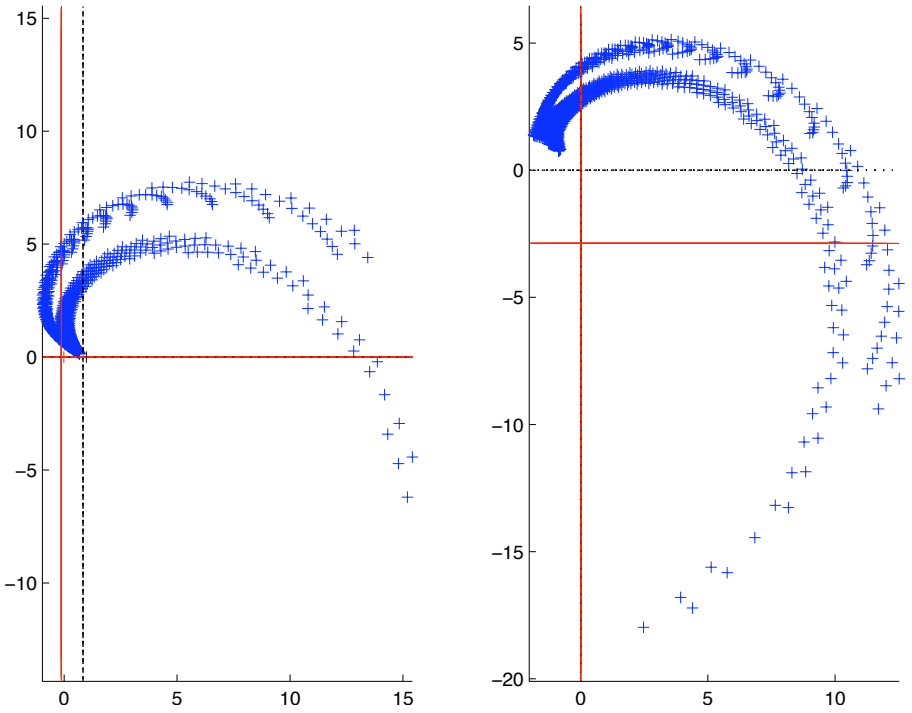

Figure 2.9: *Conjugate points. On the left is the position plane and on the right is the velocity plane,* $\beta = \bar{\beta}$, $\alpha = \bar{\alpha}$, $\Delta\beta = 0.005$, $\Delta\alpha = 0.005$, $|p_{\dot{q}}| = |\bar{p}_{\dot{q}}|$, *number of computed points for each extremal used is* $N = 1000$, $T_{\max} = 10$N.

Note that the circular tube, described by the satellite after the end of the transfer, is narrowed as the radius r decreases. This is consistent with the fact that when the spacecraft is closer to the Moon, the Earth's influence decreases.

Henceforth on the LO radius r is fixed at its initial value *i.e.* $r = 0.034$. Our goal is to reach low thrusts ($T_{\max} = 0.3$N corresponding to the SMART-1 mission). Unfortunately the technique used to compute initialization for $T_{\max} =$ 10N and 1N did not succeed for lower thrusts. Thus, we consider once again a discrete continuation on the maximal thrust $T_{\max}$ starting from 1N thereby, trying to reach the lowest possible thrust. This homotopy is delicate. It is more complicated than that for the target L_2. We reach a thrust of 0.8N using very small homotopic steps *i.e.* 10^{-7}N, unfortunately the homotopy does not make progress. Note that in figure 2.13 we obtain extremals of different shapes. The spacecraft executes an additional revolution around the first primary *i.e.* the Earth when the thrust decreases from 1N to 0.9N. Between these two thrusts, there are intermediate steps: The spacecraft does not manage to perform the whole revolution. The corresponding extremals have minimal final times $t_{f\min}$ practically twice the $t_{f\min}$ corresponding to the extremals for $T_{\max} = 1$ and 0.9N as shown in table 2.5. The same process happens between 0.9 et 0.84N. This may justify that small homotopic steps are required.

Let us now focus on the local optimality of the computed solutions. This time the target is not just a point but a submanifold of $\mathbf{R}^8$: The orbit around the Moon LO. The notion of conjugate points is non sufficient. We, there-

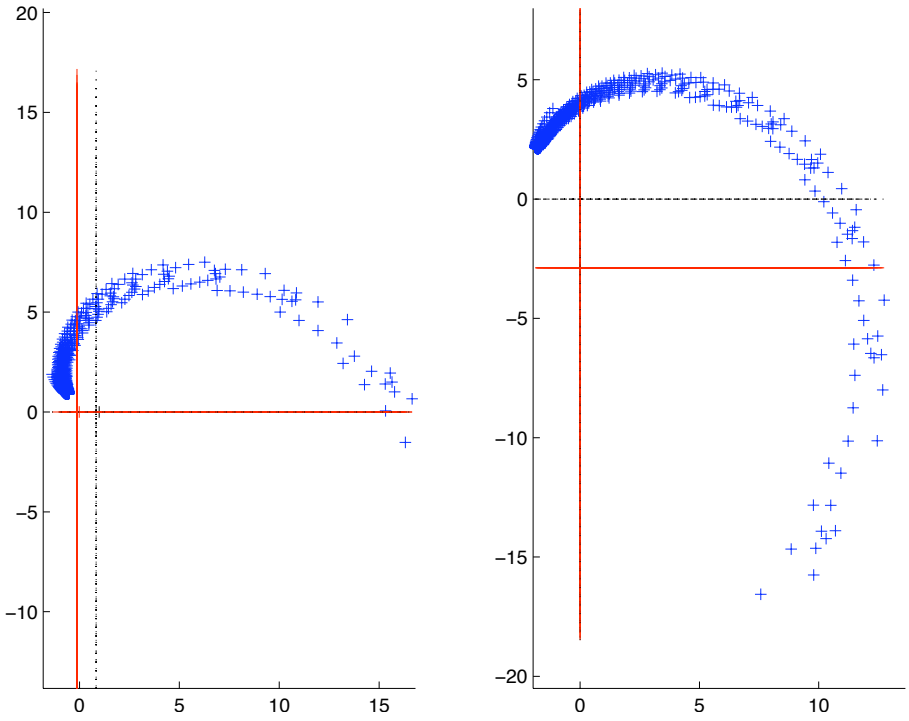

Figure 2.10: *Conjugate points. On the left is the position plane and on the right is the velocity plane,* $\beta = \bar{\beta}$, $\alpha = \bar{\alpha}$, $\Delta\beta = 0.005$, $\Delta\alpha = 0.005$, $|p_{\dot{q}}| = |\bar{p}_{\dot{q}}|+4\delta|p_{\dot{q}}|$, *number of computed points for each extremal used is* $N = 1000$, $T_{\max} = 10$N.

fore, introduce a more generalized notion: The focal points. Let $z = (x, p)$ be a reference extremal. It is a smooth solution of $\dot{z} = \overrightarrow{H}(z)$ where $\overrightarrow{H}(z) = (\frac{\partial H}{\partial p}(x,p), -\frac{\partial H}{\partial x}(x,p))$, defined on $[0, t_f]$, satisfying the transversality condition $z(t_f) \in {X_f}^{\perp}$, here X_f does not only denote the final condition on the state but it denotes the final conditions both on the state and the costate (deriving from the transversality conditions) thus here X_f is a submanifold of $\mathbf{R}^8$. As in the Riemannian case [19], focal points are related to local optimality of trajectories [8].

Proposition 2.5.1. *[1, 5, 6] A regular reference trajectory z is locally optimal up to first focal time.*

The method to compute focal times is the following [5, 6].
In the minimum time case the final time is free. The computation is the same as for conjugate points but we integrate backwards in time. Consider the vector space of dimension $n-1$ generated by the Jacobi fields $J_i = (\delta x_i, \delta p_i)$, $i = 1, \ldots, n-1$, such that $J(0) \in T_{z(t_{\text{focal}})} {X_f}^{\perp}$ are normalized by the condition:

$$\langle p(t_{\text{focal}}), \delta p_i(0) \rangle$$

The time t_{focal} is a focal time whenever

$$\text{rank}(\delta x_1(-t_{\text{focal}}), \delta x_2(-t_{\text{focal}}), \delta x_3(-t_{\text{focal}})) < n-1.$$

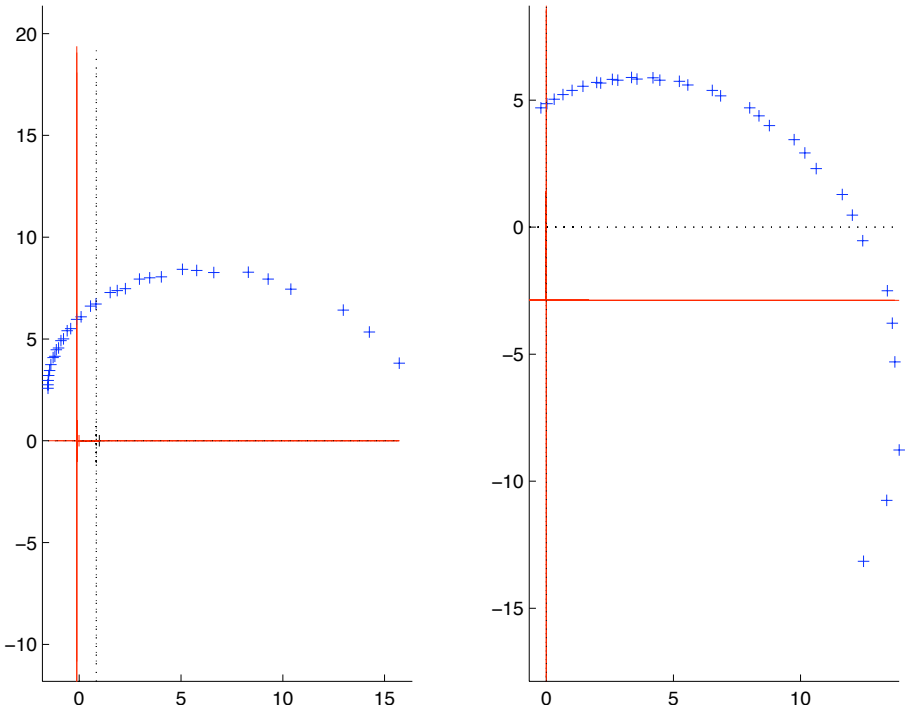

Figure 2.11: *Conjugate points. On the left is the position plane and on the right is the velocity plane,* $\beta = \bar{\beta}$, $\alpha = \bar{\alpha}$, $\Delta\beta = 0.005$, $\Delta\alpha = 0.005$, $|p_{\dot{q}}| = |\bar{p}_{\dot{q}}| + 7\delta|p_{\dot{q}}|$, *number of computed points for each extremal used is* $N = 1000$, $T_{\max} = 10\text{N}$.

As in conjugate time the rank tests may be written using the dynamics $\dot{x}$ as follows.

$$\det(\delta x_1(-t_{\text{focal}}), \ldots, \delta x_{n-1}(-t_{\text{focal}}), F(x(-t_{\text{focal}}), u(x(-t_{\text{focal}}), p(-t_{\text{focal}})))) = 0$$

An extremal is locally optimal if the first focal time t_{focal_1} satisfies $t_{\text{focal}_1} < 0$. The numerical rank tests resumed in table 2.5 show that the computed extremals for different maximal thrust value are locally optimal.

As shown the discrete continuation on $T_{\max}$ does not perform well and does not permit us to reach low thrusts. Thus we search for another continuation method.

2.6 Differential path following

The discrete continuation is based on a heuristic choice of problem sequence $(P_{\lambda_k})_{k\in\{1,\ldots,N\}}$ and no convergence is ensured at the end of the homotopy. In fact, there is no theoretical reason for the existence of a convergent sequence $(\lambda_k)_{k\in\{1,\ldots,N\}}$, hence one can only hope that the chosen sequence is a "good" one, in addition, the zeros path is roughly known: We have only some points on the zeros path. Thus a more sophisticated method is used: The differential homotopy. This method is based on following the zeros path precisely using

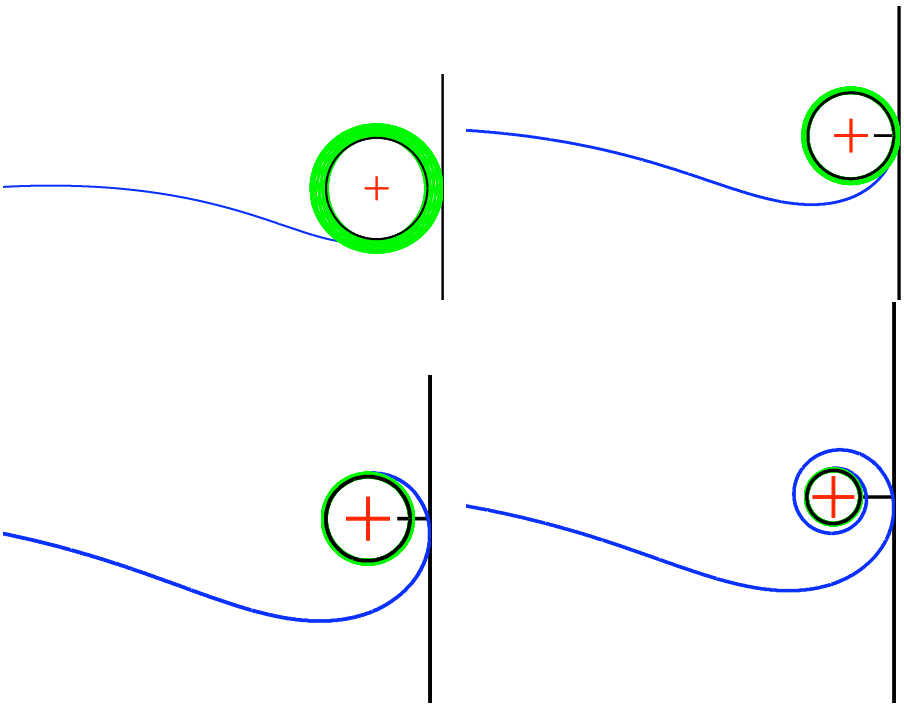

Figure 2.12: *Optimal trajectories (in blue) to LO and free trajectories (in green) after the end of the transfer, zoom on the Moon, for different radius r values:* 0.034*,* 0.02*,* 0.015 *and* 0.01*,* $T_{max} = 10N$*. The final orbit is more stable when the spacecraft is closer to the Moon.*

numerical integration, hence the sequence $(\lambda_k)_{k\in\{1,\dots,N\}}$ is automatically computed and tuned. A comparison between discrete and differential homotopy is drawn up in figure 2.14.

Definition 2.6.1. Let Ω be an open bounded set of $\mathbf{R}^n$. An homotopy is a continuous application h:

$$\begin{aligned} h\ :&\bar{\Omega}\times[0,1]\ \rightarrow\ \mathbf{R}^n \\ &(z,\lambda)\ \mapsto\ h(z,\lambda) \end{aligned}$$

Remark 2.6.1. In our case, we simply use $h(z,\lambda) = S_\lambda(z)$.

As shown in figure 2.14, the differential homotopy principle is simple: The initial guess for the next step z_{k+1} is computed using the tangent to the curve $h(z,\lambda) = 0$ at the point (z_k, λ_k). The Predictor-Corrector method is a classic differential continuation method widely used, the principle is the following: After computing the next step guess z_{k+1}, a correction is made to ensure that the considered point is on the zeros path. In our study, we consider another issue. It consists of computing precisely the zeros path using numerical integration, more details are displayed later. Let us now define the theoretical framework relative to the differential homotopy. First, we focus on the existence of the zeros path.

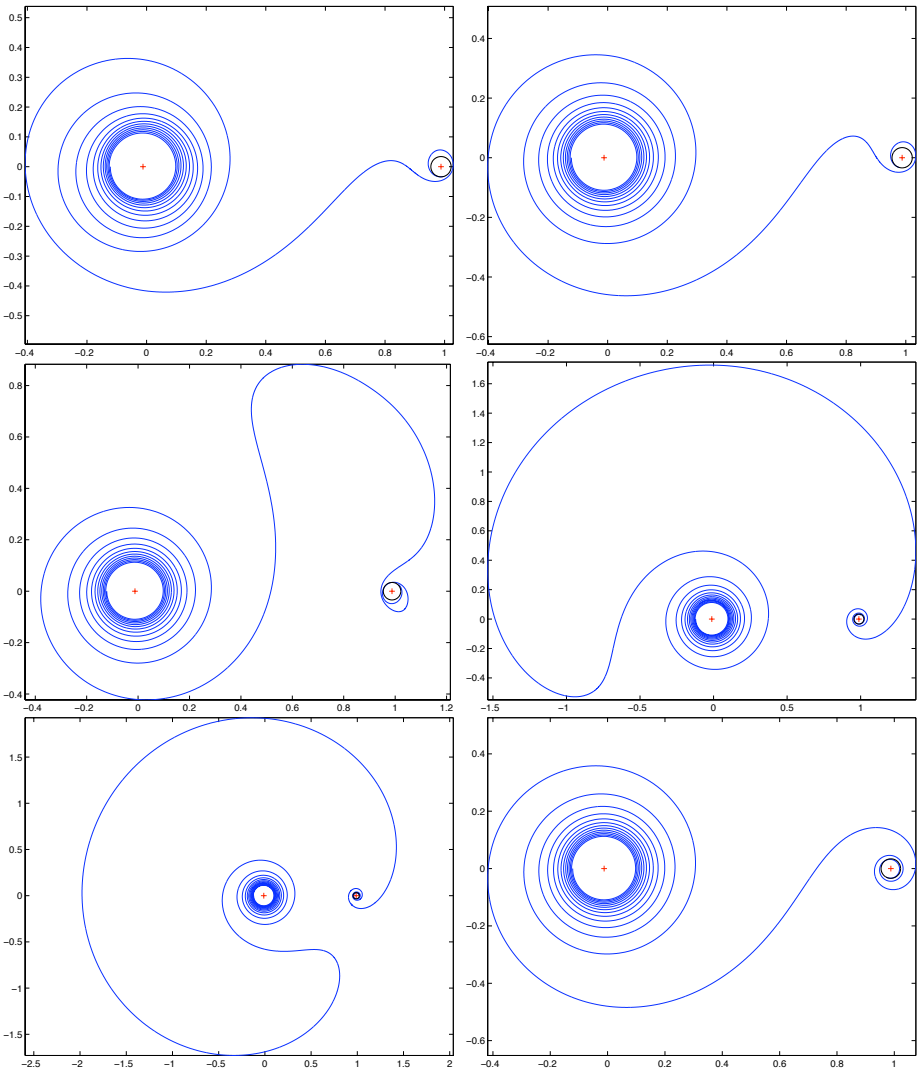

Figure 2.13: *Minimum time trajectories to LO for different maximal thrust values* $T_{\max} = 1,\ 0.97,\ 0.96,\ 0.93,\ 0.91$ *and* 0.9N.

Theorem 2.6.1. *[20] Let* Ω *be an open bounded set of* $\mathbf{R}^n$ *and* $h = \bar{\Omega} \times [0,1] \to \mathbf{R}^n$ *a continuously differentiable homotopy such that:*

$$(H1)\ \forall (x,\lambda) \in h^{-1}(0),\ rang(h'(x,\lambda)) = n$$
$$(H2)\ \forall (x,0) \in h^{-1}(0),\ rang(\frac{\partial h}{\partial x}(x,0)) = n$$
$$\forall (x,1) \in h^{-1}(0),\ rang(\frac{\partial h}{\partial x}(x,1)) = n$$

Then $h^{-1}(0)$ *consists of:*

(i) *finite number of closed curves (with finite length in* $\bar{\Omega} \times [0,1]$*);*

Table 2.5: minimum final time and first focal time for different thrust, target *LO*

T_{max}(N)	$t_{f\,min}$	$t_{f\,min}$(days)	t_{focal1}
10	1.5156935549669	6.580	no focal points
1	9.1466354940112	39.71	-19.22
0.97	9.4741602733410	41.13	-27.50
0.96	13.100227991760	56.88	-21.21
0.95	14.383235352751	62.45	-21.90
0.94	15.520169634928	67.38	-27.23
0.93	16.624801498058	72.18	-22.16
0.92	17.803899709383	77.30	-27.01
0.91	18.914781658733	82.12	-27.30
0.9	10.798706053581	46.89	-38.07
0.89	13.639710938615	59.22	-21.56
0.88	15.416426217668	66.93	-27.08
0.87	16.724698757257	72.61	-27.05
0.86	18.061441083624	78.42	-32.02
0.85	19.465091553847	84.51	-27.08
0.83	14.227707740650	61.77	-26.62
0.82	16.372790232075	71.09	-27.17
0.81	17.873436170790	77.60	-27.16
0.8	19.491254557340	84.63	-27.16

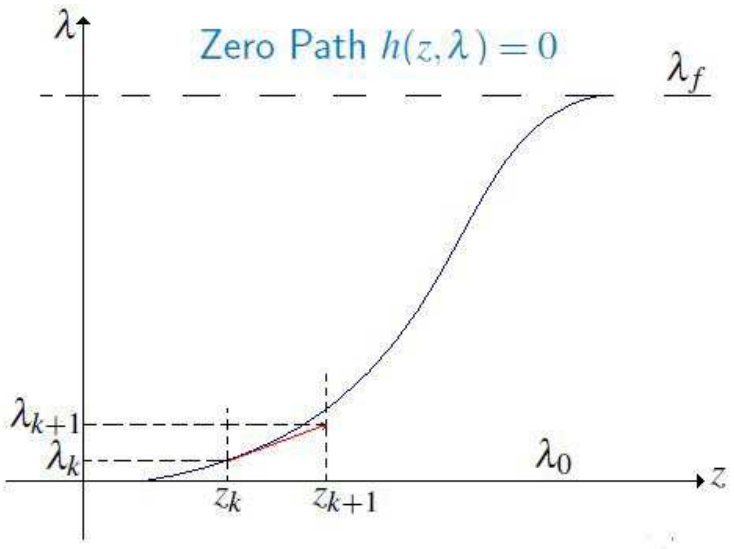

Figure 2.14: Discrete and differential homotopy. The initial guess given by the differential method z_{k+1} is clearly pretty much closer to the zeros path than the solution for the previous step *i.e.* discrete method z_k.

(*ii*) *finite number of finite length arcs with endpoints in* $\partial\Omega \times [0,1]$.

(*i*) *and* (*ii*) *are disjoint and continuously differentiable.*

The connected component of the zeros set beginning at (z_0, λ_0) is a differentiable curve that we can parametrize by arc length, s. In the curvilinear coordinates, $c(s) = (z(s), \lambda(s))$ is the solution of the following differential equation:

$$\begin{cases} \dot{c}(s) = \overrightarrow{T}(c(s)), \\ c(0) = (z_0, \lambda_0). \end{cases}$$

Where $\overrightarrow{T}(c)$ is the unit tangent vector defined, up to orientation, by $\overrightarrow{T}(c) \in Ker h'(c)$ (c is not critical so the kernel is one dimensional). In contrast with the established Predictor-Corrector method, we follow the path of zeros by merely integrating the differential equation using a high order numerical scheme without making any correction step. At step $(k+1)$, the $\overrightarrow{T}(c_{k+1})$ orientation is heuristically chosen such that $\overrightarrow{T}(c_k).\overrightarrow{T}(c_{k+1})$ is non negative.

For numerical computation, we use the `hampath`[10] compiler. In fact, a shooting algorithm is used to compute zeros of the shooting function for λ_0 and λ_f, and a zeros path following algorithm realizing the differential homotopy, as described before, is used.

Let us first consider the homotopy on the parameter μ for the target L_2. We aim to retrieve the results found by the discrete homotopy. Hence we compute the zeros path from $\mu(s=0) = \mu_{Earth-Moon}$ to $\mu(s_f) = 0.5$. The computed path with respect to the final time t_f variable ($z = (t_f, p_0)$) is portrayed in Fig. 2.15. We retrieve the same extremals computed by the discrete continuation method. At a point $c(s) = (t_f(s), p_0(s), \lambda(s))$, second order sufficient conditions

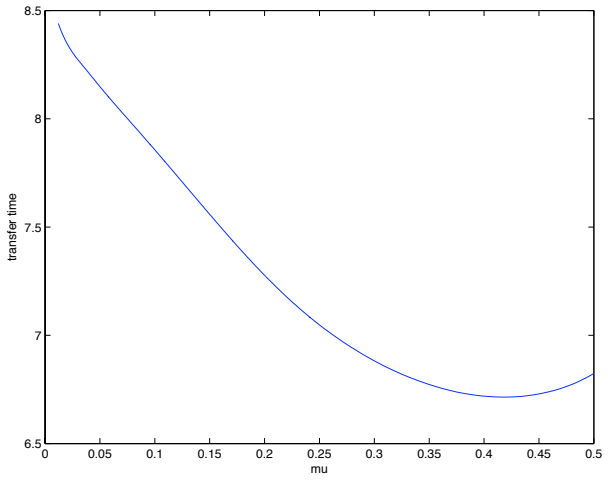

Figure 2.15: Homotopy on μ, $T_{\max} = 1$N, minimum time transfer towards L_2 Lagrange point. The value function $\mu \mapsto t_f(\mu)$ is portrayed.

are checked using a simple numerical rank evaluation. Indeed, at time $t \in (0, t_f(s)]$, Jacobi fields span the image of the differential with respect to (t, p_0) of

$$(t, p_0, \lambda) \mapsto x(t, x_0, p_0, \lambda).$$

Hence verifying that this mapping has a full rank derivative at all $(t, p_0(s))$ for $t \in (0, t_f(s)]$ ensures that we have a $\mathscr{C}^0$-local minimizer at $t_f(s)$. This eventually implies that $\partial S/\partial z(c(s))$ has full rank, so the path can be parameterized locally not only by s but also by λ (no *turning point*).

The aim of introducing the differential path following is to manage to reach low thrusts when computing transfers towards *LO* since the discrete continuation does not cover maximal thrust ranges lower than 0.8N, there we rely on the differential continuation method to enable us to reach a maximal thrust of 0.3N. Unfortunately, this is not as easy as we expected. In fact, we are faced with several issues. Paths may have turning points associated with rank drops in the partial derivative of the shooting function that prevent the verification of second order sufficient conditions. See for instance Fig. 2.16 and 2.17. Moreover, to ensure global optimality, for a given $T_{\max}$ one has to compare costs on the different connected components of the set of zeros, and it emerges that one has to jump from one component to another. While a given branch is followed using differential homotopy, switching branches is obtained by discrete homotopy. Combining both approaches allows us to obtain extremals whose local optimality is checked by second order conditions and whose global optimality is tested by comparing various branches [12].

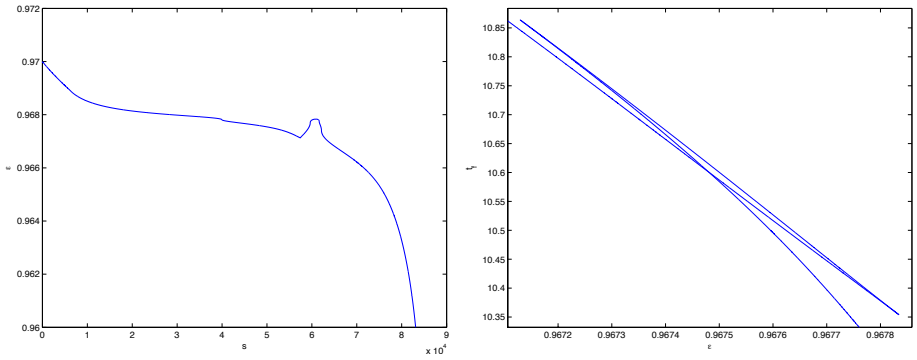

Figure 2.16: Homotopy on $T_{\max}$, Earth-Moon case ($\mu \simeq 1.21e-2$), minimum time transfer towards a circular orbit around the second primary. On both subgraphs. On the left, the ordinate is the homotopic parameter *i.e.* $T_{\max}$, the abscissa is the curvilinear abscissa on the path and two turning points are observed (see also Fig. 2.17). The corresponding cusp points on $T_{\max} \to t_f(T_{\max})$ are observed on the right. Optimality is necessarily lost past the self-intersection point near $T_{\max} \simeq 9.675e-1$ (see also Fig. 2.21).

Homotopy on $T_{\max}$ in the previous section suggests that different connected components of the path are associated solutions of different homological nature: Either winding around the second primary changes from positive to negative, or the sign remains constant but the winding number changes. A coarse classification can be made by using homology of (closed) curves in X^1_μ. (The classification is coarse as it takes into account neither the velocity coordinate, nor the adjoint p).

First restricting to extremals with boundary conditions on $x_2 = 0$ (the line defined by the two punctures in X^1_μ), one can associate to any such extremal

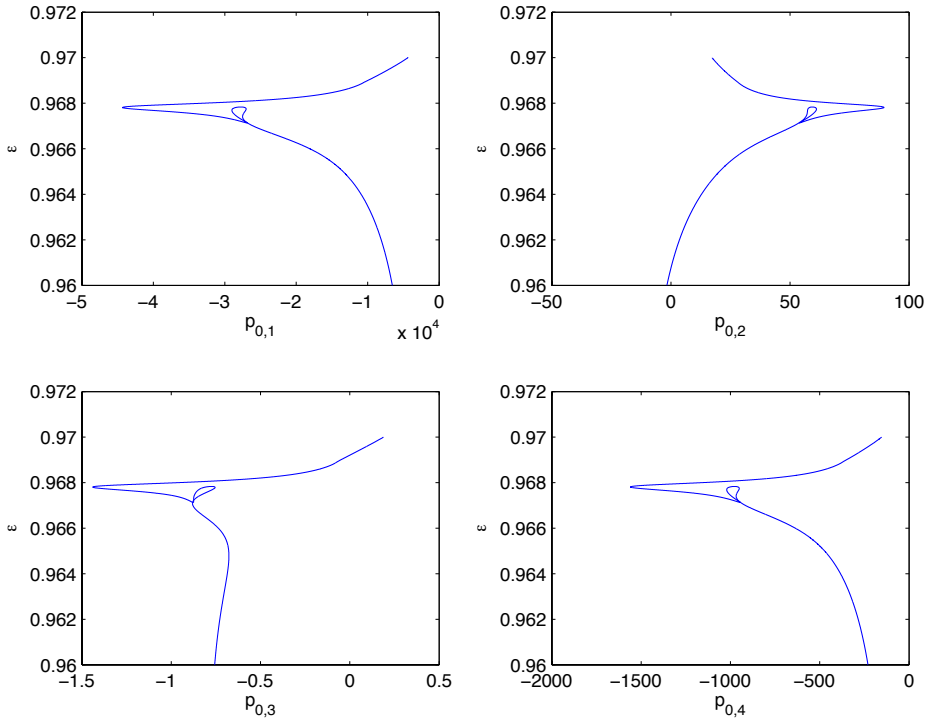

Figure 2.17: Homotopy on $T_{\max}$, Earth-Moon case ($\mu \simeq 1.21e-2$), minimum time transfer towards LO. The four components of the adjoint state p_0 are portrayed. The same two turning points as in Fig. 2.16 are observed.

a closed curve by patching it to the curve symmetric with respect to $x_2 = 0$ (and orientation reversed), see Fig. 2.19. The homology of this curve turns to be sufficient to classify the different types of solutions observed on disjoint components of the homotopy path. For arbitrary boundary conditions, the same symmetric closure has to be performed on the truncation of the position-projection of the extremal from its first intersection with $x_2 = 0$ until the final one.

As a case study, the path between $T_{\max} = 1$N and $T_{\max} = 0.96$N is discussed in Fig. 2.20. The optimality status of each homology class is analyzed in Fig. 2.21. It is a matter of future investigation to integrate homological constraints [16] to remove sub-optimal components from the path.

Let us remind the reader that the goal of using the differential continuation on $T_{\max}$ was first to reach lower thrusts than 0.8N (already reached by the discrete continuation). Actually we are faced by the same issue as in the discrete homotopy, that is, the spacecraft executes an additional revolution around the Earth. This fact makes the differential path following unsuitable. Indeed, following precisely the zeros path by numerical integration leads to following the appearance of an additional revolution around the Earth by the spacecraft. Thus the transfer time increases but when the revolution is accomplished, the transfer time suddenly plummets, the differential continuation is unable to fol-

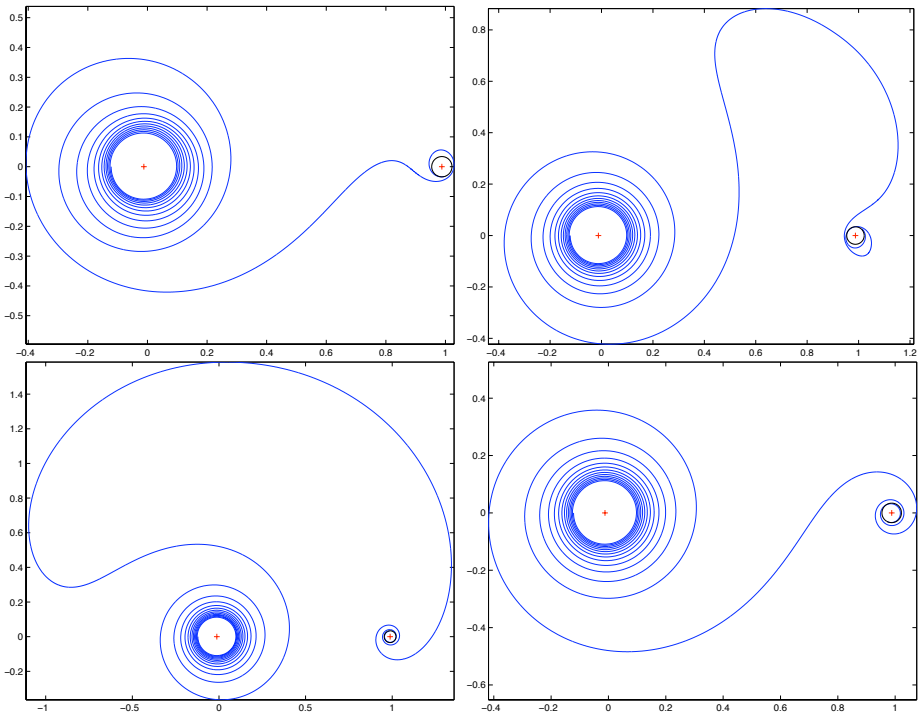

Figure 2.18: Homotopy on $T_{\max}$, Earth-Moon case ($\mu \simeq 1.21e-2$), minimum time transfer towards a circular orbit around the second primary. Top pictures are transfers for $T_{\max} = 1$N (left) and $T_{\max} = 0.96$N (right), respectively. Bottom pictures are transfers for $T_{\max} = 0.94$N (left) and $T_{\max} = 0.9$N (right), respectively. While the two previous trajectories wind up positively around the two primaries, both transfers wind up negatively around the second primary, illustrating a first difference of homological nature. Moreover, the last transfer differs from the three others in having one more revolution around the first primary.

low the minimum final time variation and the minimum time solution is a priori in another branch. However, the discrete continuation allows us to jump from one branch to another as from 0.91N to 0.9N but it is not guaranteed all times as for instance, when performing differential homotopy from $T_{\max} = 0.8$N to lower values. Faced with this fact, we aim to figure out the different zeros paths and compare optimality of different path. We choose to focus our study on the range from 1N to 0.9N since we have different initializations for both of them more than for the thrust 0.8N.

During this chapter optimal solutions of (P_t) are given for different μ values and for different maximal thrust $T_{\max}$ values. The homotopy on the parameter μ is used to connect two and three-body problems then a homotopy on the maximal thrust is built to reach low thrusts. Relevant results are found for transfer towards the libration point L_2. Low thrust extremals are computed thanks to the discrete homotopy on $T_{\max}$. Moreover extremals are also computed for different μ values from $\mu = 0$ to $\mu = 0.5$ using both discrete and differential continuations methods, a comparison between two methods is supplied. The un-

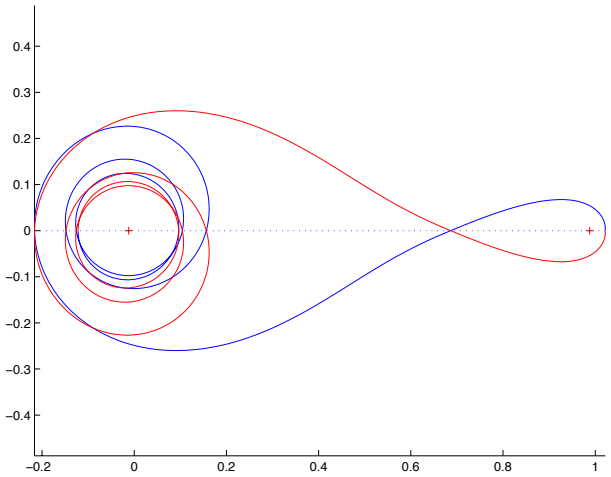

Figure 2.19: Closure by symmetrization. The extremal (blue) is truncated if necessary so that endpoints lie on $x_2 = 0$. Concatenating the symmetric curve (red) with reversed orientation results in a closed curve whose homotopy class and homology are well defined ($(7, -1)$, here).

accomplished task in the resolution of (P_t) is to compute low thrust trajectories towards the target LO. Unfortunately neither the discrete nor the differential homotopic method allows us to perform the homotopy on $T_{\max}$. The discrete method does not effect any progress after reaching $T_{\max} = 0.8$N. The differential method is more complicated than the discrete method. This method is totally unsuitable for the homotopy on $T_{\max}$. Its benefit is to inform us of the existence of many zero paths and, so as to reach low thrusts one has to jump from one zero path branch to another. We think that more time is needed to undertake numerical simulations to solve the low thrust minimum time transfer towards LO, however we have not enough time to deal with it, we have decided to concentrate on solving the minimum fuel consumption problem, which is the main goal of the PhD.

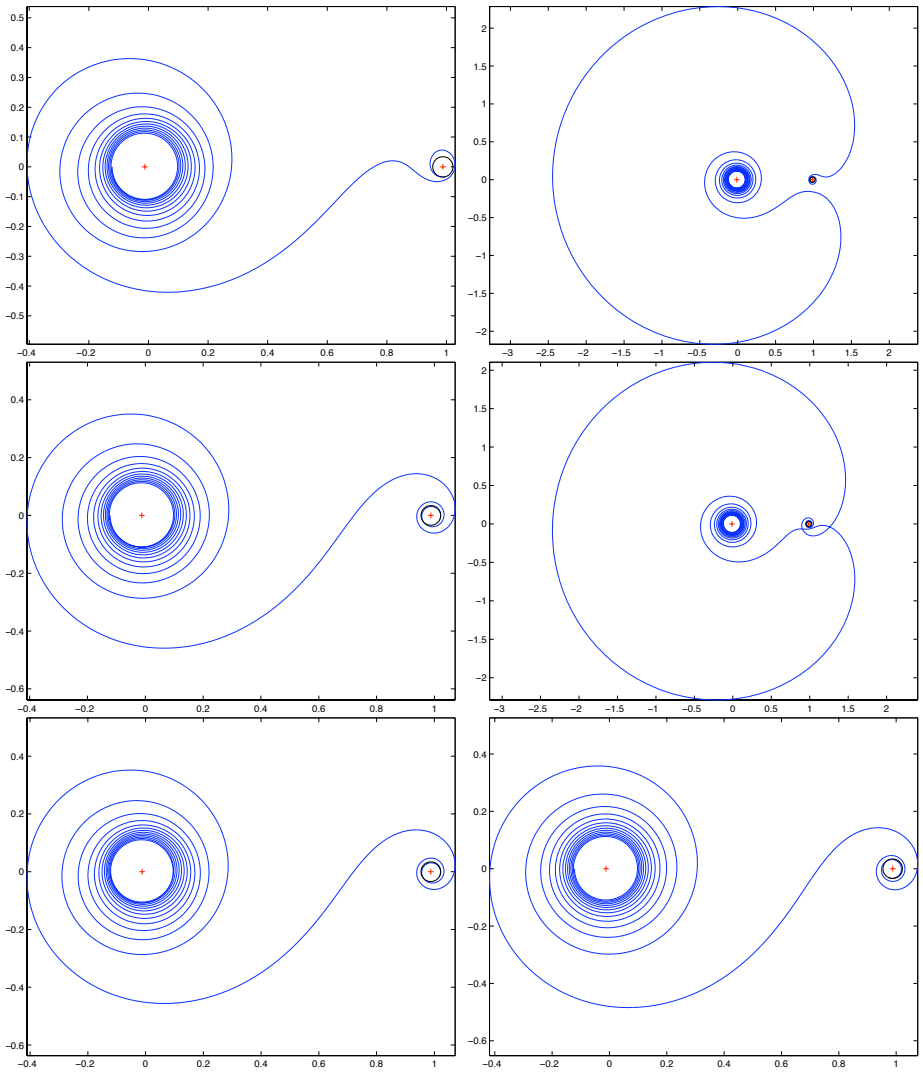

Figure 2.20: Homotopy on $T_{\max}$, Earth-Moon case ($\mu \simeq 1.21e-2$), minimum time transfer towards a circular orbit around the second primary. Top pictures are transfers for $T_{\max} = 1$N (left) and $T_{\max} = 0.904$N (right), respectively. The two extremals belong to the same branch, labeled I (see Fig. 2.16) and have the same homology (positively winding up around both primaries). Middle pictures are transfers for $T_{\max} = 1$N (left) and $T_{\max} = 0.9003$N (right), respectively. Extremals belong to the same branch, labelled II, and have the same homology (now negatively winding up around the second primary). Bottom pictures are transfers for $T_{\max} = 1$N (left) and $T_{\max} = 0.9$N (right), respectively. Extremals belong to the same branch, labeled III, and have the same homology (negatively winding up around the second primary with one more revolution around the first one that those on branches I and II).

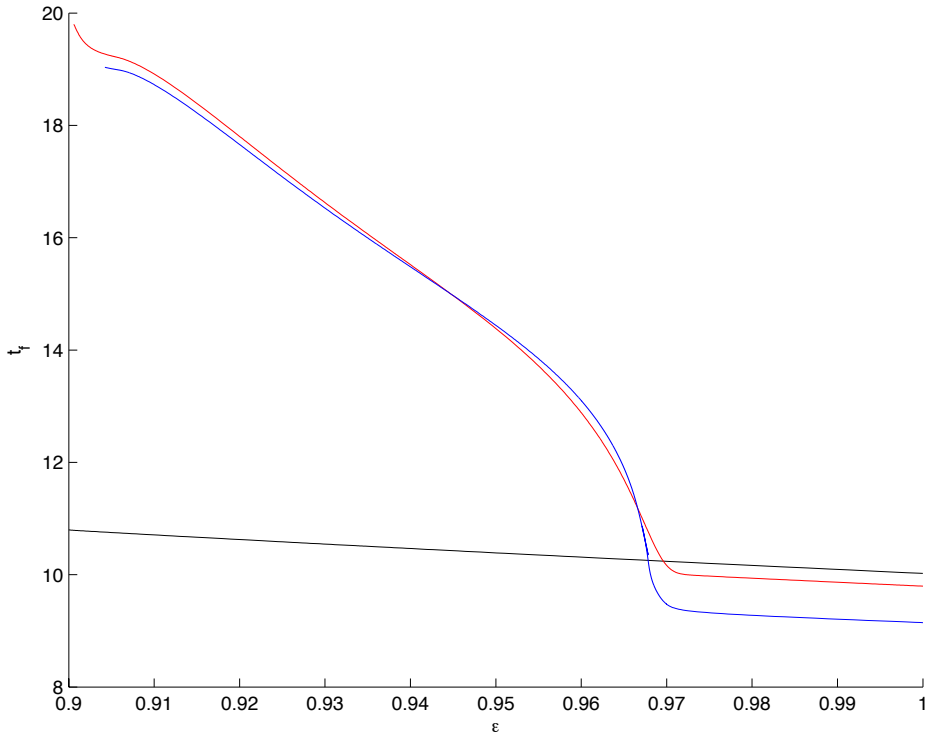

Figure 2.21: Homotopy on $T_{\max}$, Earth-Moon case ($\mu \simeq 1.21e-2$), minimum time transfer towards a circular orbit around the second primary. Each curve represents the function $T_{\max} \mapsto t_f(T_{\max})$ evaluated along the three disjoint branches I (blue), II (red) and III (black) of the homotopy (see Fig. 2.20). Slightly below $T_{\max} \simeq 0.97$N, branch II provides a better criterion than I, but both have already become worse than branch III. The infimum of the three curves provides an upper bound for the value function $T_{\max} \mapsto t_f(T_{\max})$.

Chapter 3

Minimum fuel consumption transfer

3.1 Existence and structure of controls

Once the minimum time transfer is solved, one can start the resolution of the minimum consumption transfer. The transfer time is fixed. It is then normal to begin by computing minimum time trajectories so that we may estimate the minimum time transfer. The knowledge of the minimum time $t_{f_{\min}}$ is crucial for two reasons. The first reason is a natural and important one: When fixing the transfer time t_f we have to ensure that $t_f > t_{f_{\min}}$ otherwise the transfer does not make any sense. The second reason is a technical one: Usually the transfer time t_f is fixed between 1.5 and 3 times the minimum transfer time $t_{f_{\min}}$. Indeed this choice ensures that the optimal steering is far enough from the minimum time steering *i.e.* $|u| = 1, \forall t \in [0, t_{f_{\min}}]$, then one can observe the optimal control shape relative to the minimum consumption problem. In addition, our goal is to compute low thrust trajectories *i.e.* $T_{\max} \to 0$, in this case when t_f is higher, the cost (*i.e.* the fuel consumption) is lower. Thus, it is convenient to choose t_f such that $t_f >> t_{f_{\min}}$.

Once t_f is fixed, we investigate the resolution of the problem. As in the minimum time transfer case two transfers are considered: The initial point X_0 is the same for both, however, there are two targets X_f, the libration point L_2 and the lunar orbit LO, as defined in the previous chapter.

The minimum consumption transfer is also known in the mathematical vocabulary as the minimization of the L^1-norm of the control *i.e.* $\min \int_0^{t_f} |u| \mathrm{d}t$, t_f being the transfer time and $|.|$ being the Euclidian norm, since the mass variation is proportional to $|u|$. In fact, the fuel consumption is introduced by the mass variation equation of the spacecraft: $\dot{m} = -\beta T_{\max}|u|$. The fuel mass is a significant portion of the entire mass which decreases as the engine gear is switched on, in this context the problem is also called maximization of the final mass.

In this chapter, the variation of the mass will be neglected for the following reasons: (i) The mass varies only slightly during the transfer (this fact is verified numerically); (ii) In the two body problem {Earth, spacecraft} the numerical results are almost the same when omitting or not the mass variation equation

for minimum time transfer or minimum consumption transfer; (iii) Mathematically, the inclusion of the mass dynamic leads to a more complicated system of equations, therefore the system is reduced to equations of motion alone.

In the next chapter, we shall consider the mass variation equation. Connection is made to the fixed mass case (current case) by the means of an homotopy on the parameter β, it is then shown that the mass variation does not effect neither the transfer design nor the optimal steering shape with minimal differences in the value function.

Remark 3.1.1. β is an intrinsic parameter of the spacecraft. $\beta = \frac{1}{I_{sp} g_0}$ whereby I_{sp} is the specific impulse of the spacecraft motor and g_0 is the acceleration of gravity at the Earth surface.

Let us write our optimal control problem as thus:

$$(P) \begin{cases} \min J(u) = \int_0^{t_f} |u| \mathrm{d}t \\ \dot{x} = F(x,u) = F_0(x) + \frac{T_{\max}}{m} \sum_{i=1}^{m=3} u_i F_i(x),\ x \in X_\mu^1 \\ |u| \leq 1 \\ x(0) \in X_0 \\ x(t_f) \in X_f \end{cases}$$

Remark 3.1.2. The dynamics of x are written using the ratio $\frac{T_{\max}}{m}$ instead of ε. In fact, the notation ε is used later for another purpose.

Our goal is to compute optimal steering $u = (u_1, u_2, u_3)$ transferring the spacecraft from X_0 to X_f in preset time t_f with minimum fuel consumption. First of all one has to know about the existence of such optimal steering. As in the minimum time chapter Filippov theorem is again used to state the following proposition.

Note that, contrary to the minimum time case, the final time t_f is not free, thus one has to prove the existence of admissible trajectories for a given fixed time t_f, and consider then the existence of optimal ones. One is sure that at least there exists an admissible trajectory for $t_f = t_{f_{\min}}$ *i.e.* the minimum time trajectory. We are interested in transfer from X_0 to two different targets L_2 and LO. We aim to build an admissible trajectory for each target for a final time t_f sufficiently higher than $t_{f_{\min}}$:

- The libration point L_2: consider the trajectory which combines the minimum time solution to L_2 for $t \in [0, t_{f_{\min L_2}}]$ and then takes the free trajectory $u = 0$ for $t \in [t_{f_{\min L_2}}, t_f]$, as L_2 is an equilibrium point of the system. The third body (spacecraft) remains in this point at least until t_f, then this constructed trajectory is an admissible one, let us note it as $\mathscr{C}_{L_2}$.

- The orbit around the Moon LO: This case is more complicated than the previous because the initial orbit around the Earth and the final orbit around the Moon are unstable in the CRTBP. The idea is to build an admissible trajectory with an intermediate step at the libration point L_2. The trajectory is built as follows. The first step is the minimum time solution from X_0 to L_2 (let $t_{f_{\min 1}}$ be the time transfer, we already have $t_{f_{\min 1}} = t_{f_{\min L_2}}$), the second step is such that $u = 0$ (spacecraft stays on L_2) and third step is the minimum time solution from L_2 to LO (let

$t_{f_{\min 2}}$ be the transfer time). The spacecraft remains at L_2 with $u = 0$ for a period t_{L_2} such that $t_f - t_{f_{\min 1}} - t_{f_{\min 2}} = t_{f_{L_2}}$. thus this trajectory built in this way is an admissible one, let us note it as $\mathscr{C}_{LO}$

Let T be a positive real such that $T > t_{f_{\min 1}} + t_{f_{\min 2}}$, we have already demonstrated that for all final time $t_f > T$, there exists an admissible trajectory transferring the spacecraft from X_0 to X_f. Henceforth the final time is chosen such that $t_f > T$. This assumption corresponds with our goal to minimize fuel consumption since, higher the final time, lower the cost.

Proposition 3.1.1. *For all $T_{\max} > 0$, $m > 0$ and $\mu \in (0, 1)$, for all $t_f > T$ a steering u realizing the minimum consumption transfer in time t_f exists .*

Proof. The proof is similar to the minimum time case, only two points must be added.

- The set of admissible trajectories is not empty. This is demonstrated above.
- $\forall x \in X^1_\mu$, the set $\{(z^0, z), z^0 \geq |u|, z = F(x, u),\ u \in U\}$ is convex as a cartesian product of two convex sets $\{z^0,\ z^0 \geq |u|,\ u \in U\} \times F(x, U)$ ($F(x, u)$ is an affine function of u so $F(x, U)$ is convex).

We may then conclude with Filippov theorem. □

Thus we ensure the existence of the optimal solution for the problem (P). Let us now try to find it. We apply the Pontrjagin Maximum principle. The costate (p^0, p) is introduced, and the Hamiltonian of the system is written as follows in the 3-dimensionnal case.

$$H(x, u, p) = -p^0|u| + H_0 + u_1\frac{T_{\max}}{m}H_1 + u_2\frac{T_{\max}}{m}H_2 + u_3\frac{T_{\max}}{m}H_3$$

where $H_i = \langle p, F_i(x)\rangle$ for $i \in \{0, 1, 2, 3\}$. The application of the maximum principle yields:

$$\dot{x} = \frac{\partial H}{\partial p}(x, u, p) \tag{3.1}$$

$$\dot{p} = -\frac{\partial H}{\partial x}(x, u, p) \tag{3.2}$$

$$u(t) = \text{argmax}_{|v|\leq 1} H(x(t), v, p(t)) \text{ a.e. on } [0, t_f]. \tag{3.3}$$

Proposition 3.1.2. *If $t_f > T$ then $p^0 \neq 0$.*

Proof. Suppose that $p^0 = 0$ then by Cauchy-Schwartz,

$$H(x, u, p) \leq H_0 + \frac{T_{\max}}{m}|\varphi(p)||u|.$$

Where $\varphi(p) = (H_1, H_2, H_3) = (p_4, p_5, p_6)$, equality happens when u and $\varphi(p)$ are collinear. The function $\varphi(p) = (H_1, H_2, H_3)$ has no zeros or a finite number of zeros, the demonstration is identically similar to the proof of the proposition

2.2.1 in the previous chapter. Thus the maximization condition yields to $u = \frac{\varphi(p)}{|\varphi(p)|}$ and $|u| = 1$, a.e. on $[0, t_f]$. Then

$$J(u) = \int_0^{t_f} |u| \mathrm{d}t = \int_0^{t_f} \mathrm{d}t = t_f$$

Let us check if this solution is an optimal one. In this study, we consider two targets:

- The libration point L_2, the trajectory $\mathscr{C}_{L_2}$ is admissible for our problem and is better since $t_{f_{\min}} < t_f$, absurd.
- The orbit around the Moon LO, the trajectory $\mathscr{C}_{LO}$ is admissible for our problem and is better since $t_f > t_{f_{\min 1}} + t_{f_{\min 2}}$, absurd.

□

Remark 3.1.3. In the previous proof, the hypothesis $t_f > T$ does not hinder the problem resolution for two reasons:

- Firstly when computing optimal solutions we may choose t_f which is sufficiently higher than $t_{f_{\min 1}} + t_{f_{\min 2}} > t_{f_{\min}}$. This corresponds with our goal to minimize fuel consumption since, as we stated previously, higher the final time, lower the cost.
- Numerical resolution shows that the solutions are bang-bang *i.e.* alteration in time between $u = 0$ and $|u| = 1$. In this case one is sure that the cost is strictly lower than t_f thus the solution $|u| = 1$, $\forall t \in [0, t_f]$ is not optimal.

Hence, in the remainder of this chapter, we are interested in the normal case *i.e.* $p^0 \neq 0$, the costate (p^0, p) is normalized such that $p^0 = -1$. We calculate then the optimal control u thanks to the maximization condition: By Cauchy-Schwartz,

$$H(x, u, p) \leq H_0 + (\frac{T_{\max}}{m}|\varphi(p)| - 1)|u|.$$

where $\varphi(p) = (H_1, H_2, H_3) = (p_4, p_5, p_6)$, with equality case when u and $\varphi(p)$ are collinear. Let us introduce then the function $\psi(p) = \frac{T_{\max}}{m}|\varphi(p)| - 1$, it is called the switching function since the control value is determined according to the sign of ψ as below.

(i) $\psi(p) > 0 \Rightarrow |u| = 1 \Rightarrow u = \frac{\varphi(p)}{|\varphi(p)|}$,

(ii) $\psi(p) < 0 \Rightarrow |u| = 0 \Rightarrow u = 0$,

(iii) $\psi(p) = 0 \Rightarrow |u| \leq 1 \Rightarrow u = \alpha \frac{\varphi(p)}{|\varphi(p)|}$, $\alpha \in [0, 1]$.

Definition 3.1.1. The switching surface is the submanifold of $\mathbf{R}^6$ defined by $\psi(p) = 0$. An order one contact with the switching surface happens when the curve (x, p) crosses the switching surface *i.e.* if $\bar{t}$ is a switching time of order one then $\psi(\bar{t}) = 0$ and $\dot{\psi}(\bar{t}) \neq 0$.

Let p_r be the costate with respect to the position $r = (x_1, x_2, x_3)$ and p_v the costate relative to the velocity $v = (x_4, x_5, x_6)$. Let $\bar{t}$ be a switch time of order one. Then $\psi(\bar{t}) = 0$ and $\dot{\psi}(\bar{t}) \neq 0$.

$$\begin{aligned}
\dot{\psi}(\bar{t}) = 0 &\Leftrightarrow \frac{T_{\max}}{m} \frac{\dot{H}_1 H_1 + \dot{H}_2 H_2 + \dot{H}_3 H_3}{\sqrt{H_1^2 + H_2^2 + H_3^2}} = 0 \\
&\Leftrightarrow \dot{H}_1 H_1 + \dot{H}_2 H_2 + \dot{H}_3 H_3 = 0 \\
&\Leftrightarrow \dot{p_4} p_4 + \dot{p_5} p_5 + \dot{p_6} p_6 = 0 \\
&\Leftrightarrow -\frac{\partial H}{\partial x_4}(x,u,p)p_4 - \frac{\partial H}{\partial x_5}(x,u,p)p_5 - \frac{\partial H}{\partial x_6}(x,u,p)p_6 = 0 \\
&\Leftrightarrow p_1(\bar{t})p_4(\bar{t}) + p_2(\bar{t})p_5(\bar{t}) + p_3(\bar{t})p_6(\bar{t}) = 0 \\
&\Leftrightarrow \langle p_x(\bar{t}), p_v(\bar{t}) \rangle = 0
\end{aligned}$$

We may enunciate the following proposition.

Proposition 3.1.3. *If $\langle p_x, p_v \rangle \neq 0$, then the contacts with the switching surface are of order one and there is a finite number of switches.*

Proof. Suppose that there is an infinity of switching time $(t_i)_{i \in \mathbf{N}}$ where $t_i \in [0 \ t_f] \, \forall i \in \mathbf{N}$. Then there exists a convergent subsequence $(t_{\varphi(i)})_{i \in \mathbf{N}}$ of limit $\bar{t}$. By the continuity of ψ we have $\psi(\bar{t}) = 0$. ψ is C^1 thus

$$\dot{\psi}(\bar{t}) = \lim_{i \to \infty} \frac{\psi(t_{\varphi(i)}) - \psi(\bar{t})}{t_{\varphi(i)} - \bar{t}} = 0 \text{ absurd}$$

therefore the switching number is finite. □

Remark 3.1.4. The function $\psi = \frac{T_{\max}}{m}\sqrt{H_1^2 + H_2^2 + H_3^2} - 1$ is C^1 where $H_1^2 + H_2^2 + H_3^2 \neq 0$. If $\bar{t}$ is a switching time then $\psi(\bar{t}) = 0$ and $H_1^2 + H_2^2 + H_3^2 = (\frac{m}{T_{\max}})^2 \neq 0$ thus ψ is C^1 at the switching times.

We define the corresponding shooting functions S^{L_2} and S^{LO} relative to the targets L_2 and LO respectively as below.

$$S^{L_2} \ : \ z = p(0) \ \mapsto \ \begin{pmatrix} x_1(t_f) - x_{L_2}(\mu) \\ x_2(t_f) \\ x_3(t_f) \\ x_4(t_f) \end{pmatrix}$$

and

$$S^{LO} \ : p(0) \ \mapsto \ \begin{pmatrix} x_1^2(t_f) + x_2^2(t_f) - r^2 \\ x_3^2(t_f) + x_4^2(t_f) - v^2 \\ x_1(t_f)x_3(t_f) + x_2(t_f)x_4(t_f) \\ x_1(t_f)p_2(t_f) - x_2(t_f)p_1(t_f) + x_3(t_f)p_4(t_f) - x_4(t_f)p_3(t_f) \end{pmatrix}.$$

Remark 3.1.5. The initial and final conditions of the considered transfers are in the CRTBP plane, hence transfers are taking place in the CRTBP plane. The shooting functions are written in the planar case (*i.e.* $x \in \mathbf{R}^4$).

To compute optimal transfers from X_0 to L_2 or LO, one has to find a suitable guess to solve $S^{L_2}(z) = 0$ and $S^{LO}(z) = 0$.The true Hamiltonian expression after

maximization (PMP principle) is $H(x,p) = H_0 + \psi_+(p)$ where $\psi_+(p) = \psi(p)$ if $\psi(p) > 0$ and $\psi_+(p) = 0$ elsewhere. The true Hamiltonian is then non smooth and only continuous. The optimal control is bang-bang: $|u|$ switches between zero and one. As in the two body case [21, 22], this fact makes it difficult if not impossible, to find zeros of the shooting functions. This happens because the cost function ($F^0 : (x,u) \mapsto |u|$) is only concave but not strictly concave with respect to u, and so is the Hamiltonian $H(x,p,u)$ with respect to u, thus we are not sure of the continuity of the control solution (in this case u is bang-bang). In fact, only if the Hamiltonian is strictly concave, the maximization condition of the PMP yields to a continuous control u depending only on (x,p).

In this case (minimum consumption transfer problem (P)), the initialization task is complicated since it involves switches (bang-bang). In addition the number of switches increases when considering lower thrust which is confirmed by numerical computation. In fact, to have an initial guess to solve $S^{L_2}(z) = 0$ or $S^{LO}(z) = 0$ with a Newton-type method requires knowing a priori the structure of the optimal control switches (see [21] for more details). To address this concern, we use continuation methods as in the two-body case [21, 22]. Since the optimal control shape is causing this inconvenience, our goal is to construct a continuation method that regularizes the optimal control shape as a first step and thus facilitates the initialization and secondly then ensures connection with our real problem.

We introduce a family of optimal control problems $(P_\lambda)_{\lambda\in[\lambda_0,\lambda_f]}$, a parameter λ is insert in the cost function F^0 to regularize it and to transform it into a strictly concave function.

$$(P_\lambda)\begin{cases} \min J_\lambda(u) = \int_0^{t_f} F^0(x(t),u(t),\lambda)\mathrm{d}t \\ \dot{x} = F(x,u) \\ |u| \leq 1 \\ x(0) \in X_0 \\ x(t_f) \in X_f \end{cases}$$

The resolution of (P_λ), for the two transfer cases, amounts, by the PMP application, to finding a zero of the shooting function $S_\lambda^{L_2}$ and a zero of S_λ^{LO}. The parameter λ is such that:

- The cost function is strictly concave with respect to u for $\lambda < \lambda_f$ and so is the true Hamiltonian, thus we are sure that the optimal control solution $u(x,p)$ is at least continuous. For $\lambda = \lambda_f$ we retrieve the beginning problem (*i.e.* $(P_{\lambda_f}) = (P)$).

- It is easy or known how to find a zero of $S_{\lambda_0}(z)$ *i.e.* to solve (P_{λ_0}).

The resolution strategy is simple: Once a zero of S_{λ_0} is found, then we follow the zeros path of the shooting function S_λ from $\lambda = \lambda_0$ to $\lambda = \lambda_f$. This leads us to the following paragraphs.

Remark 3.1.6. The parameter λ only changes the cost function and does not intervene in writing the final transfer conditions, thus the shooting function $S^{L_2}(z)$ and $S^{LO}(z)$ expressions remain unchanged. We add the index λ to refer to the problem (P_λ).

3.2 Energy-Consumption homotopy

In this section, we shall focus on the energy-consumption homotopy, also called $L^2 - L^1$ homotopy since it connects the minimization of the L^2-norm of the control (*i.e.* the energy $\int_0^{t_f} |u|^2 \mathrm{d}t$) to the L^1-norm. The connection is made in a convex manner *i.e.*:

$$F^0(x(t), u(t), \lambda) = \lambda|u| + (1-\lambda)|u|^2.$$

It is obvious that when $\lambda = 1$, we have our main problem (P). When $\lambda = 0$ the problem is called energy minimization problem. In this case, note that $\lambda_0 = 0$ and $\lambda_f = 1$. It is known to be much easier to solve as numerical computation demonstrate in the two-body case [22]. In fact, introducing the L^2-norm in the cost function makes the Hamiltonian smooth therefore finding a zero of the shooting function is much easier. Resolution of this problem *i.e.* $(p(0))$ is detailed in the next paragraph.

We write our modified optimal control problem as thus:

$$(P_\lambda) \begin{cases} \min J_\lambda(u) = \int_0^{t_f} \lambda|u| + (1-\lambda)|u|^2 \mathrm{d}t \\ \dot{x} = F(x,u) \\ |u| \leq 1 \\ x(0) \in X_0 \\ x(t_f) \in X_f \end{cases}$$

First, we focus on the existence of solution to this optimal control problem and as usual we use the Filippov theorem.

Proposition 3.2.1. *For all $t_f > T$, $\lambda \in [0,1]$, $T_{\max} > 0$, $m > 0$, $\mu \in (0,1)$, a steering u_λ solution of (P_λ) exists.*

Proof. The same proof as for the problem (P), with a slight difference since the cost function is now $(x,u) \mapsto \lambda|u| + (1-\lambda)|u|^2$:

- $\forall \lambda \in [0,1]\, \forall x \in X^1_\mu$, the set $\{(z^0, z), z^0 \geq \lambda|u| + (1-\lambda)|u|^2, z = F(x,u),\ u \in U\}$ is convex as a cartesian product of two convex sets $\{z^0,\ z^0 \geq \lambda|u| + (1-\lambda)|u|^2,\ u \in U\} \times F(x,U)$ ($F(x,u)$ is an affine function of u so $F(x,U)$ is convex, the first set is convex thanks to the triangular inequality and the convexity of the function $u \mapsto |u|^2$).

Subsequently we may conclude with the Filippov theorem. □

The corresponding Hamiltonian is:

$$H_\lambda(x,u,p) = -\lambda|u| - (1-\lambda)|u|^2 + H_0 + u_1 \frac{T_{\max}}{m} H_1 + u_2 \frac{T_{\max}}{m} H_2 + u_3 \frac{T_{\max}}{m} H_3$$

Note that for $\lambda < 1$ the Hamiltonian $H_\lambda(x,u,p)$ is strictly concave with respect to u, then the control solution u is writing as a continuous function of (x,p). Let us calculate it. By Cauchy-Schwartz,

$$H_\lambda(x,u,p) \leq \underbrace{H_0 + (\frac{T_{\max}}{m}|\varphi(p)| - \lambda)|u| - (1-\lambda)|u|^2}_{g_\lambda(|u|)}$$

The maximization condition implies, for $\lambda < 1$ (the case $\lambda = 1$ has already treated in the previous section):

$$\begin{aligned} & g'_\lambda(|u|) = 0 \\ \Leftrightarrow\ & 2(1-\lambda)|u| = (\frac{T_{\max}}{m}|\varphi(p)| - \lambda) \\ \Leftrightarrow\ & |u| = \alpha_\lambda(p) = \frac{(\frac{T_{\max}}{m}|\varphi(p)| - \lambda)}{2(1-\lambda)} \text{ and } \lambda \neq 1 \end{aligned} \tag{3.4}$$

As the control is constrained to the condition $|u| \leq 1$ then:

(i) $\alpha_\lambda(p) > 1 \Rightarrow |u_\lambda| = 1 \Rightarrow u_\lambda = \frac{\varphi(p)}{|\varphi(p)|}$,

(ii) $\alpha_\lambda(p) < 0 \Rightarrow |u_\lambda| = 0 \Rightarrow u_\lambda = 0$,

(iii) $0 \leq \alpha_\lambda(p) \leq 1 \Rightarrow u_\lambda = \alpha_\lambda(p)\frac{\varphi(p)}{|\varphi(p)|}$.

Remark 3.2.1. The optimal control u_λ is continuous and not smooth so the true Hamiltonian in this case is also only continuous and non smooth.

The homotopy consits in solving $(P_{\lambda=0})$ then let λ get as close as possible to 1. One can ask a question about the variation of the criterion $J_\lambda(u)$ with respect to the homotopic parameter λ and its convergence when λ tends towards 1. We enunciate the following results:

Proposition 3.2.2. *[21, 22] Let (x_λ, u_λ) be a solution of the problem (P_λ) then for $0 \leq \lambda \leq \lambda' \leq 1$, we have:*

(i) $J_\lambda(u_\lambda) \leq J_{\lambda'}(u_{\lambda'}) \leq J_1(u_1) \leq J_1(u_\lambda)$

(ii) $|J_\lambda(u_\lambda) - J_1(u_\lambda)|$ *tend to* 0 *when* λ *tend to* 1.

(iii) $J_\lambda(u_\lambda)$ *and* $J_1(u_\lambda)$ *tend to* $J_1(u_1)$ *when* λ *tend to* 1.

Proof. (i) For all $u \in B_c(0,1)$ and for all $0 \leq \lambda \leq \lambda' \leq 1$:

$$\begin{aligned} \lambda'|u| + (1-\lambda')|u|^2 &= \lambda|u| + (1-\lambda)|u|^2 + (\lambda' - \lambda)(|u| - |u|^2) \\ &\geq \lambda|u| + (1-\lambda)|u|^2 \end{aligned}$$

Thus $J_\lambda(u) \leq J_{\lambda'}(u)$ for all admissible control. Since the set of admissible control is the same for all $\lambda \in [0,1]$, we have the following inequality:

$$J_\lambda(u_\lambda) \leq J_\lambda(u_{\lambda'}) \leq J_{\lambda'}(u_{\lambda'})$$

(ii) The function $l(u,\lambda) = \lambda|u| + (1-\lambda)|u|^2$ is continuous on the compact $B_c(0,1) \times [0,1]$ thus it is uniformly continuous *i.e.*:

$$\forall \varepsilon > 0, \exists \eta > 0,\ |\lambda - 1| < \eta \Rightarrow |l(u,\lambda) - l(u,1)| < \varepsilon$$

Therefore:

$$|J_\lambda(u_\lambda) - J_1(u_\lambda)| \leq \int_0^{t_f} |l(u,\lambda) - l(u,1)| \mathrm{d}t < \varepsilon t_f$$

hence the result.

(iii) Obvious.

□

Once we are sure of the existence of solution and the criteria convergence, we begin extremals computation. To launch the energy-consumption homotopy one has to solve the minimum energy transfer problem ($p(0)$). To facilitate the numerical resolution, we omit the constraint on the control $|u| \leq 1$, this makes the control and the true Hamiltonian smooth. In fact, let us consider the following problem:

$$(P)^{L^2} \begin{cases} \min \int_0^{t_f} |u|^2 \mathrm{d}t \\ \dot{x} = F(x,u) \\ x(0) \in X_0 \\ x(t_f) \in X_f \end{cases}$$

One can see that $(P)^{L^2} = (P_{\lambda=0})$ when the control solution verifies $|u(t)| \leq 1$, $\forall t \in [0, t_f]$. Let us consider the Hamiltonian of the problem:

$$\begin{aligned} H^{L^2}(x,u,p) &= -|u|^2 + H_0 + u_1 \frac{T_{\max}}{m} H_1 + u_2 \frac{T_{\max}}{m} H_2 + u_3 \frac{T_{\max}}{m} H_3 \\ &= -(u_1^2 + u_2^2 + u_3^2) + H_0 + u_1 \frac{T_{\max}}{m} H_1 + u_2 \frac{T_{\max}}{m} H_2 + u_3 \frac{T_{\max}}{m} H_3 \end{aligned}$$

The maximization condition implies (no constraint on u):

$$\begin{aligned} & \frac{\partial H^{L^2}}{\partial u} = 0 \\ \Leftrightarrow & \begin{pmatrix} -2u_1 + \frac{T_{\max}}{m} H_1 \\ -2u_2 + \frac{T_{\max}}{m} H_2 \\ -2u_3 + \frac{T_{\max}}{m} H_3 \end{pmatrix} = \begin{pmatrix} 0 \\ 0 \\ 0 \end{pmatrix}. \\ \Leftrightarrow & \begin{pmatrix} u_1 \\ u_2 \\ u_3 \end{pmatrix} = \frac{1}{2} \begin{pmatrix} \frac{T_{\max}}{m} H_1 \\ \frac{T_{\max}}{m} H_2 \\ \frac{T_{\max}}{m} H_3 \end{pmatrix}. \\ \Leftrightarrow & u = \frac{1}{2} \frac{T_{\max}}{m} \varphi(p) \end{aligned}$$

The true Hamiltonian is then:

$$H^{L^2}(x,p) = H_0 + \frac{1}{4} (\frac{T_{\max}}{m})^2 (H_1^2 + H_2^2 + H_3^2).$$

Thanks to cancellation the constraint on u, the true Hamiltonian is smooth and finding a zero of the shooting functions $S_{L^2}^{L_2}$ and $S_{L^2}^{LO}$ is much easier ($S_{L^2}^{L_2} = S_{\lambda=0}^{L_2}$ and $S_{L^2}^{LO} = S_{\lambda=0}^{LO}$).
The final time t_f is fixed. The initialization strategy is defined as below:

- 1^{st} An initialization to solve $(P)^{L^2}$ for $t_f = t_{f\min}$ is found easily.
- 2^{nd} Increase the final time value t_f until the constraint on the control *i.e.* $\forall t \in [0, t_f]$, $|u| < 1$ is verified [4].

Remark 3.2.2. The control is restricted to $|u| < 1$ to ensure the Hamiltonian smoothness at the beginning of the homotopy, this is helpful for the differential path following.

3.2.1 Target libration point L_2

During this study we consider in our numerical calculations two transfer targets: The libration point L_2 and the orbit LO around the Moon. In this section, we will focus only on transfer to the point L_2 and we will detail the numerical strategy followed to design the transfer from X_0. The same techniques are used again when the target is LO and the results are given next section. The goal is this section is to emphasize the numerical techniques by taking as a supporting example: Transfer from X_0 to L_2. The numerical simulations are provided in the planar case since initial and final conditions are in the CRTBP plane.

As in the minimum time transfer, we consider the same spacecraft mass characteristics: Initial mass $m = 1500$kg and we neglect the mass variation along the transfer. Let us first consider a medium thrust *i.e.* $T_{\max} = 10$N. We have not focused on low thrusts at the beginning because our goal is first to understand the transfer design and then extend the strategy to the low thrust. In fact, when considering low thrust the time transfer is very high this leads to more cumulative integration errors; this could cause the shooting algorithm divergence, in addition time computation is very long in this case.

The initialization strategy is known: An arbitrary initialization produces solution for $t_f = t_{f_{\min}}$. We assume intuitively that when the transfer time increases the maximum of $|u|$ is decreases, thus an extremal ensuring the constraint $|u| < 1$ may be found. This method is detailed in table 3.1. In this table, we have the the ratio $t_f/t_{f_{\min}}$, the maximum value of the control norm along the transfer and the corresponding initialization $p(0)$. For the forthcoming numerical

Table 3.1: Minimum energy transfer initialization table - target L_2, $T_{\max} = 10$N. $max_{[0,t_f]}|u|$ decreases regularly when the transfer time increases.

$t_f/t_{f_{\min}}$	$max_{[0,t_f]}\|u\|$	$p(0)$
1.0	2.00	$[10^{-2}10^{-2}10^{-2}10^{-2}]$
1.1	1.50	$[10^{-2}10^{-2}10^{-2}10^{-2}]$
1.2	1.20	$[10^{-2}10^{-2}10^{-2}10^{-2}]$
1.3	1.02	$[10^{-2}10^{-2}10^{-2}10^{-2}]$
1.4	0.86	$[10^{-2}10^{-2}10^{-2}10^{-2}]$
1.5	0.75	$[10^{-2}10^{-2}10^{-2}10^{-2}]$

simulations *i.e.* energy-consumption homotopy, the extremal corresponding to $c_{t_f} = t_f/t_{f_{\min}} = 1.5$ is chosen. The extremal and the control norm are demonstrated respectively in figure 3.1 and figure 3.2. Let us use the same method for a lower thrust for instance $T_{\max} = 5$N. We resume in table 3.2 the different steps to solve the minimum energy problem. Discrete homotopic step means that the solution of the previous step is introduced as an initialization for the current step, the homotopic parameter is the ratio $c_{t_f} = t_f/t_{f_{\min}}$. In table 3.2, one can identify two points: Firstly, arbitrary initializations are not valid when the final time increases thus we introduce a discrete homotopy on c_{t_f}, secondly, when increasing the final time we can not ensure that $max_{[0,t_f]}|u|$ decreases automatically, in fact $max_{[0,t_f]}|u|$ is increased from $c_{t_f} = 1.6$ to $c_{t_f} = 1.7$. The extremal corresponding to $t_f/t_{f_{\min}} = 1.6$ is chosen to perform the next step.

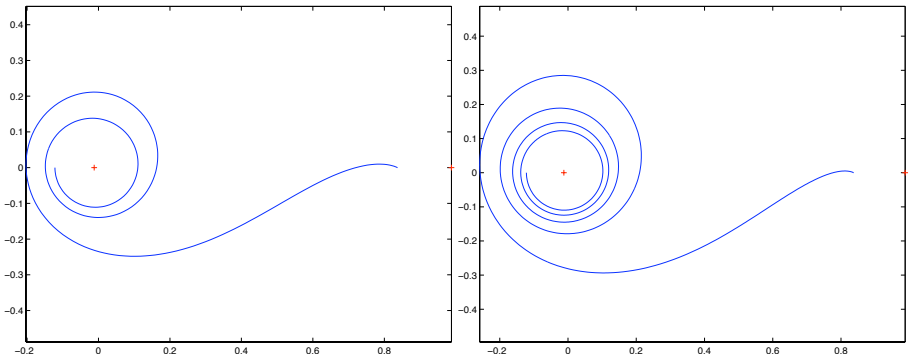

Figure 3.1: Minimum energy optimal trajectory to L_2, $T_{\max} = 10$N left and $T_{\max} = 5$N right, CR3BP frame.

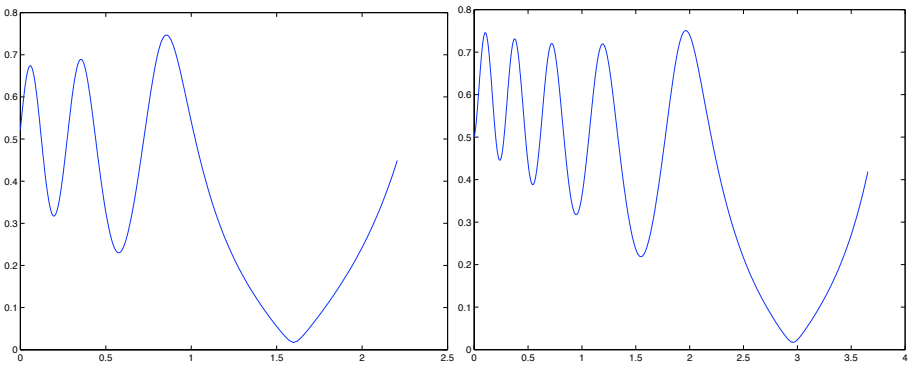

Figure 3.2: Control norm $|u|$ versus time - minimum energy case - target L_2, $T_{\max} = 10$N and $t_f = 1.5 t_{f\,\min}$ left and $T_{\max} = 5$N and $t_f = 1.6 t_{f\,\min}$ right.

The extremal and the control norm are portrayed respectively in figure 3.1 and figure 3.2.

This initialization method is used successfully for medium thrusts. however, when thrust decreases, this method is not efficient. We use another method for low thrusts, the new method has the same principle as explained before: start from an initialization for $t_f = t_{f\,\min}$ and then increase the final time in order to obtain $|u| < 1$ but the way to find the first initialization and to increase the time is not the same. This is detailed in the following paragraph supported by an example of $T_{\max} = 0.3$N (this corresponds with SMART-1 maximal acceleration).

The process is the following. The initialization solution of the minimum time transfer is a suitable guess for the shooting algorithm of (P^{L^2}) for $t_f = t_{f\,\min}$. The control norm of the solution is higher than 1, which we aim the to reduce. We introduce an homotopy on the final time t_f starting from $t_f = t_{f\,\min}$, then t_f is increased until the norm control satisfies the constraint $|u| < 1$. This time the discrete continuation does not work so a differential one is used. A summary is given in table 3.3.

As shown in the table 3.3, differential homotopy on t_f enables us to produce

Table 3.2: Minimum energy transfer initialization table, target L_2, $T_{\max} = 5$N.

$t_f/t_{f_{\min}}$	$max_{[0,t_f]}\|u\|$	$p(0)$
1.0	2.33	$[10^{-2}10^{-2}10^{-2}10^{-2}]$
1.1	1.44	$[10^{-2}10^{-2}10^{-2}10^{-2}]$
1.2	1.51	$[10^{-2}10^{-2}10^{-2}10^{-2}]$
1.3	1.24	$[10^{-2}10^{-2}10^{-2}10^{-2}]$
1.4	1.03	$[10^{-2}10^{-2}10^{-2}10^{-2}]$
1.5	0.88	discrete homotopic step
1.6	0.75	discrete homotopic step
1.7	0.77	discrete homotopic step

Table 3.3: Minimum energy transfer initialization table - target L_2, $T_{\max} = 0.3$N. $max_{[0,t_f]}|u|$ decreases regularly when the transfer time increases.

$t_f/t_{f_{\min}}$	$max_{[0,t_f]}\|u\|$
1.0	2.34
1.1	1.91
1.2	1.59
1.3	1.34
1.4	1.13
1.5	0.91
1.6	0.75
1.7	0.67

solutions such that $|u| < 1$. For the forthcoming numerical simulations *i.e.* energy-consumption homotopy, the extremal corresponding to $c_{t_f} = t_f/t_{f_{\min}} = 1.7$ is chosen. One can notice that solutions for $c_{t_f} = 1.5$ and $c_{t_f} = 1.6$ are also admissible but numerical tests show that when the control norm is smaller the computations of the energy-consumption homotopy are faster and more efficient because the control saturates the constraint *i.e.* $|u| = 1$ when λ is close to 1 (towards the end of the energy-consumption homotopy). The chosen extremal and the corresponding control norm are demonstrated respectively in figure 3.3 and figure 3.4.

Remark 3.2.3. When the maximum thrust decreases, the number of the control norm oscillations as well as the number of revolution around the first primary increases. For instance for $T_{\max} = 0.3$ there is tens of control norm oscillations, this high number affects the numerical calculations as it will be detailed later.

As afore mentioned, the maximum principle is essentially a first order necessary condition. To ensure local optimality, second order necessary conditions are introduced. Since in the minimum energy case the Hamiltonian is smooth, one can test optimality of the computed extremals for the different thrusts 10 5 and 0.3N. The notion of conjugate point was introduced in the previous chapter, however there is a different issue this time: That is, the final time is fixed (final time was free in the minimum time problem). Thus we recall the theoretical

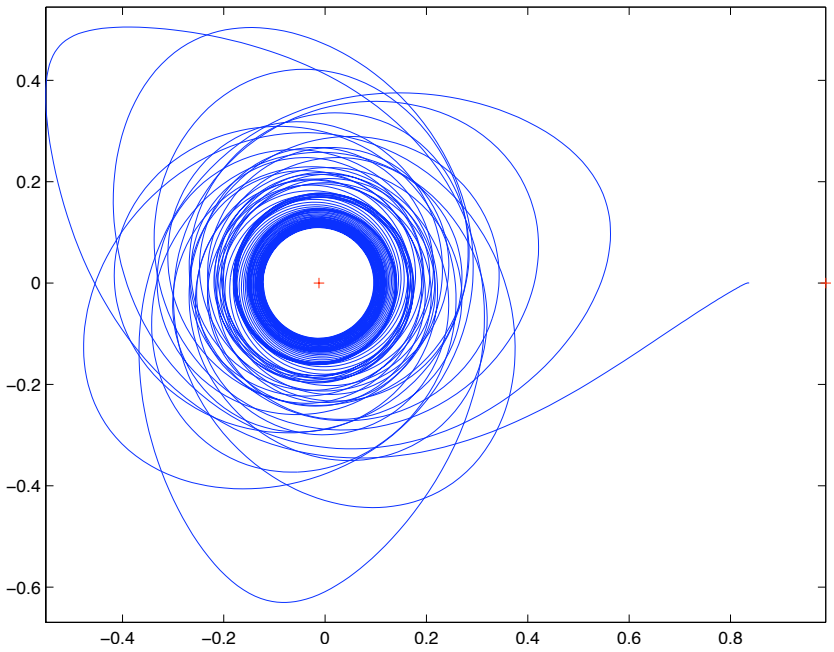

Figure 3.3: Minimum energy optimal trajectory to L_2, $T_{\max} = 0.3$N, CR3BP frame.

framework and then we shall explain the suitable numerical tests for this case. The Hamiltonian is noted H for the sake of generality.

Let $z = (x, p)$ be a reference extremal. It is a smooth solution of $\dot{z} = \overrightarrow{H}(z)$ where $\overrightarrow{H}(z) = (\frac{\partial H}{\partial p}(x,p), -\frac{\partial H}{\partial x}(x,p))$, defined on $[0, t_f]$, satisfying the initial and final conditions *i.e.* $x(0) \in (X_0 = \text{GEO perigee})$ and $x(t_f) \in (X_f = L_2)$.

Definition 3.2.1. The variational equation on $[0, t_f]$, $\dot{\delta z}(t) = \overrightarrow{H}'(z(t))\delta z(t)$ is called the *Jacobi equation* along $z(.)$. A *Jacobi field* is a non trivial solution $J(t) = (\delta x(t), \delta p(t))$ of the Jacobi equation along $z(.)$, its is said to be vertical at time t if $\delta x(t) = d\Pi(z(t))(J(t)) = 0$ where $\Pi : (x, p) \mapsto x$ is the standard projection.

Definition 3.2.2. Let $z(t, z_0) = (x(t, x_0, p(0)), p(t, x_0, p(0)))$ be a solution of $\dot{z} = \overrightarrow{H}(z)$ for the initial condition $z_0 = (x_0, p(0))$. We define the exponential mapping by

$$\exp_{x_0}(t, p(0)) = x(t, x_0, p(0)).$$

Definition 3.2.3. We say that $t_c > 0$ is a conjugate time if there exists a Jacobi field $J = (\delta x, \delta p)$ vertical at 0 and t_c. The associated point $x(t_c)$ is said to be conjugate to x_0.

Definition 3.2.4. An extremal is said to be regular if the strong Legendre condition holds along the extremal *i.e.*:

$$\frac{\partial^2 H}{\partial u^2} < 0 \ \textit{i.e.}\ \frac{\partial^2 H}{\partial u^2} \text{ is negative definite.}$$

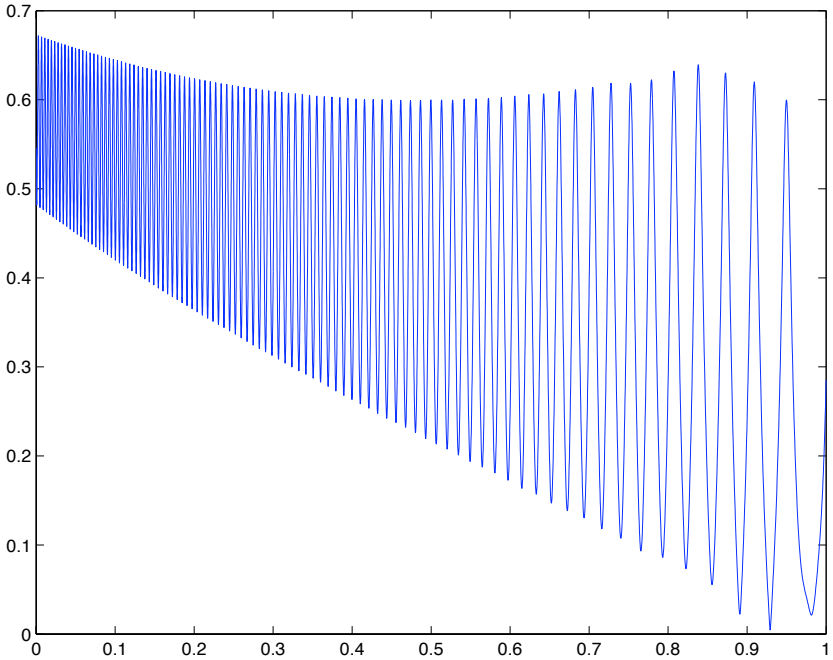

Figure 3.4: Control norm $|u|$ versus time - minimum energy case - target L_2, $T_{\max} = 0.3\text{N}$, $t_f = 1.7 t_{f_{\min}}$, the time t is scaled by t/t_f.

Proposition 3.2.3. *Minimum energy transfer extremals are regular.*

Proposition 3.2.4. *t_c is a conjugate time if and only if the mapping $\exp_{x_0}(t_c, .)$ is not an immersion at $p(0)$.*

Proposition 3.2.5. *[1, 5, 6] A regular reference trajectory z is locally optimal up to first conjugate time.*

The method to compute conjugate times is the following [5, 6].
In the minimum consumption case the final time is fixed. The method to compute conjugate times is the following. One has to compute numerically the jacobi fields $J_i = (\delta x_i, \delta p_i),\ i = 1, \ldots, n = 4$, corresponding to the initial conditions $\delta x_i(0) = 0$ and $\delta p_i(0) = e_i$, $i = 1, \ldots, n$ where $(e_i)_{1 \leq i \leq n}$ represents the canonical basis of $\mathbf{R}^n$. The time t_c is conjugate time whenever

$$\text{rank}(\delta x_1(t_c), \delta x_2(t_c), \delta x_3(t_c), \delta x_4(t_c)) < n.$$

An extremal is locally optimal if the first conjugate time t_{c1} satisfies $t_{c1} > t_f$. The numerical rank tests show that the computed extremals for $T_{\max} = 10\text{N}$, $T_{\max} = 5\text{N}$ and $T_{\max} = 0.3\text{N}$ are locally optimal.

Once the minimum energy problem *i.e.* $S^{L_2}_{\lambda=0}(p(0))$ is solved. The energy-consumption homotopy *i.e.* resolution of $(P_\lambda)_{\lambda>0}$ begins. We use the differential path following. The solution of (P_0) is used to initialize the differential homotopy on λ. We give similar results for the two different thrusts $T_{\max} = 10\text{N}$ and $T_{\max} = 5\text{N}$. Tables 3.4 and 3.5 summarize the homotopic steps and gives the precision on the shooting function norm at the end of the step. The control norm

variation along the homotopy is represented for different λ values in Fig. 3.5 and Fig. 3.6. The bang-bang (norm of the) control is approximated as λ tends to one.

Table 3.4: Energy-Consumption homotopy, target L_2, $T_{\max} = 10$N.

Homotopic Step λ	Shooting Function $\lvert S_\lambda^{L_2} \rvert$
$0.0 \rightarrow 0.1$	$\sim 10^{-10}$
$0.1 \rightarrow 0.2$	$\sim 10^{-9}$
$0.2 \rightarrow 0.3$	$\sim 10^{-12}$
$0.3 \rightarrow 0.4$	$\sim 10^{-11}$
$0.4 \rightarrow 0.5$	$\sim 10^{-10}$
$0.5 \rightarrow 0.6$	$\sim 10^{-8}$
$0.6 \rightarrow 0.7$	$\sim 10^{-7}$
$0.7 \rightarrow 0.8$	$\sim 10^{-6}$
$0.8 \rightarrow 0.9$	$\sim 10^{-6}$
$0.9 \rightarrow 0.9935$	$\sim 10^{-5}$

Table 3.5: Energy-Consumption homotopy, target L_2, $T_{\max} = 5$N.

Homotopic Step λ	Shooting Function $\lvert S_\lambda^{L_2} \rvert$
$0.0 \rightarrow 0.1$	$\sim 10^{-12}$
$0.1 \rightarrow 0.2$	$\sim 10^{-13}$
$0.2 \rightarrow 0.3$	$\sim 10^{-12}$
$0.3 \rightarrow 0.4$	$\sim 10^{-12}$
$0.4 \rightarrow 0.5$	$\sim 10^{-12}$
$0.5 \rightarrow 0.6$	$\sim 10^{-12}$
$0.6 \rightarrow 0.7$	$\sim 10^{-6}$
$0.7 \rightarrow 0.8$	$\sim 10^{-4}$
$0.8 \rightarrow 0.9$	$\sim 10^{-4}$
$0.9 \rightarrow 0.999$	$\sim 10^{-3}$

We can see in Fig. 3.7 that the cost criteria $J(u_\lambda) = \int_0^{t_f} |u_\lambda| \mathrm{d}t$ tends, by superior values, to a limit value when λ tends to one and the criteria $J_\lambda(u_\lambda) = \int_0^{t_f} (\lambda|u_\lambda| + (1-\lambda)|u_\lambda|^2) \mathrm{d}t$ tends, by inferior values, to the same limit value when λ tends to one, this limit value as stated before is $J(u) = \int_0^{t_f} |u| \mathrm{d}t$. The numerical simulations are consistent with the proposition 3.2.2. Both of the extremal trajectories for $\lambda = 0.9935$ and $T_{\max} = 10$N and for $\lambda = 0.999$ and $T_{\max} = 5$N are plotted in the CR3BP-rotating frame (*cf.*Fig. 3.8). Red points indicate (maximum) thrust locations on the extremal trajectories. Until now results have been given for medium thrusts: 10N and 5N, similar results are also obtained for 7N and 3N. Let us see what happens to low thrust for instance, $T_{\max} = 0.3$N. As already has been accomplished for 10N and 5N,

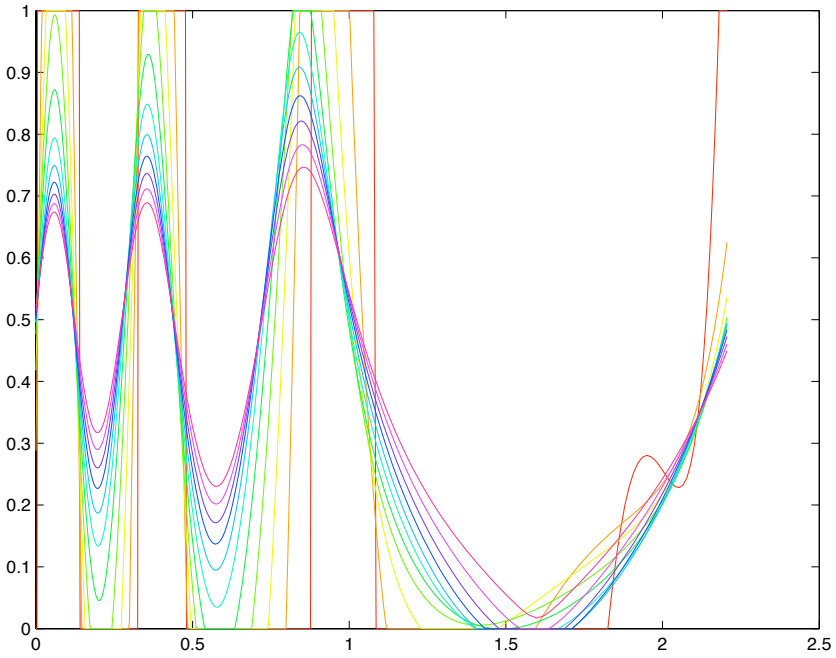

Figure 3.5: Control norm $|u_\lambda|$ versus time for λ equal to 0.0 till 0.9935 (red), energy-consumption homotopy, target L_2, $T_{\max} = 10$N.

The solution of (P_0) is used to initialize the differential homotopy on λ. Table 3.6 summarizes the homotopic steps and gives the precision on the shooting function norm at the end of the step. Actually, the derivative of the shooting function is computed using the variational equation method which is a proper method when the control is smooth, in the energy-consumption case this method continues to work if the switches of the control to 1 or to 0 as defined at (3.4) are of order one *cf.* figure 3.10 *i.e.* the function $\alpha_\lambda(p)$ is equal to 0 or 1 in isolated points *i.e.* crosses the lines of $l_1 = 0$ and $l_2 = 1$. This is verified, a posteriori in our case, by numerical computation, see figure 3.11. This fact is not penalizing for the medium thrusts (10, 7, 5 and 3N), the homotopy performs well till λ is close to 1. Unfortunately, for low thrusts this does not work well. The precision on the shooting for low thrust $T_{\max} = 0.3$N decreases faster than for medium thrusts as shown in table 3.6. The continuation is then stopped at $\lambda = 0.75$; shooting algorithm does not converge for higher λ values. In fact, figure 3.9 shows that the control norm presents a high number of oscillations, in addition, the bang-bang form appears. This causes numerical integration difficulties and shows us the limit of the used numerical method when the Hamiltonian is only continuous but not smooth.

3.2.2 Lunar orbit target

The same techniques used for the target L_2 are used here. We obtain similar results as the previous section. The difference only appears with the second order conditions. As for the target L_2 numerical tests are proceeded for medium

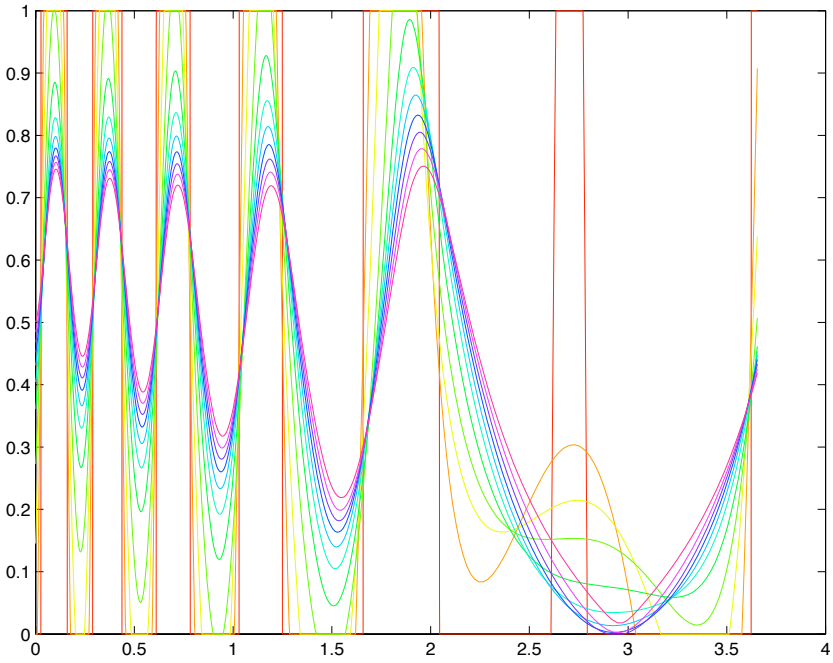

Figure 3.6: Control norm $|u_\lambda|$ versus time for λ equal to 0.0 till 0.999 (red), energy-consumption homotopy, target L_2, $T_{\max} = 5$N.

thrusts *i.e.* 10, 7, 5 and 3N. We give results for two thrust 10 and 5N. We have no results for low thrust for instance 0.3N like for target L_2 because we have not managed to solve (P^{L^2}) (nor (P_t) as yet) for the target LO.

The initialization strategy is known: An arbitrary initialization provides a solution for $t_f = t_{f_{\min}}$, then we assume intuitively that when the transfer time increases the maximum of $|u|$ decreases, thus an extremal which ensures the constraint $|u| < 1$ may be found.This method is detailed in table 3.7. This table exhibit the ratio $t_f/t_{f_{\min}}$, the control norm maximum value along the transfer and the corresponding initialization $p(0)$.

For the forthcoming numerical simulations *i.e.* energy-consumption homotopy, the extremal corresponding to $c_{t_f} = t_f/t_{f_{\min}} = 1.6$ is chosen. The extremal and the control norm are given respectively in figure 3.12 and figure 3.13.

Let us use the same method for a lower thrust for instance $T_{\max} = 5$N. We resume in table 3.8 the different step to solve the minimum energy problem.

As in the previous chapter we recall that discrete homotopic step means that the solution of the previous step is introduced as an initialization for the current one, the homotopic parameter is the ratio $c_{t_f} = t_f/t_{f_{\min}}$. From the table 3.8, one can identify two points: Firstly arbitrary initializations are not valid when the final time increases thus we introduce a discrete homotopy on c_{t_f}, secondly when increasing the final time we do not ensure that $max_{[0,t_f]}|u|$ is automatically decreasing, this is shown for both $T_{\max} = 10$ and 5N. The extremal corresponding to $t_f/t_{f_{\min}} = 1.7$ is chosen to perform the next step. The extremal and the control norm are given respectively in figure 3.12 and

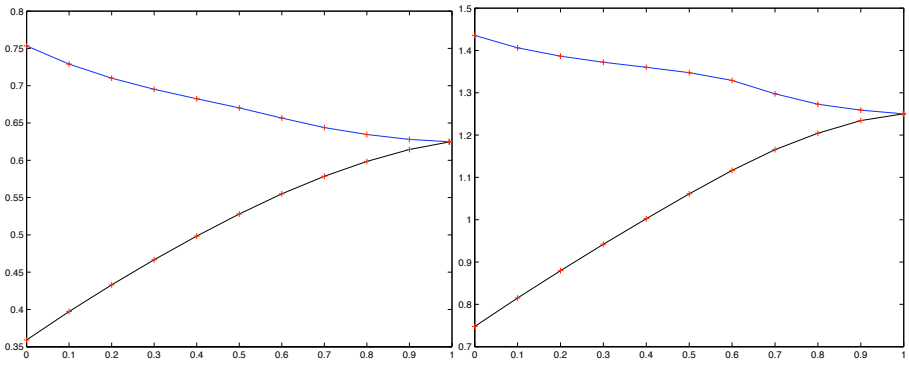

Figure 3.7: Value function for different λ, energy-consumption homotopy, target L_2, $T_{\max} = 10$N left and $T_{\max} = 5$N right, $J(u_\lambda)$ in blue and $J_\lambda(u_\lambda)$ in black, computed points in red.

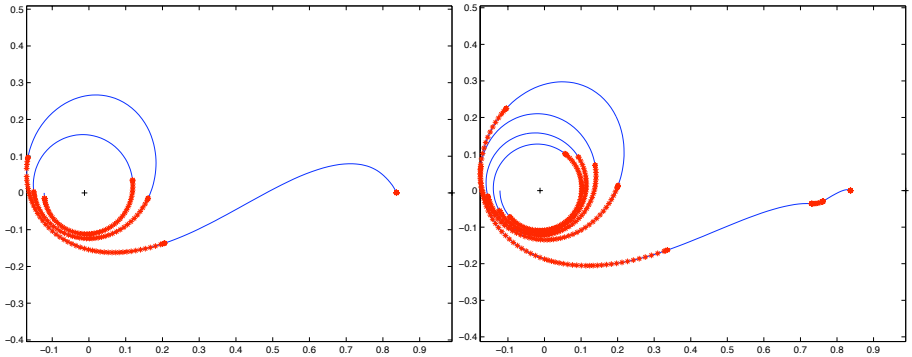

Figure 3.8: Minimum fuel consumption optimal trajectory to L_2, energy-consumption homotopy, $T_{\max} = 10$N left and $T_{\max} = 5$N right, CR3BP frame.

figure 3.13.

The maximum principle gives only a first order necessary condition. To ensure local optimality, second order necessary conditions are introduced. The Hamiltonian is the same as for the target L_2 but here the final conditions describe a submanifold: The orbit LO. As in the minimum transfer case conjugate point tests are not adequate therefore we use the focal point test. Here final time is fixed, we recall the theoretical framework and explain the suitable numerical tests for this case. The Hamiltonian is noted H for the sake of generality.

Let $z = (x, p)$ be a reference extremal. It is a smooth solution of $\dot{z} = \overrightarrow{H}(z)$ where $\overrightarrow{H}(z) = (\frac{\partial H}{\partial p}(x,p), -\frac{\partial H}{\partial x}(x,p))$, defined on $[0, t_f]$, satisfying the transversality condition $z(t_f) \in {X_f}^\perp$, here as in the previous chapter X_f does not only denote the final condition on the state but it denotes the final conditions both on the state and the costate (deriving from the transversality conditions) thus here X_f is a submanifold of $\mathbf{R}^8$.

Definition 3.2.5. The variational equation on $[0, t_f]$, $\dot{\delta z}(t) = \overrightarrow{H}'(z(t))\delta z(t)$ is called the *Jacobi equation* along $z(.)$. A *Jacobi field* is a non trivial solution $J(t) = (\delta x(t), \delta p(t))$ of the Jacobi equation along $z(.)$.

Table 3.6: Energy-Consumption homotopy, target L_2, $T_{\max} = 0.3$N.

Homotopic Step λ	Shooting Function $\lvert S_\lambda^{L_2}\rvert$
$0.0 \rightarrow 0.1$	$\sim 10^{-9}$
$0.1 \rightarrow 0.2$	$\sim 10^{-9}$
$0.2 \rightarrow 0.3$	$\sim 10^{-8}$
$0.3 \rightarrow 0.4$	$\sim 10^{-9}$
$0.4 \rightarrow 0.5$	$\sim 10^{-8}$
$0.5 \rightarrow 0.6$	$\sim 10^{-7}$
$0.6 \rightarrow 0.61$	$\sim 10^{-7}$
$0.61 \rightarrow 0.62$	$\sim 10^{-8}$
$0.62 \rightarrow 0.63$	$\sim 10^{-7}$
$0.63 \rightarrow 0.64$	$\sim 10^{-8}$
$0.64 \rightarrow 0.65$	$\sim 10^{-5}$
$0.65 \rightarrow 0.66$	$\sim 10^{-4}$
$0.66 \rightarrow 0.67$	$\sim 10^{-3}$
$0.67 \rightarrow 0.68$	$\sim 10^{-3}$
$0.68 \rightarrow 0.69$	$\sim 10^{-2}$
$0.69 \rightarrow 0.7$	$\sim 10^{-2}$
$0.7 \rightarrow 0.71$	$\sim 10^{-2}$
$0.71 \rightarrow 0.72$	$\sim 10^{-1}$
$0.72 \rightarrow 0.73$	$\sim 10^{-1}$
$0.73 \rightarrow 0.74$	$\sim 10^{-1}$
$0.74 \rightarrow 0.75$	$\sim 10^{-1}$

Definition 3.2.6. We say that $t_{\text{focal}} > 0$ is a focal time if there exists a Jacobi field $J = (\delta x, \delta p)$ such that $\delta x(0) = 0$ and $J(t_{\text{focal}})$ is tangent to ${X_f}^\perp$, $J(t_{\text{focal}}) \in T_{z(t_{\text{focal}})}{X_f}^\perp$.

Proposition 3.2.6. *[1, 5, 6] A regular reference trajectory z is locally optimal up to first focal time.*

The method to compute focal times is the following [5, 6].
In the minimum consumption case the final time is fixed. One has to consider the vector space of dimension $n = 4$ generated by the Jacobi fields $J_i = (\delta x_i, \delta p_i)$, $i = 1, \ldots, n$, such that $J(t_{\text{focal}}) \in T_{z(t_{\text{focal}})}{X_f}^\perp$ and then integrate the Jacobi equation backwards in time. The time t_{focal} is a focal time whenever

$$\text{rank}(\delta x_1(-t_{\text{focal}}), \delta x_2(-t_{\text{focal}}), \delta x_3(-t_{\text{focal}}), \delta x_4(-t_{\text{focal}})) < n.$$

An extremal is locally optimal if the the first focal time $t_{\text{focal}1}$ satisfies $t_{\text{focal}1} < 0$. The numerical rank tests show that the computed extremals for $T_{\max} = 10$N and $T_{\max} = 5$N are locally optimal.

Once the minimum energy problem *i.e.* $(S_{L^2}^{LO} p(0)) = 0$ is solved. The energy-consumption homotopy *i.e.* resolution of $(P_\lambda)_{\lambda>0}$ can be started. We use the differential path following as in the previous section. The solution of (P_0) is used to initialize the differential homotopy on λ. We give similar results for the two

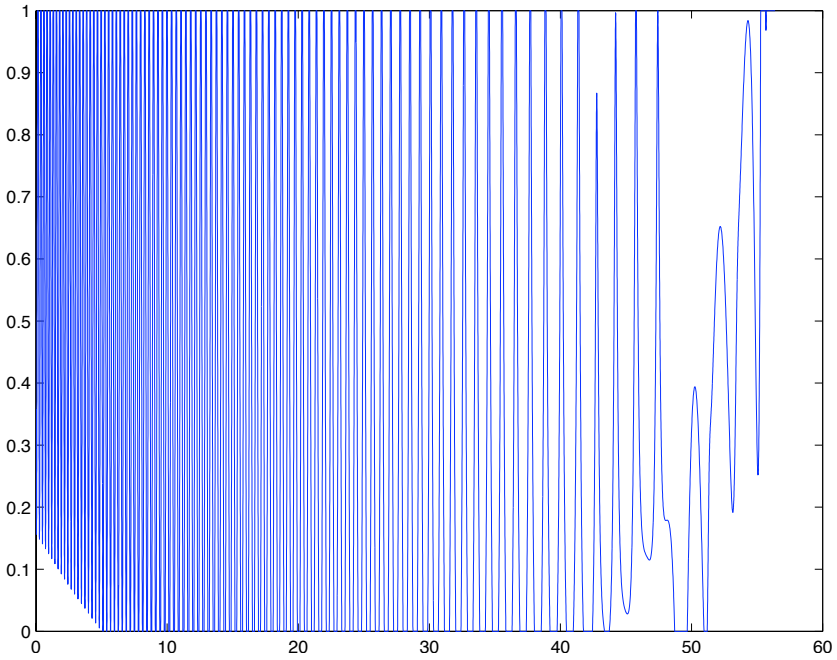

Figure 3.9: Control norm $|u_\lambda|$ versus time for $\lambda = 0.75$, energy-consumption homotopy, target L_2, $T_{\max} = 0.3$N.

different thrusts $T_{\max} = 10$N and $T_{\max} = 5$N. Tables 3.9 and 3.10 summarize the homotopic steps and gives the precision on the shooting function norm at the end of the step. The control norm variation along the homotopy is represented for different λ values in Fig. 3.14 and Fig. 3.15. The bang-bang (norm of the) control is approximated as λ tends to one.

We can see in Fig. 3.16 that the cost criteria $J(u_\lambda) = \int_0^{t_f} |u_\lambda| \mathrm{d}t$ tends, by superior values, to a limit value when λ tends to one and the criteria $J_\lambda(u_\lambda) = \int_0^{t_f} (\lambda|u_\lambda| + (1-\lambda)|u_\lambda|^2) \mathrm{d}t$ tends, by inferior values, to the same limit value when λ tends to one, this limit value as stated before is $J(u) = \int_0^{t_f} |u| \mathrm{d}t$. The numerical simulations are consistent with the preposition 3.2.2.

Both the extremal trajectories for $\lambda = 0.99$ and $T_{\max} = 10$N and for $\lambda = 0.999$ and $T_{\max} = 5$N are plotted in the CR3BP-rotating frame (*cf.*Fig. 3.17). Red points indicate (maximum) thrust locations on the extremal trajectories.

In this section, we introduce a continuation to connect minimum energy to minimum consumption transfer to find a suitable initialization to solve (P). This method gives us extremal for different medium thrusts however the control is only continuous and so is the true Hamiltonian. This fact has two drawbacks: Firstly, when the control is only continuous and non smooth, computing the derivative of the shooting function by variational (method used in *hampath*) is not an adequate method and its impact is clear: Deterioration of the precision on the shooting function when λ is close to 1 (close to the bang-bang form), this issue is detailed for the thrust $T_{\max} = 0.3$N. Secondly, we are enable to test local optimality of the computed extremals because second order conditions as defined are only valid for the smooth case.

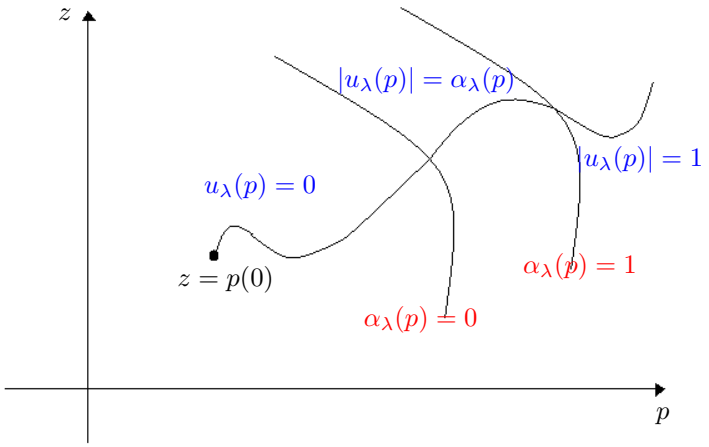

Figure 3.10: The control u_λ switches are of order one, $u_\lambda(p)$ crosses the curves $\alpha_\lambda(p) = 0$ and $\alpha_\lambda(p) = 1$.

Table 3.7: Minimum energy transfer initialization table - target LO, $T_{\max} = 10\text{N}$. $max_{[0,t_f]}|u|$ does not always decreases when the transfer time increases, see the case of $t_f/t_{f\,\min} = 1.4$ and 1.5.

$t_f/t_{f\,\min}$	$max_{[0,t_f]}\|u\|$	$p(0)$
1.0	4.12	$[10^{-2}10^{-2}10^{-2}10^{-2}]$
1.1	2.02	$5[10^{-3}10^{-3}10^{-3}10^{-3}]$
1.2	1.22	$[10^{-2}10^{-2}10^{-2}10^{-2}]$
1.3	1.02	$[10^{-2}10^{-2}10^{-2}10^{-2}]$
1.4	1.15	$5[10^{-3}10^{-3}10^{-3}10^{-3}]$
1.5	1.49	$[10^{-2}10^{-2}10^{-2}10^{-2}]$
1.6	0.83	$[10^{-2}10^{-2}10^{-2}10^{-2}]$
1.7	0.72	$[10^{-2}10^{-2}10^{-2}10^{-2}]$

3.3 Logarithmic barrier homotopy

We introduce the logarithmic barrier homotopy as follows.

$$(P_\varepsilon)\begin{cases} \min J_\varepsilon(u) = \int_0^{t_f} |u| - \varepsilon[\log|u| + \log(1-|u|)]\,\mathrm{d}t \\ \dot{x} = F(x,u) \\ x(0) \in X_0 \\ x(t_f) \in X_f \end{cases}$$

The parameter ε is strictly positive *i.e.* $\varepsilon > 0$. The original control set which was the closed ball in $\mathbf{R}^3$ is replaced by the open pointed ball thanks to the introduction of the logarithm, in fact we do not allow the control to reach $|u| = 0$ and $|u| = 1$. One can notice that when $\varepsilon = 0$, the cost function $J_\varepsilon(u)$ is identical to the cost function $J(u)$ of the problem (P).

Unfortunately, for this continuation case, we have not managed to prove the existence of optimal solution of the optimal control problem (P_ε). In fact, the

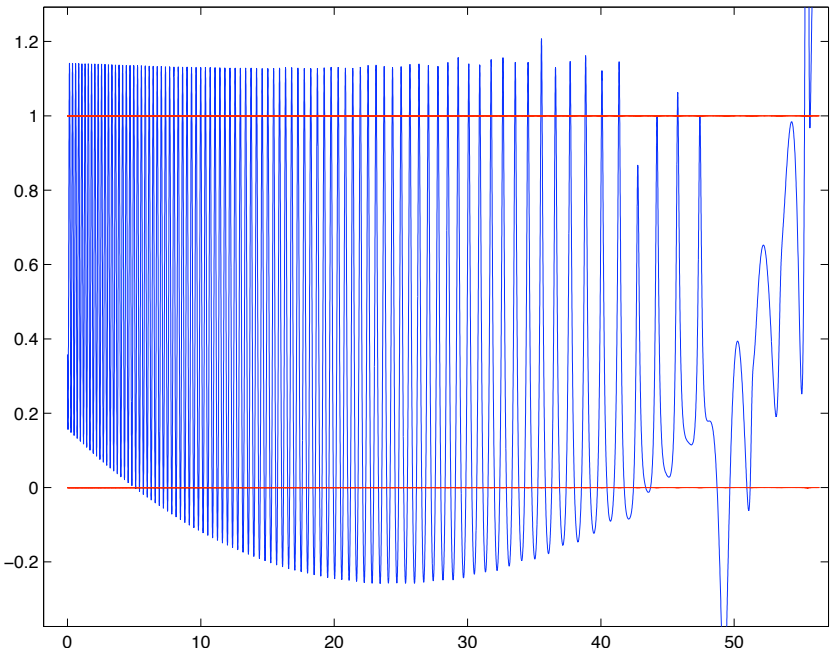

Figure 3.11: Function $\alpha_\lambda(p)$ versus time for $\lambda = 0.75$, energy-consumption homotopy, target L_2, $T_{\max} = 0.3$N.

Filippov theorem is not applicable because the admissible control values are in the open pointed ball of $\mathbf{R}^3$ *i.e.* $u \in B_o(0,1) \setminus \{0\}$ which is a non convex set. Thus we suppose that such optimal solution of (P_ε) exists. Let us then write the first order necessary condition using the PMP. The corresponding Hamiltonian is:

$$H_\varepsilon(x,u,p) = -|u| + \varepsilon(\log(|u|) + \log(1-|u|)) + H_0 + u_1 \frac{T_{\max}}{m} H_1 + u_2 \frac{T_{\max}}{m} H_2 + u_3 \frac{T_{\max}}{m} H_3.$$

By Cauchy-Schwartz,

$$H_\varepsilon(x,u,p) \leq \underbrace{H_0 + (\underbrace{\frac{T_{\max}}{m}|\varphi(p)| - 1}_{\psi(p)})|u| + \varepsilon(\log(|u|) + \log(1-|u|))}_{g_\varepsilon(|u|)}.$$

The maximization condition implies for $\varepsilon > 0$:

$$\begin{aligned} & g'_\varepsilon(|u|) = 0 \\ \Leftrightarrow\ & |u| = |u_\varepsilon| = \alpha_\varepsilon(p) \end{aligned}$$

with

$$\alpha_\varepsilon(p) = \frac{2\varepsilon}{2\varepsilon - \psi(p) + \sqrt{\psi(p)^2 + 4\varepsilon^2}}.$$

The optimal control is then:

$$u_\varepsilon = \alpha_\varepsilon(p) \frac{\varphi(p)}{|\varphi(p)|}$$

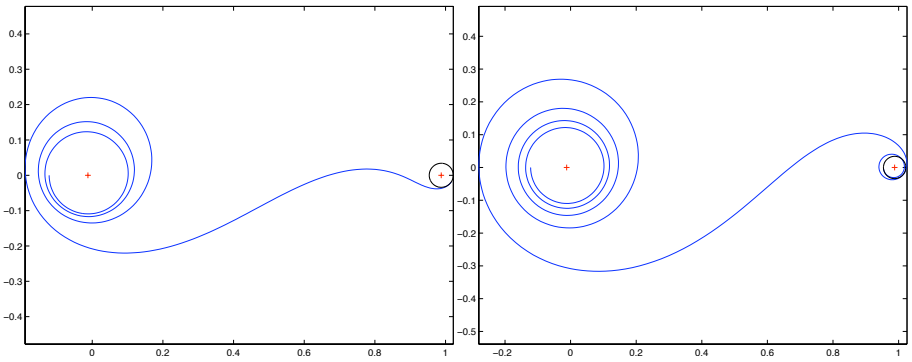

Figure 3.12: Minimum energy optimal trajectory to LO, $T_{\max} = 10$N left and $T_{\max} = 5$N right, CR3BP frame.

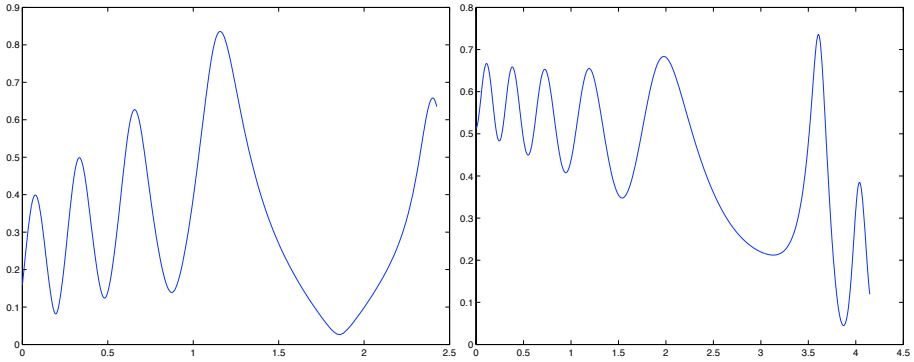

Figure 3.13: Control norm $|u|$ versus time - minimum energy case - target LO, $T_{\max} = 10$N and $t_f = 1.5 t_{f\,\min}$ left and $T_{\max} = 5$N and $t_f = 1.7 t_{f\,\min}$ right.

. The true Hamiltonian is:

$$H_\varepsilon(x,p) = H_0 + \psi(p)\alpha_\varepsilon(p) + \varepsilon[\log \alpha_\varepsilon(p) + \log(1-\alpha_\varepsilon(p))].$$

The optimal control solution and the true Hamiltonian are smooth, we say that the problem (P_ε) is regularizing the problem (P). The optimal control solution is smooth for all $\varepsilon > 0$ even if the control solution is very close to bang-bang when ε is so close to 0. This fact is very important for two reasons. First computing the shooting function using the variational equations is relevant when using *hampath*. Second one can compute second order conditions to verify optimal locality of computed solutions. Let us furnish some results concerning the criteria J_ε:

Proposition 3.3.1. *[21] For all $0 < \varepsilon \leq \varepsilon'$, if u, u_ε and $u_{\varepsilon'}$ are respectively the optimal controls solution of the problems (P), (P_ε) and $(P_{\varepsilon'})$, then*

$$J(u) \leq J(u_\varepsilon) \leq J_\varepsilon(u_\varepsilon) \leq J_{\varepsilon'}(u_{\varepsilon'}).$$

Proof. (i) We have $J(u) \leq J(u_\varepsilon)$ because the control u is the optimal control minimizing the criteria $J(u)$.

Table 3.8: Minimum energy transfer initialization table, target LO, $T_{\max} = 5$N.

$t_f/t_{f_{\min}}$	$max_{[0,t_f]}\|u\|$	$p(0)$
1.0	2.09	$[10^{-2}10^{-2}10^{-2}10^{-2}]$
1.1	1.66	$[10^{-2}10^{-2}10^{-2}10^{-2}]$
1.2	1.33	$[10^{-2}10^{-2}10^{-2}10^{-2}]$
1.3	1.16	$[10^{-2}10^{-2}10^{-2}10^{-2}]$
1.4	1.34	$5[10^{-3}10^{-3}10^{-3}10^{-3}]$
1.5	0.94	$[10^{-2}10^{-2}10^{-2}10^{-2}]$
1.6	0.86	$[10^{-2}10^{-2}10^{-2}10^{-2}]$
1.7	0.74	discrete homotopic step

Table 3.9: Energy-Consumption homotopy, target LO, $T_{\max} = 10$N.

Homotopic Step λ	Shooting Function $\|S_\lambda^{LO}\|$
$0.0 \rightarrow 0.1$	$\sim 10^{-13}$
$0.1 \rightarrow 0.2$	$\sim 10^{-12}$
$0.2 \rightarrow 0.3$	$\sim 10^{-12}$
$0.3 \rightarrow 0.4$	$\sim 10^{-13}$
$0.4 \rightarrow 0.5$	$\sim 10^{-5}$
$0.5 \rightarrow 0.6$	$\sim 10^{-5}$
$0.6 \rightarrow 0.7$	$\sim 10^{-5}$
$0.7 \rightarrow 0.8$	$\sim 10^{-4}$
$0.8 \rightarrow 0.9$	$\sim 10^{-5}$
$0.9 \rightarrow 0.99$	$\sim 10^{-4}$

(ii) We have $-\varepsilon[\log|u_\varepsilon| + \log(1-|u_\varepsilon|)] \geq 0$ since $0 < |u_\varepsilon| < 1$, then:

$$0 \leq |u_\varepsilon| \leq |u_\varepsilon| - \varepsilon[\log|u_\varepsilon| + \log(1-|u_\varepsilon|)]$$
$$\int_0^{t_f} |u_\varepsilon|\,\mathrm{d}t \leq \int_0^{t_f} |u_\varepsilon| - \varepsilon[\log|u_\varepsilon| + \log(1-|u_\varepsilon|)]\,\mathrm{d}t$$
$$J(u_\varepsilon) \leq J_\varepsilon(u_\varepsilon)$$

(iii) Let u be an admissible control. For all $0 < \varepsilon \leq \varepsilon'$, we have:

$$0 \leq |u| - \varepsilon[\log|u| + \log(1-|u|)] \leq |u| - \varepsilon'[\log|u| + \log(1-|u|)]$$
$$\int_0^{t_f} |u| - \varepsilon[\log|u| + \log(1-|u|)]\,\mathrm{d}t \leq \int_0^{t_f} |u| - \varepsilon'[\log|u| + \log(1-|u|)]\,\mathrm{d}t$$
$$J_\varepsilon(u) \leq J_{\varepsilon'}(u)$$

thus $J_\varepsilon(u_\varepsilon) \leq J_\varepsilon(u_{\varepsilon'}) \leq J_{\varepsilon'}(u_{\varepsilon'})$.

□

We have no convergence results as in the energy-consumption homotopy. Thanks to the previous proposition one is sure only of the convergence of $J_\varepsilon(u_\varepsilon)$

Table 3.10: Energy-Consumption homotopy, target LO, $T_{\max} = 5$N.

Homotopic Step λ	Shooting Function $\lvert S_\lambda^{LO}\rvert$
$0.0 \rightarrow 0.1$	$\sim 10^{-12}$
$0.1 \rightarrow 0.2$	$\sim 10^{-11}$
$0.2 \rightarrow 0.3$	$\sim 10^{-10}$
$0.3 \rightarrow 0.4$	$\sim 10^{-12}$
$0.4 \rightarrow 0.5$	$\sim 10^{-11}$
$0.5 \rightarrow 0.6$	$\sim 10^{-6}$
$0.6 \rightarrow 0.7$	$\sim 10^{-5}$
$0.7 \rightarrow 0.8$	$\sim 10^{-4}$
$0.8 \rightarrow 0.9$	$\sim 10^{-4}$
$0.9 \rightarrow 0.999$	$\sim 10^{-3}$

when ε tends to 0, the corresponding limit is high or equal to $J(u)$. In fact, to ensure the convergence of $J_\varepsilon(u_\varepsilon)$ to $J(u)$, one has to suppose that for all admissible control u for the problem (P), there exists a sequence of admissible controls $(u_{\varepsilon_k})_k$ of the problem $(P_{\varepsilon_k})_k$ such that $0 < |u_{\varepsilon_k}| < 1$ and which converges to u. Convergence of $J_\varepsilon(u_\varepsilon)$ to $J(u)$ is verified a posteriori by numerical simulations.

Let us begin the numerical resolution. The strategy is to find an initialization of (P_ε) for a certain value ε_0 of ε and then let ε tend to zero, as low as possible, since (P_ε) tends to (P) when ε tends to 0.

The difficulty is how to find a suitable initialization to solve $S_{\varepsilon_0}(z) = 0$ (shooting function of (P_{ε_0}))? and also how to find the suitable ε_0? The idea is the following: Find a value $\varepsilon_0 > 0$ and a value $\lambda_0 \in [0, 1]$ such that the initialization solution of (P_{λ_0}) (we recall that the problem (P_λ) defines the energy-consumption *i.e.* $L^2 - L^1$ continuation) is a suitable guess to solve $S_{\varepsilon_0}(z) = 0$.

We proceed by numerical tests for medium thrust as in previous section *i.e.* $L^2 - L^1$ continuation. Numerical tests are proceeded successfully for different medium maximal thrust values *i.e.* 10, 7, 5 and 3N. We focus in this section on the numerical results for two maximal thrusts $T_{\max} = 10$ and 5N. We recall that the spacecraft mass is $m = 1500$kg. The initial point transfer is as usual X_0.

3.3.1 Target libration point L_2

Let us consider first the transfer from X_0 to $X_f = L_2$. For $T_{\max} = 10$N, a $(P)_\varepsilon$ solution is obtained for $\varepsilon = 10$ using the minimum energy solution as an initial guess (*i.e.* solution of (P_λ) for $\lambda = 0$). The differential homotopy on the parameter ε is considered in order to reach lower ε values. We resume in table 3.11 the homotopic steps and we give the precision on the shooting function $S_\varepsilon^{L_2}$ at the end of the step.

The control norm variation along the homotopy is represented for different ε values Fig. 3.18. The bang-bang (norm of the) control is approximated as ε tends to zero.

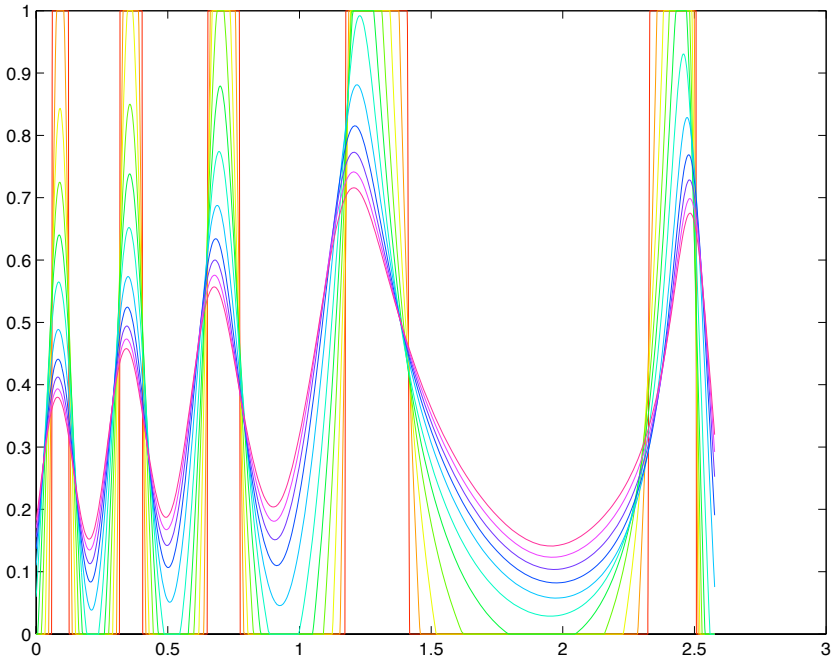

Figure 3.14: Control norm $|u_\lambda|$ versus time for λ equal to 0.0 till 0.99 (red), energy-consumption homotopy, target LO, $T_{\max} = 10\text{N}$.

Figure 3.19 shows that both cost criteria $J(u_\varepsilon) = \int_0^{t_f} |u_\varepsilon| \mathrm{d}t$ and $J_\varepsilon(u_\varepsilon) = \int_0^{t_f} (|u_\varepsilon| - \varepsilon[\log|u_\varepsilon| + \log(1 - |u_\varepsilon|)])\mathrm{d}t$ tend, by superior values, to a limit value when ε tends to zero which is consistent with proposition 3.3.1.

The extremal solution for $\varepsilon = 10^{-5}$ is plotted in the CR3BP-rotating frame (*cf.*Fig. 3.20). Red points indicate (maximum) thrust locations on the extremal.

From the minimum energy solution to the minimum consumption solution a new switch in the control norm appears. The new switch is clearer by the logarithmic barrier homotopy than that of the energy-consumption, because when the homotopic λ becomes closer to 1 (*i.e.* > 0.9935) the homotopy is not performing well *i.e.* non convergence. Thus the solution given by the logarithmic barrier is better since it is closer to the bang-bang form and its value function is better. Since the true Hamiltonian is smooth for all $\varepsilon > 0$ and the admissible control values are in an open set *i.e.* $u \in B_o(0,1) \setminus \{0\}$, one is also able to test optimal locality of computed solutions for all $\varepsilon > 0$. Before launching second order condition tests one has to ensure the regularity of the extremals *i.e.* $\frac{\partial^2 H_\varepsilon}{\partial u^2}$ is negative definite along every extremal.

Proposition 3.3.2. *Extremals solutions of* (P_ε) *are regular.*

Proof. Let (x, p, u) be an extremal of the optimal control problem (P_ε), then the Hamiltonian depends on $\alpha = |u|$ and not u:

$$H_\varepsilon(x, p, u) = H_0 + \psi(p)\alpha + \varepsilon[\log\alpha + \log(1 - \alpha)].$$

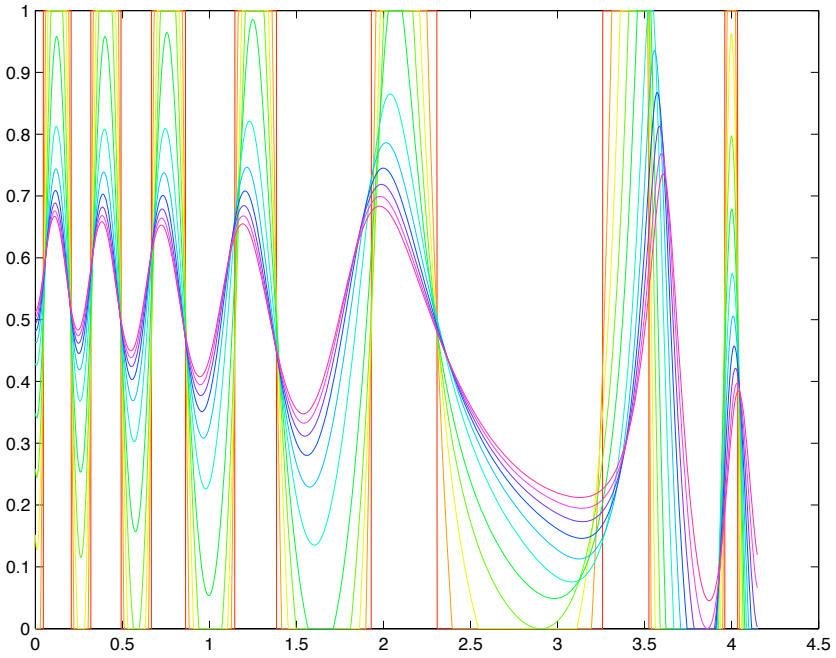

Figure 3.15: Control norm $|u_\lambda|$ versus time for λ equal to 0.0 till 0.999 (red), energy-consumption homotopy, target LO, $T_{\max} = 5$N.

Thus $\frac{\partial^2 H_\varepsilon}{\partial \alpha^2} < 0$ is sufficient to prove extremal regularity. It is obvious that: $\frac{\partial^2 H_\varepsilon}{\partial \alpha^2} = -\varepsilon(\frac{1}{\alpha^2} + \frac{1}{(1-\alpha}})^2) < 0$, then the result follows. □

Since the target is a point *i.e.* L_2, we carry out second order conditions tests using the conjugate points. Numerical rank tests show that the computed extremals for $T_{\max} = 10$N and for different ε values are locally optimal.

Let us consider a lower thrust, for instance, $T_{\max} = 5$N. The solution of the minimum energy problem *i.e.* $(P_{\lambda=0})$ is set as an initialization for the logarithmic barrier for $\varepsilon = 0.5$. The homotopic steps from $\varepsilon = 0.5$ to $\varepsilon = 1.1 \times 10^{-5}$ are summarized in the table 3.12.

The control norm variation is represented for different ε values Fig. 3.21.

Figure 3.22 shows that both cost criteria $J(u_\varepsilon) = \int_0^{t_f} |u_\varepsilon| \mathrm{d}t$ and $J_\varepsilon(u_\varepsilon) = \int_0^{t_f} (|u_\varepsilon| - \varepsilon[\log |u_\varepsilon| + \log(1 - |u_\varepsilon|)]) \mathrm{d}t$ tend, by superior values, to a limit value when ε tends to zero which is consistent with proposition 3.3.1.

The extremal solution for $\varepsilon = 1.1 \times 10^{-5}$ is plotted in the CR3BP-rotating frame (*cf.*Fig. 3.23). Red points indicate (maximum) thrust locations on the extremal.

The numerical conjugate points rank tests show that all the computed extremals for different ε values are locally optimal except the extremal relative to $\varepsilon = 1.1 \times 10^{-5}$. Here only the local optimality is verified and the solution found here is not a global optimal for sure because the solution given by the energy-consumption homotopy is better since the value function is lower. Thus we try to find a better solution, by the logarithmic barrier homotopy, which may be the same solution using the previous homotopy. Let us consider the

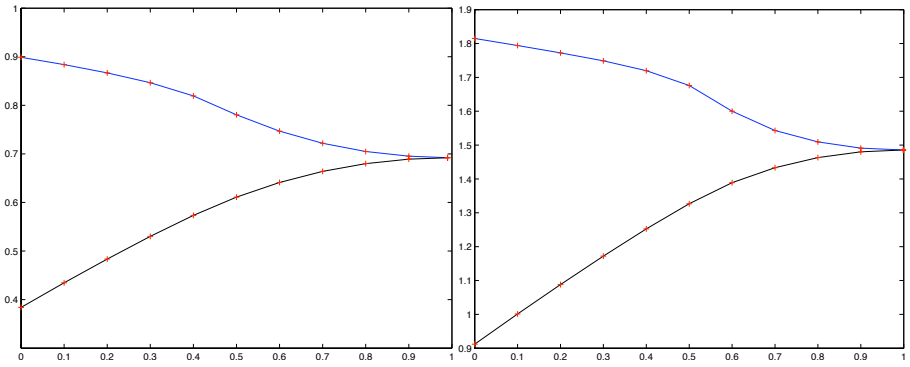

Figure 3.16: Value function for different λ, energy-consumption homotopy, target LO, $T_{\max} = 10$N left and $T_{\max} = 5$N right, $J(u_\lambda)$ in blue and $J_\lambda(u_\lambda)$ in black, computed points in red.

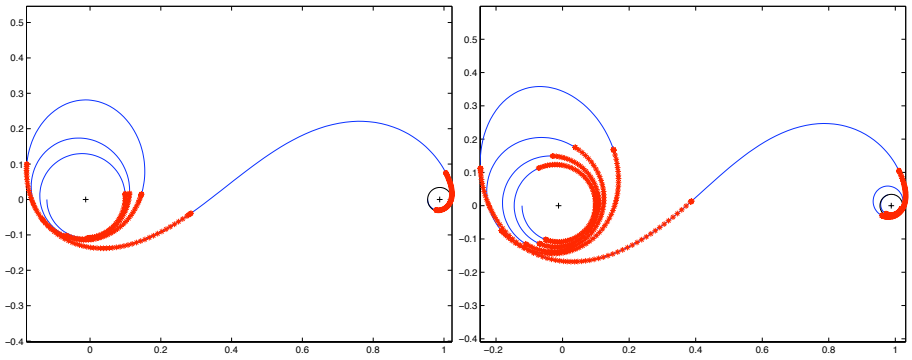

Figure 3.17: Minimum fuel consumption optimal trajectory to LO, energy-consumption homotopy, $T_{\max} = 10$N left and $T_{\max} = 5$N right, CR3BP frame.

solution of the energy-consumption homotopy (P_λ) for $\lambda = 0.4$ and embed it as an initialization to the logarithmic barrier homotopy for $\varepsilon = 0.5$. The shooting algorithm converges and the logarithmic barrier homotopy begins from $\varepsilon = 0.5$ by differential path following.

The homotopic steps from $\varepsilon = 0.5$ to $\varepsilon = 1.3 \times 10^{-5}$ are summarized in table 3.13.

The control norm variation is represented for different ε values Fig. 3.24.

Figure 3.25 shows that both cost criteria $J(u_\varepsilon) = \int_0^{t_f} |u_\varepsilon| \mathrm{d}t$ and $J_\varepsilon(u_\varepsilon) = \int_0^{t_f} (|u_\varepsilon| - \varepsilon[\log|u_\varepsilon| + \log(1 - |u_\varepsilon|)])\mathrm{d}t$ tend, by superior values, to a limit value when ε tends to zero, which is consistent with proposition 3.3.1. The extremal solution for $\varepsilon = 1.3 \times 10^{-5}$ is plotted in the CR3BP-rotating frame (*cf.* Fig. 3.26). Red points indicate (maximum) thrust locations on the extremal.

The numerical conjugate points rank tests show that all the computed extremals for different ε values are locally optimal. Here we have another solution for the minimum consumption problem better than the previous one. But, the solution found by the energy-consumption homotopy is the best compared to the solution found by the logarithmic barrier homotopy.

Table 3.11: Logarithmic barrier homotopy, target L_2, $T_{\max} = 10$N.

Homotopic Step ε	Shooting Function $\lvert S_\varepsilon^{L_2}\rvert$
$10^{1} \rightarrow 10^{0}$	$\sim 10^{-13}$
$10^{0} \rightarrow 10^{-1}$	$\sim 10^{-13}$
$10^{-1} \rightarrow 10^{-2}$	$\sim 10^{-13}$
$10^{-2} \rightarrow 10^{-3}$	$\sim 10^{-10}$
$10^{-3} \rightarrow 10^{-4}$	$\sim 10^{-3}$
$10^{-4} \rightarrow 10^{-5}$	$\sim 10^{-3}$

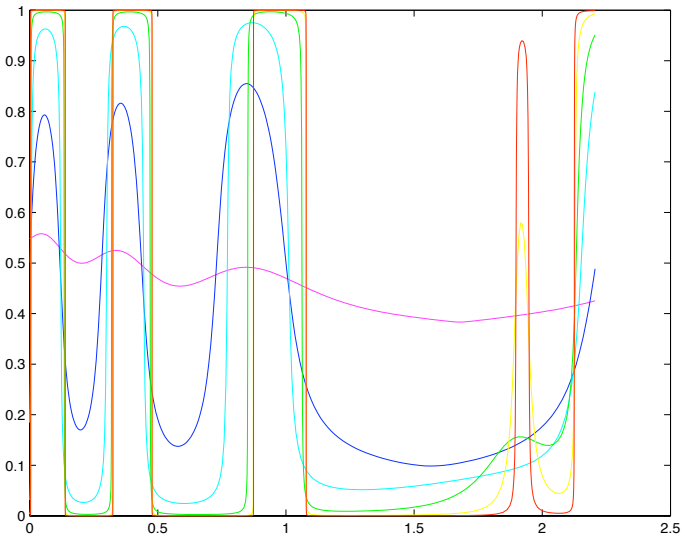

Figure 3.18: Control norm $|u_\varepsilon|$ versus time for ε equal to 1 till 10^{-5} (red), logarithmic barrier homotopy, target L_2, $T_{\max} = 10$N.

Consider a low thrust case $T_{\max} = 0.3$N. The solution of the energy-consumption homotopy (P_λ) for $\lambda = 0.0$ is a suitable guess to solve $S_\varepsilon^{L_2}(z) = 0$ for $\varepsilon = 0.5$. The logarithmic barrier homotopy is then considered starting from $\varepsilon = 0.5$. The differential continuation steps are summarized in table 3.14. We reach $\varepsilon = 10^{-5}$, the control is almost bang-bang as figure 3.28 shows. The trajectory solution for $\varepsilon = 10^{-5}$ is displayed in figure 3.27. Note that the maximum thrust points are not plotted in red this time for the sake of visibility since the extremal solution presented a high number of revolutions around the Earth. The logarithmic barrier homotopy is more efficient this time than the energy-Consumption one (failure to reach λ close to 1).

Note that for low thrust cases the transfer time is high and the number of optimal control u oscillations is high compared to the medium thrust case. Therefore we call for small homotopic steps to ensure shooting convergence till a low ε values. Figure 3.29 shows that both cost criteria $J(u_\varepsilon) = \int_0^{t_f} |u_\varepsilon| \mathrm{d}t$ and $J_\varepsilon(u_\varepsilon) = \int_0^{t_f} (|u_\varepsilon| - \varepsilon[\log|u_\varepsilon| + \log(1 - |u_\varepsilon|)])\mathrm{d}t$ tend, by superior values, to a

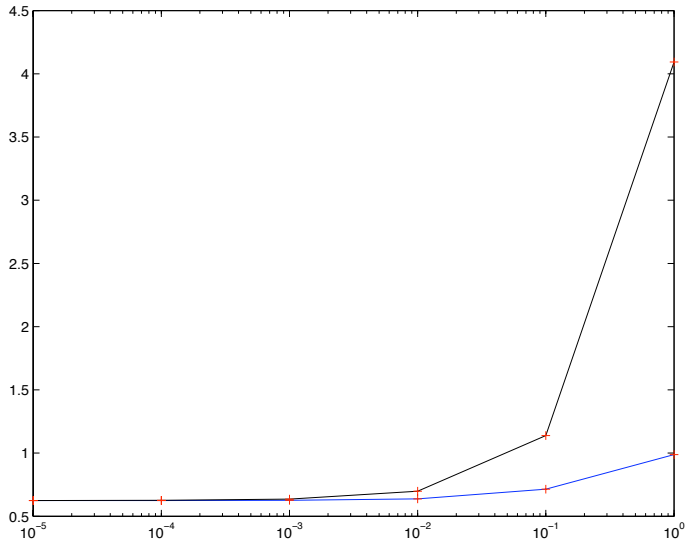

Figure 3.19: Value functions $J(u_\varepsilon)$ in blue and $J_\varepsilon(u_\varepsilon)$ in black, logarithmic barrier homotopy, target L_2, $T_{\max} = 10$N, computed points in red.

Table 3.12: Logarithmic barrier homotopy, target L_2, $T_{\max} = 5$N.

Homotopic Step ε	Shooting Function $\lvert S_\varepsilon^{L_2} \rvert$
$5 \times 10^{-1} \rightarrow 10^{-1}$	$\sim 10^{-11}$
$10^{-1} \rightarrow 10^{-2}$	$\sim 10^{-12}$
$10^{-2} \rightarrow 10^{-3}$	$\sim 10^{-6}$
$10^{-3} \rightarrow 1.5 \times 10^{-4}$	$\sim 10^{-6}$
$1.5 \times 10^{-4} \rightarrow 1.1 \times 10^{-5}$	$\sim 10^{-4}$

limit value when ε tends to zero which is consistent with proposition 3.3.1.

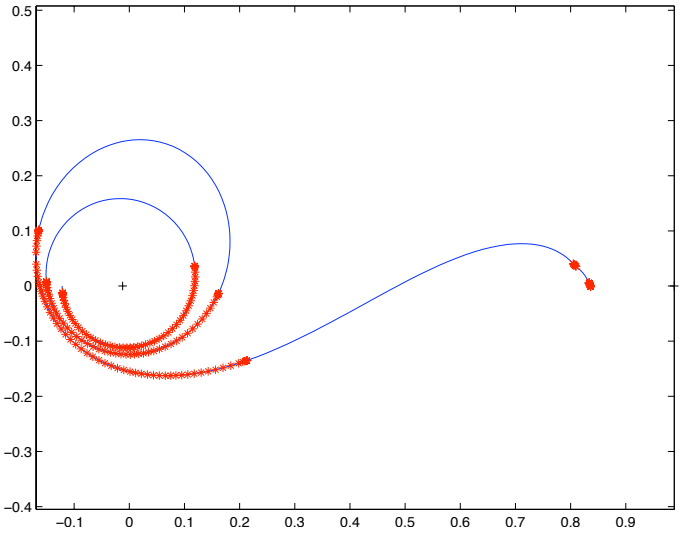

Figure 3.20: Minimum fuel consumption optimal trajectory to L_2, logarithmic barrier homotopy, $T_{\max} = 10$N, CR3BP frame.

Table 3.13: Logarithmic barrier homotopy - second initialization, target L_2, $T_{\max} = 5$N.

Homotopic Step ε	Shooting Function $\lvert S_\varepsilon^{L_2} \rvert$
$5 \times 10^{-1} \rightarrow 10^{-1}$	$\sim 10^{-12}$
$10^{-1} \rightarrow 10^{-2}$	$\sim 10^{-11}$
$10^{-2} \rightarrow 10^{-3}$	$\sim 10^{-5}$
$10^{-3} \rightarrow 10^{-4}$	$\sim 10^{-4}$
$10^{-4} \rightarrow 1.3 \times 10^{-5}$	$\sim 10^{-3}$

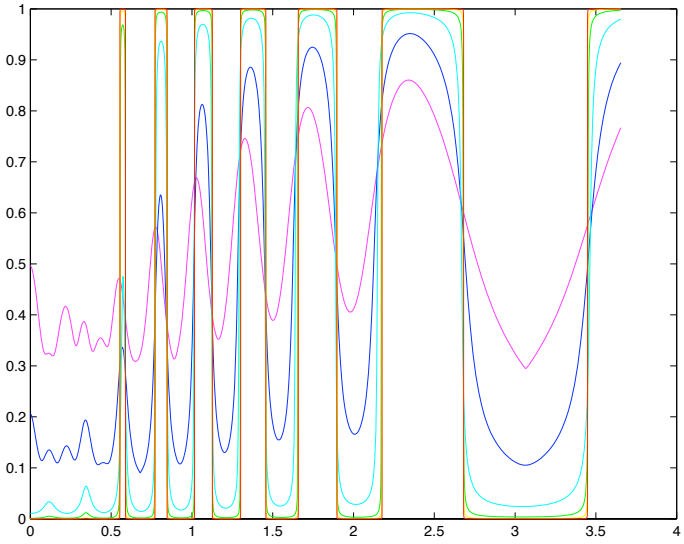

Figure 3.21: Control norm $|u_\varepsilon|$ versus time for ε equal to 0.5 till 1.1×10^{-5} (red), logarithmic barrier homotopy, target L_2, $T_{\max} = 5$N.

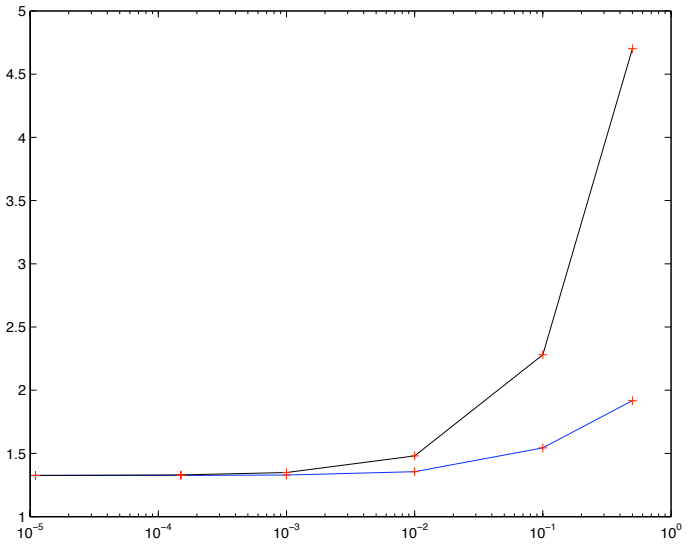

Figure 3.22: Value functions $J(u_\varepsilon)$ in blue and $J_\varepsilon(u_\varepsilon)$ in black, logarithmic barrier homotopy, target L_2, $T_{\max} = 5$N, computed points in red.

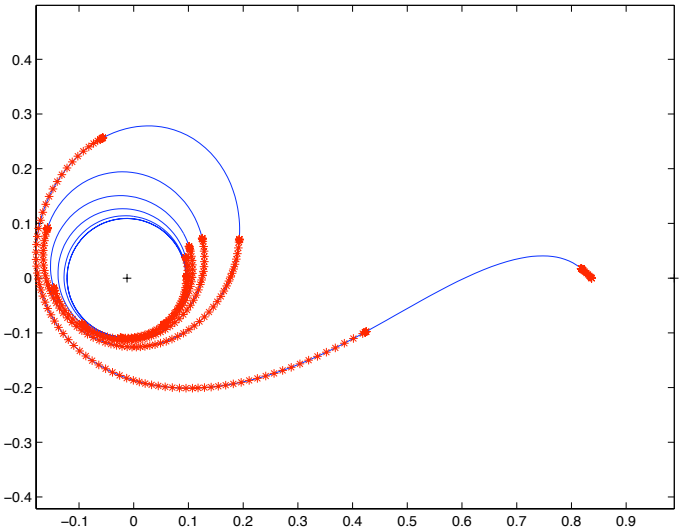

Figure 3.23: Minimum fuel consumption optimal trajectory to L_2, CR3BP frame, logarithmic barrier homotopy, $T_{\max} = 5\text{N}$.

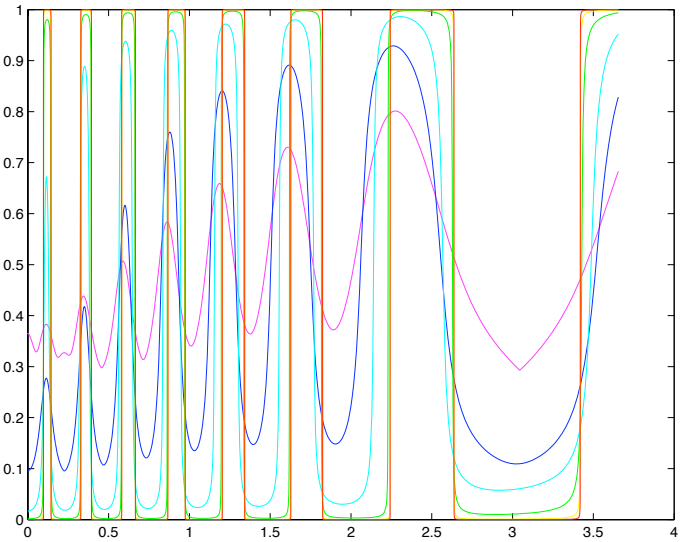

Figure 3.24: Control norm $|u_\varepsilon|$ versus time for ε equal to 0.5 till 1.3×10^{-5} (red), logarithmic barrier homotopy - second initialization, target L_2, $T_{\max} = 5\text{N}$.

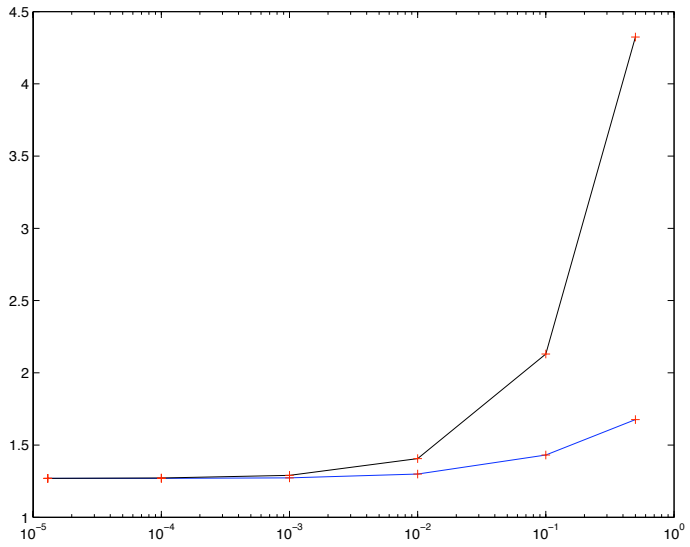

Figure 3.25: Value functions $J(u_\varepsilon)$ in blue and $J_\varepsilon(u_\varepsilon)$ in black, logarithmic barrier homotopy - second initialization, target L_2, $T_{\max} = 5$N, computed points in red.

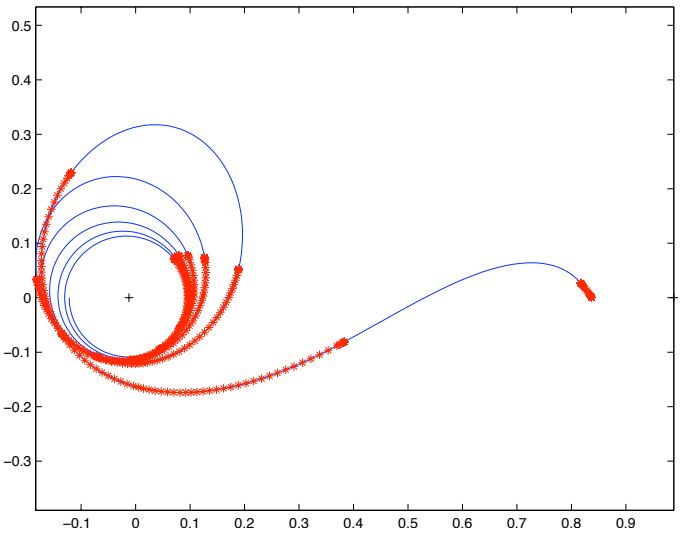

Figure 3.26: Minimum fuel consumption optimal trajectory to L_2, CR3BP frame, logarithmic barrier homotopy - second initialization, target L_2, $T_{\max} = 5$N.

Table 3.14: Logarithmic barrier homotopy, target L_2, $T_{\max} = 0.3$N.

Homotopic Step ε	Shooting Function $\lvert S_\varepsilon^{L_2} \rvert$
$5 \times 10^{-1} \ \rightarrow \ 4 \times 10^{-1}$	$\sim 10^{-10}$
$4 \times 10^{-1} \ \rightarrow \ 3 \times 10^{-1}$	$\sim 10^{-10}$
$3 \times 10^{-1} \ \rightarrow \ 2 \times 10^{-1}$	$\sim 10^{-10}$
$2 \times 10^{-1} \ \rightarrow \ 10^{-1}$	$\sim 10^{-11}$
$10^{-1} \ \rightarrow \ 9 \times 10^{-2}$	$\sim 10^{-9}$
$9 \times 10^{-2} \ \rightarrow \ 8 \times 10^{-2}$	$\sim 10^{-9}$
$8 \times 10^{-2} \ \rightarrow \ 7 \times 10^{-2}$	$\sim 10^{-8}$
$7 \times 10^{-2} \ \rightarrow \ 6 \times 10^{-2}$	$\sim 10^{-7}$
$6 \times 10^{-2} \ \rightarrow \ 5 \times 10^{-2}$	$\sim 10^{-8}$
$5 \times 10^{-2} \ \rightarrow \ 4 \times 10^{-2}$	$\sim 10^{-9}$
$4 \times 10^{-2} \ \rightarrow \ 3 \times 10^{-2}$	$\sim 10^{-7}$
$3 \times 10^{-2} \ \rightarrow \ 2 \times 10^{-2}$	$\sim 10^{-7}$
$2 \times 10^{-2} \ \rightarrow \ 10^{-2}$	$\sim 10^{-7}$
$10^{-2} \ \rightarrow \ 9 \times 10^{-3}$	$\sim 10^{-8}$
$9 \times 10^{-3} \ \rightarrow \ 8 \times 10^{-3}$	$\sim 10^{-7}$
$8 \times 10^{-3} \ \rightarrow \ 7 \times 10^{-3}$	$\sim 10^{-8}$
$7 \times 10^{-3} \ \rightarrow \ 6 \times 10^{-3}$	$\sim 10^{-7}$
$6 \times 10^{-3} \ \rightarrow \ 5 \times 10^{-3}$	$\sim 10^{-6}$
$5 \times 10^{-3} \ \rightarrow \ 4 \times 10^{-3}$	$\sim 10^{-8}$
$4 \times 10^{-3} \ \rightarrow \ 3 \times 10^{-3}$	$\sim 10^{-7}$
$3 \times 10^{-3} \ \rightarrow \ 2 \times 10^{-3}$	$\sim 10^{-6}$
$2 \times 10^{-3} \ \rightarrow \ 10^{-3}$	$\sim 10^{-6}$
$10^{-3} \ \rightarrow \ 10^{-4}$	$\sim 10^{-4}$
$10^{-4} \ \rightarrow \ 10^{-5}$	$\sim 10^{-4}$

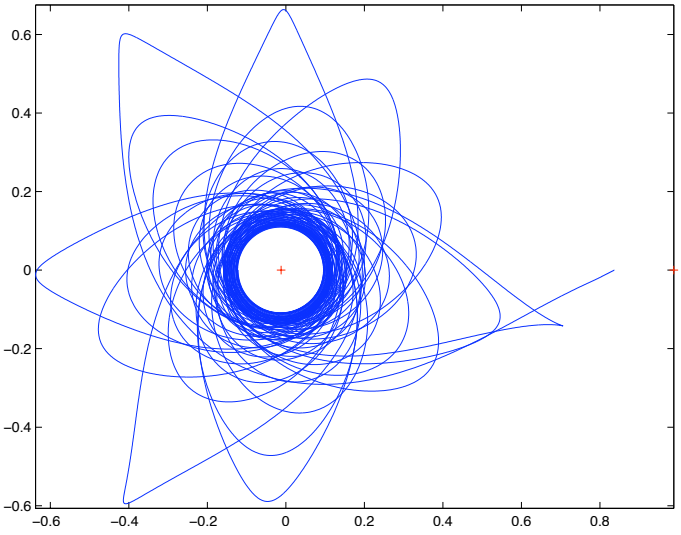

Figure 3.27: Minimum fuel consumption optimal trajectory to L_2, CR3BP frame, logarithmic barrier homotopy, target L_2, $T_{\max} = 0.3$N.

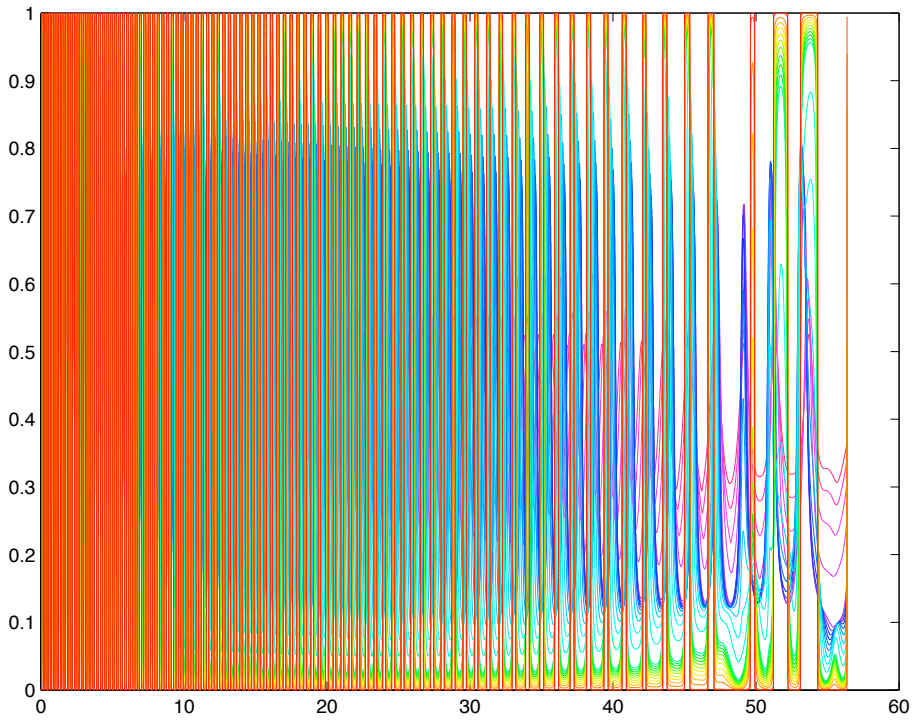

Figure 3.28: Control norm $|u_\varepsilon|$ versus time for for ε equal to 0.5 till 10^{-5} (red), logarithmic barrier homotopy, target L_2, $T_{\max} = 0.3$N.

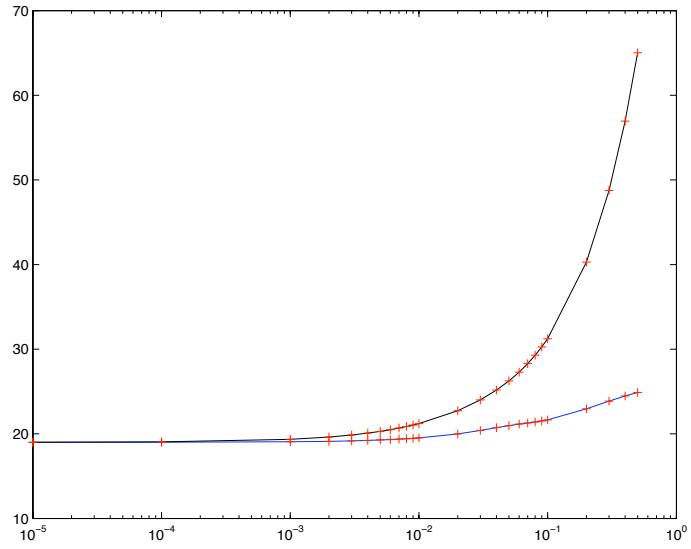

Figure 3.29: Value functions $J(u_\varepsilon)$ in blue and $J_\varepsilon(u_\varepsilon)$ in black, logarithmic barrier homotopy - second initialization, target L_2, $T_{\max} = 0.3$N, computed points in red.

The numerical conjugate points rank tests show that all the computed extremals for different ε values are locally optimal, no comparison with the energy-consumption continuation this time is possible because of the failure of this continuation.

3.3.2 Lunar orbit target

As for the energy-consumption homotopy, we exhibit results concerning the transfer starting from X_0 to the orbit around the Moon LO. Numercial simulations are accomplished for medium maximal thrusts *i.e.* $T_{\max} = 10$, 7, 5 and 3N. We have no results for low thrusts. In this section are detailed numerical computation for maximal thrusts $T_{\max} = 10$ and 5N. Let us first consider $T_{\max} = 10$. The final time is fixed at $t_f = 1.6 t_{f\,\min}$. The solution of $(P_{\lambda=0})$ is a suitable guess to solve $S_\varepsilon^{LO}(z) = 0$ for $\varepsilon \simeq 0.5$. The differential homotopy on the parameter ε is then considered in order to reach lower ε values. We resume in table 3.15 the homotopic steps and we give the precision on the shooting function at the end of the step.

The control norm variation along the homotopy is represented for different ε values Fig. 3.30. The bang-bang (norm of the) control is approximated as ε tends to zero.

Figure 3.31 shows that both cost criteria $J(u_\varepsilon) = \int_0^{t_f} |u_\varepsilon| \mathrm{d}t$ and $J_\varepsilon(u_\varepsilon) = \int_0^{t_f} (|u_\varepsilon| - \varepsilon[\log|u_\varepsilon| + \log(1 - |u_\varepsilon|)])\mathrm{d}t$ tend by superior values to a limit value when ε tends to zero which is consistent with proposition 3.3.1.

The extremal solution for $\varepsilon = 2.5 \times 10^{-5}$ is plotted in the CR3BP-rotating frame (*cf.*Fig. 3.32). Red points indicate (maximum) thrust locations on the extremal.

In this case, we obtain the same optimal solution computed via the energy-

Table 3.15: Logarithmic barrier homotopy, target LO, $T_{\max} = 10\text{N}$.

Homotopic Step ε	Shooting Function $\lvert S_\varepsilon^{LO}\rvert$
$5 \times 10^{-1} \rightarrow 10^{-1}$	$\sim 10^{-12}$
$10^{-1} \rightarrow 10^{-2}$	$\sim 10^{-12}$
$10^{-2} \rightarrow 10^{-3}$	$\sim 10^{-10}$
$10^{-3} \rightarrow 10^{-4}$	$\sim 10^{-5}$
$10^{-4} \rightarrow 2.5 \times 10^{-5}$	$\sim 10^{-5}$

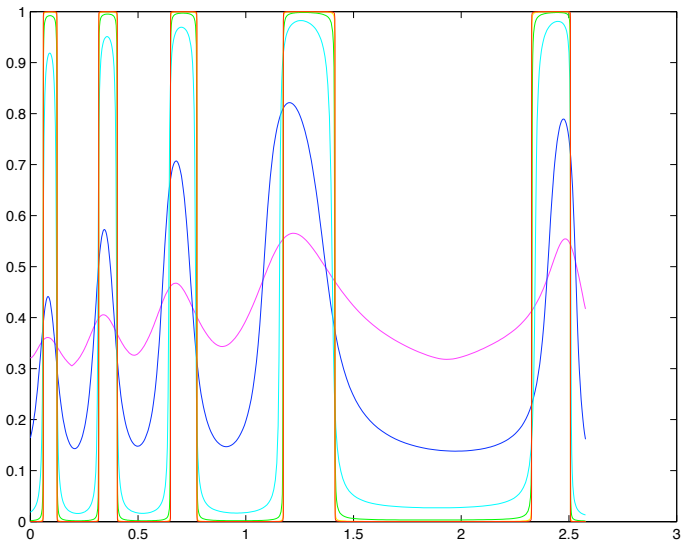

Figure 3.30: Control norm $|u_\varepsilon|$ versus time for ε equal to 1 till 2.5×10^{-5} (red), logarithmic barrier homotopy, target LO, $T_{\max} = 10\text{N}$.

consumption homotopy. Both continuations (P_λ) and (P_ε) are efficient. The advantage of the logarithmic barrier homotopy in this case is here: One can test second order optimality conditions. The target is a submanifold defined by LO, we carry out second order conditions tests using the focal points. Numerical rank tests show that the computed extremals for $T_{\max} = 10\text{N}$ and for different ε values are locally optimal (first focal times are negative).

Maximal thrust is now $T_{\max} = 5\text{N}$. The final time is fixed at $t_f / = 1.7 t_{f\,\min}$. Let us consider the solution of the energy-consumption homotopy for $\lambda = 0.1$ and embed it as an initialization to the logarithmic barrier homotopy for $\varepsilon = 0.5$. The shooting algorithm converges and we start the logarithmic barrier homotopy from $\varepsilon = 0.5$. The homotopic steps from $\varepsilon = 0.5$ to $\varepsilon = 10^{-5}$ are summarized in the table 3.16.

The control norm variation along the homotopy is represented for different ε values Fig. 3.33. The bang-bang (norm of the) control is approximated as ε tends to zero.

Figure 3.31 shows that both cost criteria $J(u_\varepsilon) = \int_0^{t_f} |u_\varepsilon| \mathrm{d}t$ and $J_\varepsilon(u_\varepsilon) =$

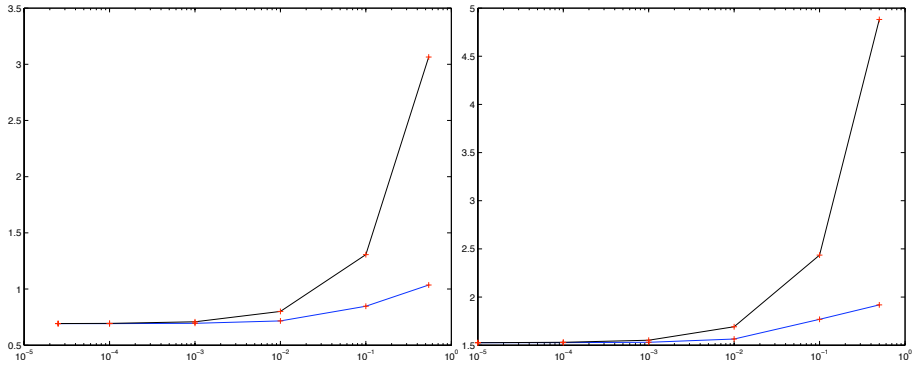

Figure 3.31: Value functions $J(u_\varepsilon)$ in blue and $J_\varepsilon(u_\varepsilon)$ in black, logarithmic barrier homotopy, target LO, $T_{\max} = 10$N left and $T_{\max} = 5$N right, computed points in red.

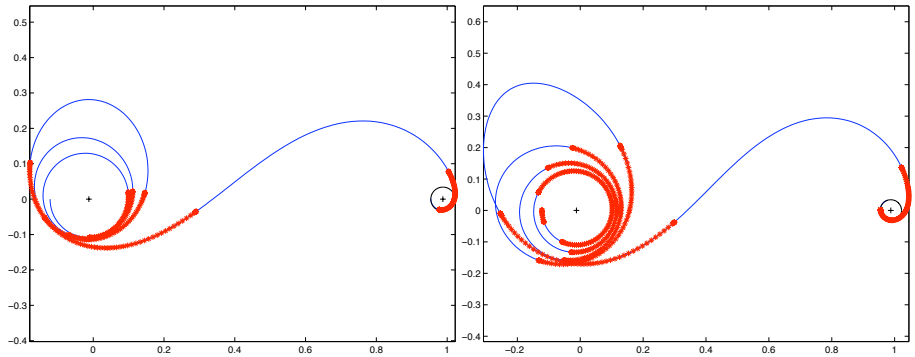

Figure 3.32: Minimum fuel consumption optimal trajectory to LO, logarithmic barrier homotopy, $T_{\max} = 10$N left and $T_{\max} = 5$N right, CR3BP frame.

$\int_0^{t_f} (|u_\varepsilon| - \varepsilon[\log|u_\varepsilon| + \log(1 - |u_\varepsilon|)])\mathrm{d}t$ tend by superior values to a limit value when ε tends to zero which is consistent with proposition 3.3.1. The extremal solution for $\varepsilon = 10^{-5}$ is plotted in the CR3BP-rotating frame (*cf.* Fig. 3.32). Red points indicate (maximum) thrust locations on the extremal. The numerical focal points rank tests show that all the computed extremals for different ε values are locally optimal. Here, only the local optimality of the solution is verified and it is certainly not globally optimal, because the solution given by the energy-consumption homotopy is better, since the value function is lower.

In this chapter, the minimum consumption transfer (P) is solved for two different targets L_2 and LO. The resolution method is based on continuation methods: The energy-consuption homotopy (P_λ) (or the L^2-L^1 homotopy) and the logarithmic barrier homotopy (P_ε). Many numerical results are stipulated in this chapter nevertheless we do not demonstrate all the numerical results, for instance those concerning maximal thrusts 7 and 3N. These pages summarize months of numerical simulations in order to implement a numerical strategy to solve (P). The main goal is to obtain an extremal of the optimal control (P) for low thrust of $T_{\max} = 0.3$N for both targets L_2 and LO to enable comparison with the mission SMART-1. In fact, when the spacecraft mass is fixed, a maximal

Table 3.16: Logarithmic barrier homotopy, target an orbit around the Moon, $T_{\max} = 5\text{N}$.

Homotopic Step ε	Shooting Function $\lvert S_\varepsilon^{LO}\rvert$
$5 \times 10^{-1} \rightarrow 10^{-1}$	$\sim 10^{-11}$
$10^{-1} \rightarrow 10^{-2}$	$\sim 10^{-10}$
$10^{-2} \rightarrow 10^{-3}$	$\sim 10^{-5}$
$10^{-3} \rightarrow 10^{-4}$	$\sim 10^{-4}$
$10^{-4} \rightarrow 10^{-5}$	$\sim 10^{-3}$

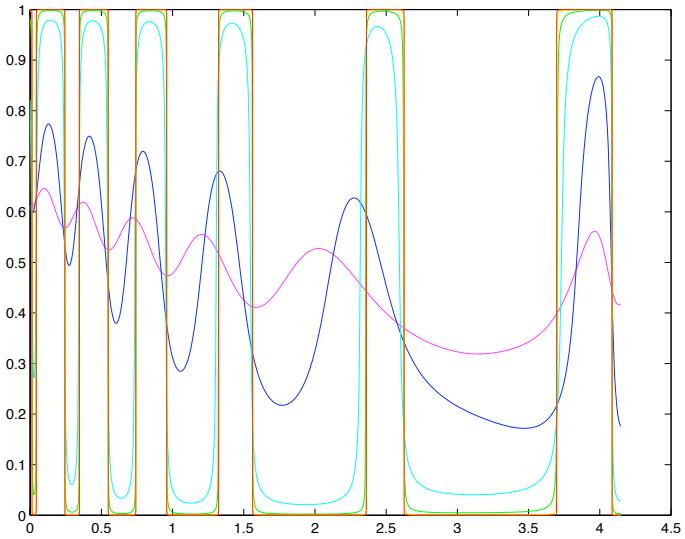

Figure 3.33: Control norm $\lvert u_\varepsilon\rvert$ versus time for ε equal to 0.5 till 10^{-5} (red), logarithmic barrier homotopy, target LO, $T_{\max} = 5\text{N}$.

thrust of 0.3N for a mass of 1500kg (our case) is equivalent to a maximal thrust of 0.07N for a mass of 350kg (SMART-1 case) since $\frac{0.3}{1500} = \frac{0.07}{350} = 2.10^{-4}\text{m.s}^{-2}$. We begin with numerical tests for medium thrusts *i.e.* 10, 7, 5 and 3N to figure out the suitable method for finding an initialization to solve $S^{L_2}(z) = 0$ and $S^{LO}(z) = 0$. For this maximal thrust range, both homotopies are done successfully. However, on the one hand, the logarithmic barrier homotopy is better since: It allows us to be closer to the bang-bang control with higher precision on the shooting function norm. It also allows us to perform second order condition tests to ensure local optimality of the computed extremals, because the true Hamiltonian verifies the Legendre strong condition which ensure the control smoothness, even if we are so close to the bang-bang shape. On the other hand, the energy-consumption homotopy is better since: It always leads to the better solution in terms of cost values. It is also consolidated by a theoretical background. In fact we are sure of existence of a global maximizer for the optimal control (P_λ) and that the cost criteria $J(u_\lambda)$ tends towards $J(u)$ when λ tends

to to 1, u is control solution of (P). Nevertheless for low thrust the logarithmic barrier homotopy is better since it provides us with a control which is very close to the bang-bang form with high precision on the shooting function. However, the (P_λ) homotopy fails, this homotopy is limited for low thrust transfers. This is mainly due to the numerical method used to compute the shooting function derivative which is more adequate for the smooth cases. The unaccomplished point in this work is the following: No numerical results for low thrust *i.e.* 0.3N concerning the target LO. This could also be a consequence of the failure of solving (P_t) for these parameters, because the solution of $S_t^{LO}(z) = 0$ is needed to initialize the resolution of $S_{L^2}^{LO}(z) = 0$ as for the target L_2 case. Or maybe another numerical strategy should be found to deal with transfers to the target LO for low thrusts. We pay more attention to this point when considering the SMART-1 mission in the next chapter.

Chapter 4

Application: The SMART1 mission

4.1 Mission definition

In the two previous chapters, some methods were put forward to solve minimum time and minimum fuel consumption transfers in the Earth-Moon system, modeled by the CRTBP. In this chapter, we use those method for a real mission case. We choose to simulate the European Space Agency mission to Moon SMART-1 [31, 32] (first Small Missions for Advanced Research in Technology) and then compare our transfer performance with that of the real mission. The SMART-1 mission is a spacecraft transfer from the GTO orbit around the Earth to a polar orbit around the Moon. The starting orbit around the Earth (GTO) is characterized by:

- Perigee altitude: $h_p = 742$km.
- Apogee altitude: $h_a = 36016$km.
- Argument of perigee: $\omega = 178°$.
- Inclination relative to the equator: $i = 7°$.
- Argument of the ascending node: Free.

As a reminder, the Earth's mean radius orbit is $R_{Earth} = 6378$km and the Moon's mean radius orbit is $R_{Moon} = 1737$km. The targeted orbit around the Moon (perilune near to the south-pole) is defined by:

- Perilune altitude: $h_p = 1000$km.
- Apolune altitude: $h_a = 10000$km.
- Argument of perilune: $\omega = 270°$.
- Inclination relative to the lunar equator: $i = 90°$.
- Argument of the ascending node: Free.

Henceforth, we note the targeted orbit around as the Moon *POM* (Polar Orbit around the Moon).

The SMART-1 spacecraft uses an electric propulsion thruster, the *PPS1350*. It provides a nominal thrust of $T_{\max} = 70$mN at $I_{sp} = 1640$s specific impulse. The equation of the vehicule's mass variation due to propellant expulsion is: $\dot{m} = -\frac{T}{I_{sp} g_0}$ where g_0 is the gravitational acceleration at sea level *i.e.* $g_0 = 9.8\text{m.s}^{-2}$ and T is the thrust generated by a propulsion system, the initial mass is $m_0 = 350$kg (*cf.* http://smart.esa.int/). The thrust T is normalized as follows: $T = T_{\max} u$, u is a vector of $\mathbf{R}^3$ such that $|u| \leq 1$. u is the engine control.

In this study, the transfer takes place in the Circular Restricted Three-Body Problem CRTBP. Let us consider the rotating frame (x_1, x_2, x_3) relative to the CRTBP. The plane (x_1, x_2) is the Moon's orbital plane (the plane containing the Earth and two different positions of the Moon when orbiting around the Earth). The parameters of the initial orbit and the arrival orbit are given relative to the equator plane and the lunar equator plane respectively. Thus those two planes have to be situated relative to Moon's orbital plane. let us recall that the ecliptic plane is the Earth's orbital plane relative to the Sun. Then (*cf.* figure 4.1):

- The plane (x_1, x_2) *i.e.* the Moon's orbital plane is tilted 5.145° relative to the ecliptic. The lunar equator is tilted 1.5424° relative to the ecliptic and so, 6.687° relative to the plane (x_1, x_2).

- The equator is tilted 23.44° relative to the ecliptic and the equator plane is fixed relative to the ecliptic, when the Earth is orbiting around the Sun. Thus the orbital plane of the Moon *i.e.* the plane (x_1, x_2) is tilted between 18.29° and 28.58° relative to the equator because this plane *i.e.* (x_1, x_2) is in revolution around the Sun.

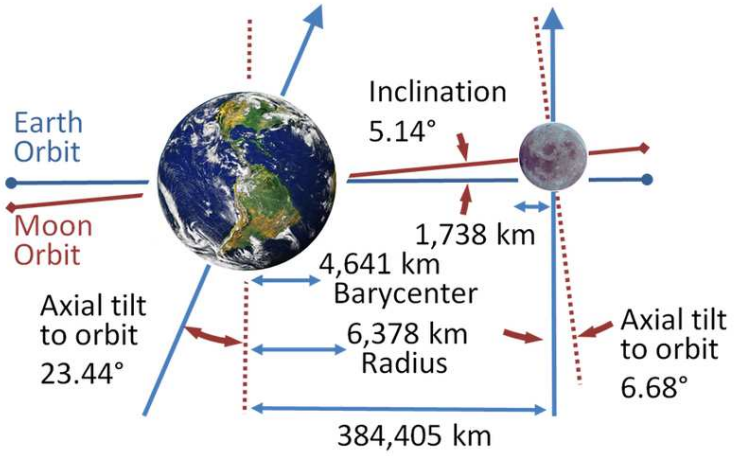

Figure 4.1: Different planes position in the Earth-Moon system.

We suppose that the plane (x_1, x_2) is inclined by 23° (mean inclination between 18.29° and 28.58°) relative to the equator, when the transfer starts. If

it is not the case, a continuation on the inclination angle is utilized to reach the desired inclination at the beginning of the transfer.

We aim in this chapter to compute optimal steering, realizing the transfer from GTO to POM, for a fixed time transfer t_f with respect to the optimization criteria: Minimum fuel consumption, which is equivalent to maximum spacecraft final mass $\max m(t_f)$, or $m(t_f) = m(0) - \frac{T_{\max}}{I_{sp} g_0} \int_0^{t_f} |u(t)| \mathrm{d}t$ thus $\max m(t_f) \iff \min \int_0^{t_f} |u(t)| \mathrm{d}t$. The dynamic of the system is augmented by the equation of mass variation.

$$\begin{cases} \dot{x} = F(x,u) = F_0(x) + \frac{T_{\max}}{m} \sum_{i=1}^{3} F_i(x) u_i \\ \dot{m} = -\beta T_{\max} |u|, \ \beta = \frac{1}{I_{sp} g_0} \end{cases}$$

Let us first focus on the controllability of the system with mass variation. We are inspired by the demonstration given in the two-body case [14] to enunciate the following result.

Proposition 4.1.1. *For any $T_{\max} > 0$, there is a proper mass $\chi_0 > 0$ of the spacecraft that makes the system controllable.*

Proof. Controllability of the constant mass system *i.e.*

$$\dot{x} = F_0(x) + \sum_{i=1}^{3} \gamma_i F_i(x) \tag{4.1}$$

$$|\gamma| \leq T_{\max}/m^0 \tag{4.2}$$

comes from the proposition 1.5.2. The controllability of the system with varying mass is then established by setting

$$m = m^0 \exp(-\beta \int_0^t |\gamma| \mathrm{d}s) > 0$$
$$u = m\gamma / T_{\max}$$

where γ controls 4.1 and 4.2. Indeed, $\dot{m} = -\beta T_{\max} |u|$ and $|u| \leq m^0 \gamma / T_{\max} \leq m^0 (T_{\max}/m^0)/T_{\max} = 1$. If t_f is the resulting final transfer time, the proper mass $\chi_0 = m^0 \exp(-t_f \beta T_{\max}/m^0) > 0$ is obviously such that $m \geq \chi_0$ on $[0, t_f]$. □

4.2 Minimum time transfer

One has to compute first the minimum final time $t_{f_{\min}}$ of the mission in order to fix the final time $t_f > t_{f_{\min}}$. Hence, we investigate first the minimum time transfer. The optimal control problem minimizing the final time is written as follows.

$$(P_t) \begin{cases} \min t_f = \int_0^{t_f} \mathrm{d}t \\ \dot{x} = F(x,u) = F_0(x) + \frac{T_{\max}}{m} \sum_{i=1}^{3} F_i(x) u_i \\ \dot{m} = -\beta T_{\max} |u|, \ \beta = \frac{1}{I_{sp} g_0} \\ |u| \leq 1 \\ x(0) \in GTO \\ x(t_f) \in POM \\ m(0) = 350\text{kg} \\ m(t_f) \text{ free} \end{cases}$$

We apply the Pontryagin Maximum Principle and we consider the normal case. Thus if (x, m, u) is an optimal solution of (P_t) then there exists a non identical zero vector $(p_x, p_m) \in \mathbf{R}^6 \times \mathbf{R}$ such that:

$$\begin{aligned}
\dot{x} &= \frac{\partial H}{\partial p_x}(x, m, p_x, p_m, u) \\
\dot{m} &= \frac{\partial H}{\partial p_m}(x, m, p_x, p_m, u) \\
\dot{p}_x &= -\frac{\partial H}{\partial x}(x, m, p_x, p_m, u) \\
\dot{p}_m &= -\frac{\partial H}{\partial m}(x, m, p_x, p_m, u) \\
u &= argmax_{|v|\leq 1} H(x, m, p_x, p_m, v)
\end{aligned}$$

Where H is the Hamiltonian, defined by:

$$\begin{aligned}
&H(x, m, p_x, p_m, u) = -1 + p_x F(x, u) - p_m \beta T_{\max} |u| \\
&= -1 + \underbrace{p_x F_0(x)}_{H_0} + \frac{T_{\max}}{m} \sum_{i=1}^{3} u_i \underbrace{p_x F_i(x)}_{H_i = p_{x\,i+3} = \varphi_i(p_x)} - p_m \beta T_{\max} |u|,\ \varphi(p_x) = (p_{x4}, p_{x5}, p_{x6}) \\
&= -1 + H_0 + \frac{T_{\max}}{m} \langle \varphi(p_x), u \rangle - p_m \beta T_{\max} |u| \\
&\leq -1 + H_0 + \frac{T_{\max}}{m} |\varphi(p_x)||u| - p_m \beta T_{\max} |u| \text{ (Cauchy-Schwartz)} \\
&\leq -1 + H_0 + T_{\max} \underbrace{\left(\frac{|\varphi(p_x)|}{m} - p_m \beta \right)}_{\psi(x, m, p_x, p_m)} |u|
\end{aligned}$$

Equality happens when $u = \alpha \frac{\varphi(p_x)}{|\varphi(p_x)|}$, $0 \leq \alpha \leq 1$. Let us focus then on the sign of $\psi(x, m, p_x, p_m)$. We have:

$$\begin{aligned}
\dot{p}_m &= -\frac{\partial H}{\partial m}(x, m, p_x, p_m, u) \\
&= \frac{T_{\max}}{m^2} \langle \varphi(p_x), u \rangle \\
&= \frac{T_{\max}}{m^2} \langle \varphi(p_x), \alpha \frac{\varphi(p_x)}{|\varphi(p_x)|} \rangle \\
&= \alpha \frac{T_{\max}}{m^2} |\varphi(p_x)| \geq 0
\end{aligned}$$

Since the final mass is free, transversality condition 2.6 gives $p_m(t_f) = 0$, provided that the function p_m is an increasing one ($\dot{p}_m \geq 0$) thus $p_m \leq 0$ and $\psi(x, m, p_x, p_m) \geq 0$. The maximization condition yields to $|u| = 1$ and then $u = \frac{\varphi(p_x)}{|\varphi(p_x)|}$, a.e. on $[0, t_f]$.

Once the optimal control is calculated, we aim to compute optimal trajectories from GTO to POM. The starting orbit GTO is inclined by 7° relative to the equator, we assume that this inclination is in the same direction with the inclination between the equator and the Moon orbital plane *i.e.* the plane (x_1, x_2), hence the inclination of GTO relative to the plane (x_1, x_2) is the sum

of the two inclinations *i.e.* $23^\circ + 7^\circ = 30^\circ$. It follows that the starting orbit is an ellipse around the Earth situated on the plane inclined by 30° relative to (x_1, x_2). We suppose that the major axis of this ellipse is situated on the plane (x_1, x_3). The starting point is also fixed: The perigee of the *GTO* which is supposed to be on the plane (x_1, x_3) and situated between the Earth and the Moon, is called X_0. Fixing the initial point on the starting orbit does not affect the transfer performances since the semi major axis of the *GTO* is too small compared to the Earth-Moon distance. The same numerical strategy in chapter 2 is used here to compute minimum time transfers. However, this time we deal with 3D transfers. Therefore, we reutilize the two-three body continuation. The starting orbit is the *GTO* and the targeted orbit is the lunar orbit. We use the Gauss modified coordinates $x = (P, e_x, e_y, h_x, h_y, L)$ defined in chapter 2 *cf.* figure 2.2 and the control is expressed in a ortho-radial frame attached to the spacecraft (q, s, w), defined also in chapter 2 *cf.* figure 2.2. We omit the equation of mass variation and we are first interested to constant mass transfer. The optimal control to solve is then:

$$(P_t^G) \begin{cases} min \int_0^{t_f} dt \\ \dot{x} = f_0(x) + \frac{T_{\max}}{m}(u_1 f_1(x) + u_2 f_2(x) + u_3 f_3(x)) \\ |u| \leq 1 \\ P(0), e_x(0), e_y(0), h_x(0), h_y(0), L(0) \text{ fixed} \\ P(t_f), e_x(t_f), e_y(t_f), h_x(t_f), h_y(t_f) \text{ Moon's orbit} \\ L(t_f) \text{ free} \end{cases}$$

where:

$$f_0(x) = \sqrt{\frac{\mu}{P}} \begin{pmatrix} 0 \\ 0 \\ 0 \\ 0 \\ 0 \\ W^2/P \end{pmatrix},$$

$$f_1(x) = \sqrt{\frac{P}{\mu}} \begin{pmatrix} 0 \\ \sin(L) \\ -\cos(L) \\ 0 \\ 0 \\ 0 \end{pmatrix},$$

$$f_2(x) = \sqrt{\frac{P}{\mu}} \begin{pmatrix} 2P/W \\ \cos(L) + (e_x + \cos(L))/W \\ \sin(L) + (e_y + \sin(L))/W \\ 0 \\ 0 \\ 0 \end{pmatrix},$$

$$f_3(x) = \frac{1}{W}\sqrt{\frac{P}{\mu}} \begin{pmatrix} 0 \\ -Ze_y \\ Ze_x \\ C\cos(L)/2 \\ C\sin(L)/2 \\ Z \end{pmatrix}$$

and

$$\begin{aligned} W &= 1 + e_x \cos(L) + e_y \sin(L), \\ Z &= h_x \sin(L) - h_y \cos(L), \\ C &= 1 + h_x^2 + h_y^2. \end{aligned}$$

(P_t^G) and (P_t) have the same form. The PMP application gives the same control shapes. The final longitude $L(t_f)$ is free. In fact, the position of the Moon is known at any time as t_f. However, the number of required revolution around the Earth to reach the Moon's orbit remains unknown. Then transversality condition 2.6 yields to $p_L(t_f) = 0$ (costate with respect to the state L). The corresponding shooting function is:

$$S_t^G \ : \ z = (t_f, p(0)) \ \mapsto \ \begin{pmatrix} P(t_f) - 384.402 \\ e_x(t_f) \\ e_y(t_f) \\ h_x(t_f) \\ h_y(t_f) \\ p_L(t_f) \\ H(t_f) \end{pmatrix}$$

We recall here that the spacecraft mass is 350kg, thus the maximal thrust of 60N in chapter 2 is equivalent here to $T_{\max} = 60 \times 350/1500 = 14$N. We aim to solve $S_t^G(z) = 0$ for the maximal thrust $T_{\max} = 14$N. We use the initialization solution found in chapter 2. In fact, we have the same targeted orbit *i.e.* the lunar orbit, however, the staring orbit is not the same. In fact, the semi major axis a, the eccentricity e and the inclination i are different. Let us note (a_p, e_p, i_p) the orbital element of the starting orbit considered in chapter 2, the index p refers to the planar case, and (a_t, e_t, i_t) to the orbital element of the starting orbit GTO considered in this chapter. The index t refers to a three-dimensional case. We have:

$$\begin{aligned} a_p &= 42.165\text{Mm}, & a_t &= 24.757\text{Mm}. \\ e_p &= 0.0, & e_t &= 0.7124. \\ i_p &= 0^\circ, & i_t &= 30^\circ. \end{aligned}$$

The idea is to build homotopy on the orbital elements of the starting orbit, since we have the solution to $S_t^G(z) = 0$ for starting orbit with orbital elements (a_p, e_p, i_p). We set up a three-stage homotopy respecting this order:

$$\begin{aligned} (a_p, e_p, i_p) &\longrightarrow \text{homotopy on the semimajor axis } a \longrightarrow (a_t, e_p, i_p) \\ (a_t, e_p, i_p) &\longrightarrow \text{homotopy on the eccentricity } e \longrightarrow (a_t, e_t, i_p) \\ (a_t, e_t, i_p) &\longrightarrow \text{homotopy on the inclination } i \longrightarrow (a_t, e_t, i_t) \end{aligned}$$

The continuation is performed successfully by differential path following for the three considered steps. Thus, we have an initialization $(t_f, p(0))$ solution to $S_t^G(t_f, p(0)) = 0$ for a minimum time transfer from starting orbit GTO to the lunar orbit. The same process used in chapter 2 is used here to move towards the CRTBP coordinate. In fact, we do not target directly the orbit POM, we take an intermediate step. We first target the libration point L_2, we still consider

a constant mass transfer and a maximal thrust of 14N. The correspondent shooting function is:

$$S_t^{L_2} \ : \ z = (t_f, p(0)) \ \mapsto \ \begin{pmatrix} x_1(t_f) - x_{L_2}(\mu) \\ x_2(t_f) \\ x_3(t_f) \\ x_4(t_f) \\ x_5(t_f) \\ x_6(t_f) \\ H(t_f) \end{pmatrix}$$

The goal is to find a suitable initialization to solve $S_t^{L_2}(z) = 0$ for $\mu_{Earth-Moon} = 0.012153$. We proceed as follows. An initial guess composed by $t_{f\,min}(\mu = 0)$ (solution of $S_t^G(z) = 0$) and arbitrary vector $p(0)$ is a "good" initialization to solve $S_t^{L_2}(z) = 0$ for $\mu = \mu_{Earth-Moon}$. The shooting algorithm converge and a minimum time trajectory from the starting point X_0 on the GTO to L_2 is computed in the CRTBP frame. Recall that for the moment the mass is constant along the transfer. The omission of the equation of mass variation may be seen from the following angle: The parameter β is set to 0. From this point of view, an idea to connect a constant mass transfer to a transfer with mass variation is as follows: Construct a homotopy on the parameter β starting from 0 (the solution is already found), till the real value of β. In this case, the equation $p_m(t_f) = 0$ is added to the shooting function *i.e.*:

$$S_t^{L_2} \ : \ z = (t_f, p(0)) \ \mapsto \ \begin{pmatrix} x_1(t_f) - x_{L_2}(\mu) \\ x_2(t_f) \\ x_3(t_f) \\ x_4(t_f) \\ x_5(t_f) \\ x_6(t_f) \\ p_m(t_f) \\ H(t_f) \end{pmatrix}$$

A differential continuation on β is performed successfully from $\beta = 0$ to the right value of β. Note that the homotopy on β may be used to compare trajectories for different proper impulsions I_{sp} of the spacecraft engine. Till now a minimum time transfer extremal for maximal thrust $T_{\max} = 14$N from X_0 to L_2 with mass variation is computed.

We aim now to reach low thrust, hence a continuation on $T_{\max}$ is considered. The discrete method is used here since it is more suitable for this continuation than the differential as shown in chapter 2. In the same chapter, we also showed that for the target L_2 the product $t_{f\,\min} T_{\max}$ is almost constant when $T_{\max}$ tends to zero. Thus, the initialization method is: Let $(t_{f\,\min i}, p_i(0))$ be the initialization solution for the step i (for $T_{\max i}$), the initial guess for the next step $(i+1)$ (for $T_{\max i+1}$) is $(t_{f\,\min i} \times T_{\max i}/T_{\max i+1}, p_i(0))$. The continuation is succeeded: We reach the desired thrust $T_{\max} = 0.07$N. The homotopic steps are resumed in table 4.2. The trajectory solution for $T_{\max} = 0.07$N is portrayed in figure 4.2.

We aim now to solve the optimal control (P_t) *i.e.* compute minimum time trajectory from X_0 on the GTO orbit to the POM orbit. The elements of the orbit POM given above define a family of ellipses whose major axis is the Moon

Table 4.1: Homotopic discrete steps on the maximal thrust, the product $T_{\max} t_{f_{\min}}$ is almost constant when $T_{\max}$ tends to zero, the spacecraft mass, at the end of the transfer, *i.e.* $m(t_{f_{\min}})$ is also given

T_{max}(N)	$t_{f_{min}}$	$T_{\max} t_{f_{\min}}$	$t_{f_{\min}}$(days)	$m(t_{f_{\min}})$(kg)
14	0.42895027737683	6.005303883275690	1.8624	209.8340
13	0.44898703734349	5.836831485465408	1.9494	213.7662
12	0.47201104592118	5.664132551054196	2.0494	217.7970
11	0.49970693819704	5.496776320167495	2.1696	221.7032
7	0.72044556103715	5.043118927260099	3.1280	232.2917
6	0.78734372119204	4.724062327152270	3.4184	239.7386
2	1.83173596941559	3.663471938831180	7.9529	264.4932
1.7	2.27966110556162	3.875423879454754	9.8977	259.5462
1.4	2.75658580613807	3.859220128593297	11.968	259.9244
0.8	4.39460385766865	3.515683086134920	19.080	267.9426
0.4	7.96876315378605	3.187505261514420	34.598	275.6024
0.35	9.55173231281645	3.343106309485757	41.471	271.9707
0.32	10.7960518112250	3.454736579592000	46.874	269.3652
0.2	16.9423496080589	3.388469921611780	73.559	270.9118
0.19	17.4234215325703	3.310450091188357	75.648	272.7329
0.11	29.6423382843007	3.260657211273077	128.70	273.8950
0.081	37.7312507475975	3.056231310555398	163.82	278.6664
0.0705	43.4444216051816	3.062831723165303	188.62	278.5124
0.07	43.5981688315684	3.051871818209788	189.29	278.7682

polar axis (tilted at 6.687° relative to the x_3 axis) and the perilune is situated near to the Moon south pole.

In order to facilitate the numerical simulations we suppose that the POM orbit is situated on the plane (x_1, x_3), moreover we fix the targeted point on the orbit POM: The apolune of the orbit is chosen. Choosing the targeted orbit and choosing a point to target on this orbit does not disturb the generality of the problem since the targeted orbit is very short to the Moon and its period, a few days, is very small compared to the time transfer, a few months (for instance 6 months are needed to arrive to L_2). Thus, choosing a precise point on a precise orbit of the family of the admissible targets POM may vary the time transfer more or less by a few days. This is a very slight variation so we suppose that it does not affect the transfer performances. The shooting function is written as below.

$$S_t \ : \ z = (t_f, p_x(0), p_m(0)) \ \mapsto \ \begin{pmatrix} x_1(t_f) - x_1^f \\ x_2(t_f) \\ x_3(t_f) - x_3^f \\ x_4(t_f) - x_4^f \\ x_5(t_f) \\ x_6(t_f) - x_6^f \\ p_m(t_f) \\ H(t_f) \end{pmatrix}$$

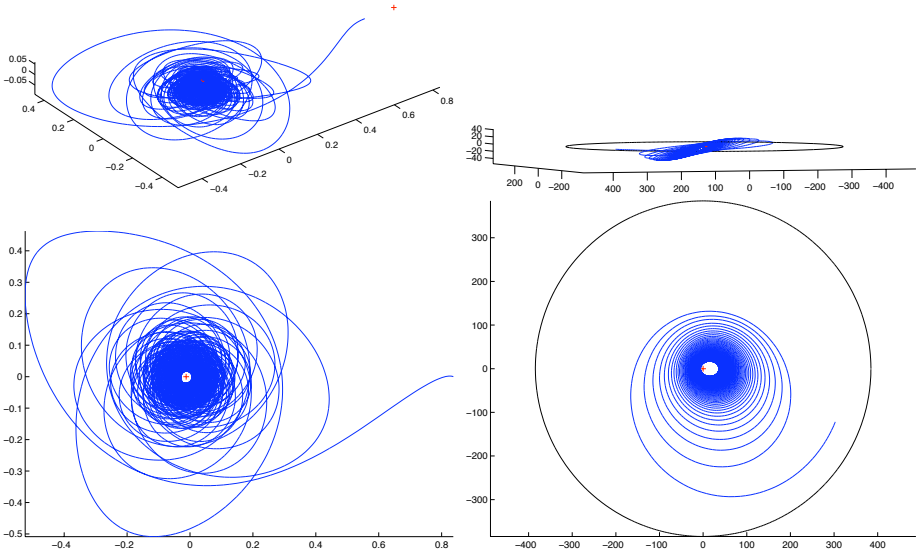

Figure 4.2: *Minimum time trajectory to L_2. Both figures on the left are in the CRTBP frame and both figures on the right are in a fixed frame around the Earth. The black circle is the Moon's orbit. Both top figures show the three dimension aspect of the transfer, both bottom figures are projection of the trajectory on the orbital plane of the Moon,* $T_{\max} = 0.07$N.

We intend to find a suitable initial guess to solve $S_t(z) = 0$ for $T_{\max} = 0.07$N. The first idea which comes to mind is to use the solution of $S_t^{L_2}(z) = 0$ as first guess. The lowest $T_{\max}$ for which it works is $T_{\max} = 1.4$N. As usual we construct a discrete continuation on $T_{\max}$ in order to reach lower thrusts. This homotopy does not work after $T_{\max} = 0.86$N. In fact, the continuation on $T_{\max}$ does not progress when the spacecraft is executing another revolution around the Earth or around the Moon *cf.* figure 4.2. This homotopy is more complicated than the same homotopy evoked in chapter 2 for the transfer towards LO, for two reasons. First, the 3D effects: The orbit LO is situated on the plane (x_1, x_2) however, the orbit POM is situated on a plane orthogonal to this plane. It is already known that when the spacecraft is outside of this plane, the attraction forces of the primaries naturally pull the spacecraft back to this plane. Secondly, the orbit is very close to the Moon thus, a two-body transfer is supposed to take place around the Moon to put the spacecraft on its course to the final orbit. Hence, the continuation is faced with problems when the spacecraft is accomplishing another revolution, not only around the Earth, but also around the Moon.

During the minimum time transfer study in the planar case or in the 3D case we notice that the continuation on $T_{\max}$ works well for transfer from the Earth to L_2, this is due to the fact that the transfer is near to a two-body transfer than a three-body one. The idea derives from the following question: Do we have the same effect around the Moon? In fact transfer from L_2 to an orbit around the Moon, for instance POM, may be near to a two-body transfer (the Earth's effect on orbits around the Moon is far more important than the

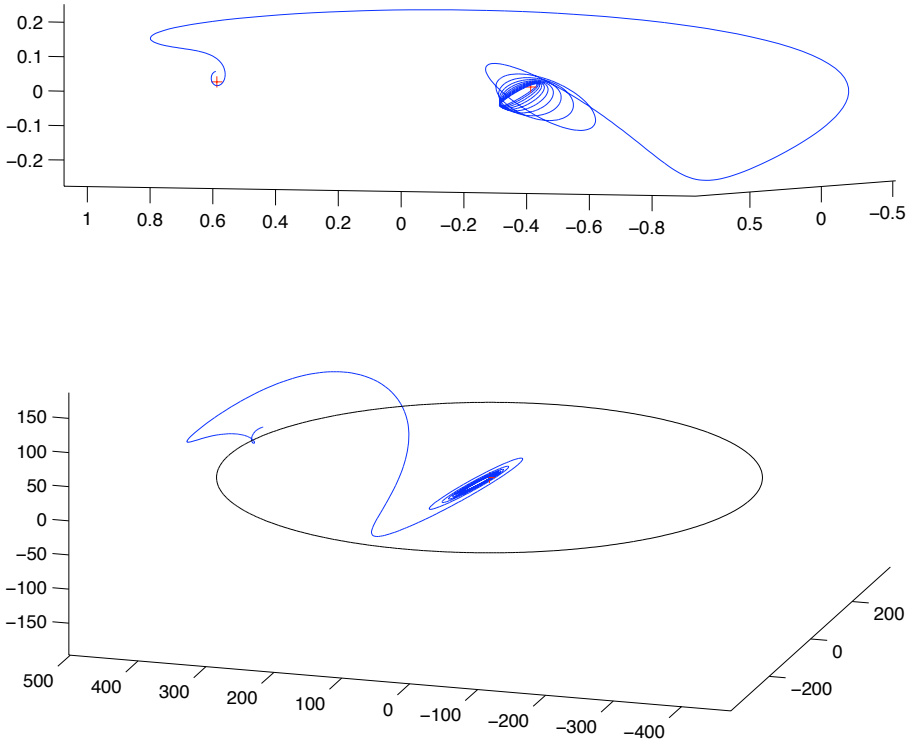

Figure 4.3: *Minimum time trajectory to POM, the top figure is in the CRTBP frame and the bottom figure is in a fixed frame around the Earth. The black circle is the Moon's orbit. The spacecraft is executing another revolution around the Earth and another revolution around the Moon at the same time,* $T_{\max} = 0.86$N.

influence of the Moon on orbits around the Earth). Hence, we tentatively divide the transfer into two parts: the first part from X_0 to L_2 has already been solved and solutions are provided for different $T_{\max}$, second part from L_2 to POM has not been solved yet. The two parts are connected to each other thanks to multiple shooting, which allows us to obtain an optimal solution for the whole transfer from X_0 to POM. We first focus on the resolution of the second part and second on the connection between the two parts.

The second part should start where the first one ends, thus the starting point is the L_2 point with null velocity and the initial mass is the mass at the end of the first part for $T_{\max} = 0.07$N *i.e.* $m_0 = 278.7682$kg. Notice that the final mass of the first step is around 270kg for $T_{\max}$ lower than 0.8N, *cf.* table 4.2, then if we consider another thrust different to 0.07N, the same initialization works a priori, this has been verified by numerical simulations, if not homotopy on the initial mass give us the right initialization.

The resolution process is the following. An initialization is found for $T_{\max} =$ 14N, then a discrete continuation on $T_{\max}$ is considered to reach lower thrusts exactly as in transfer from X_0 to L_2, this homotopy works only up to $T_{\max} =$ 0.14N. The homotopic steps are summarized in table 4.2.

Note that the product $t_{f\,\min} T_{\max}$ keeps decreasing when $T_{\max}$ decreases until

Table 4.2: Homotopic discrete steps on the maximal thrust, transfer from libration point L_2 to the orbit POM

T_{max}(N)	$t_{f_{min}}$	$t_{f_{\min}} T_{\max}$	$t_{f_{\min}}$(days)
14	0.162966431602354	2.281530042432956	0.7076
8	0.279449935507688	2.235599484061504	1.2133
4	0.383844074536392	1.535376298145568	1.6666
3	0.438289002142305	1.314867006426915	1.9029
2.5	0.477831423973761	1.194578559934403	2.0746
2	0.533398602690320	1.066797205380640	2.3159
1.5	0.620328859920913	0.930493289881370	2.6933
1.2	0.703842607492855	0.844611128991426	3.0559
1	0.789654655779306	0.789654655779306	3.4285
0.9	0.868505246038283	0.781654721434455	3.7708
0.7	1.119953722199710	0.783967605539797	4.8625
0.6	1.481156785054380	0.888694071032628	6.4308
0.5	1.816139276649490	0.908069638324745	7.8852
0.4	2.414589761122370	0.965835904448948	10.483
0.266	2.629334679162720	0.699403024657284	11.415
0.17	3.906184948950600	0.664051441321602	16.959
0.14	5.556928564801730	0.777969999072242	24.126

the thrust $T_{\max} = 0.7$N. We think that the homotopy failure is due to the three-dimension effect. In fact, we think that for low thrust the spacecraft does not have the sufficient energy to be in an orbit situated at a plane orthogonal to the Moon orbital plane, knowing that we start the transfer from L_2 with null velocity. Thus, for high and medium thrust the control application is sufficient to move the spacecraft to the POM plane and the transfer is close to a two-body transfer in the plane (x_1, x_3) *cf.* figure 4.2. However, when the maximal thrust becomes too low the 3D aspect appears clearly *cf.* figure 4.2. This inconvenience will also affect the connection between the two transfer parts as we will see later. To address this concern, it will be recommended to add an initial velocity to help the spacecraft to remain on the plane (x_1, x_3) at the beginning of the transfer.

Let us now focus on the connection between the two transfer parts. Up to now we have two optimal transfer branches: From X_0 to L_2 and then from L_2 to POM. We connect the two branchs using the multiple shooting method [35]. Consider the whole transfer from X_0 to POM, let t_f be the final time transfer. Multiple shooting splits the interval $[0, t_f]$ in N (here $N = 2$) intervals $[t_i, t_{i+1}]$, $i \in \{0, \ldots, N-1\}$ and has the values $z(t_i)$ ($z = (x, m, p_x, p_m)$) at the beginning of each sub-interval are unknown. Then, one has to take into account some matching conditions at each instant t_i (continuity condition). The Pontryagin maximum principle specifies the conditions at the limits, on the state, the adjoint vector and on the Hamiltonian (t_f is free here). By limits, we mean, the initial time, here $t_0 = 0$, the final time, here is $t_2 = t_f$, and the intermediate times, here we have one intermediate time t_1. Analogously to the simple shooting, we write the multiple boundary value problem (MBVP) corresponding to our case

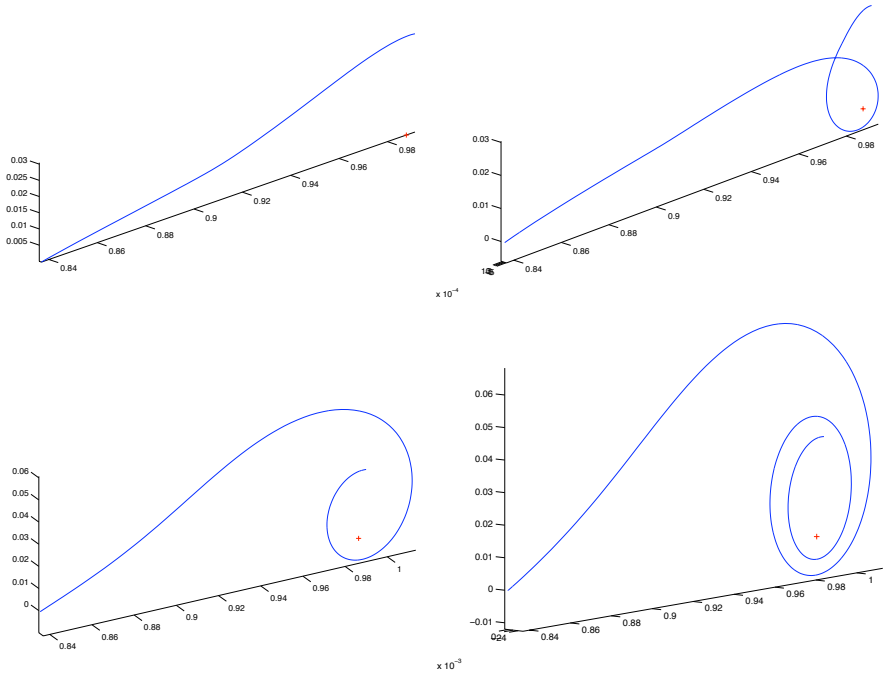

Figure 4.4: *Minimum time trajectory from* L_2 *to* POM*,* $T_{\max} = 14$*(top corner left),* 8*(top corner right),* 1*(bottom corner left) and* 0.7N*(bottom corner right), the transfer is taking place almost on the plane* (x_1, x_3)*.*

as below.

$$(MBVP)\begin{cases} \dot{z}(t) = \overrightarrow{H}(z),\ t \in [t_i, t_{i+1}] \\ z(t_i) = z_i,\ i = 0, \ldots, N-1 \\ z(t_{i+1}, t_i, z_i) - z_{i+1} = 0,\ i = 0, \ldots, N-2, \text{ continuity condition} \\ b_f(z(t_f, t_{N-1}, z_{N-1})) = 0 \\ H(t_f) = 0 \text{ final time is free .} \end{cases}$$

Where $\overrightarrow{H}(z) = (\frac{\partial H}{\partial p_x}, \frac{\partial H}{\partial p_m}, -\frac{\partial H}{\partial x}, -\frac{\partial H}{\partial m})$ the Hamiltonian vector field on each sub-interval, note that in our case we have the same Hamiltonian for each sub-interval but generally we can have different Hamiltonian. t_i, $i = 1, \ldots, N-1$ and z_i, $i = 0, \ldots, N-1$ are the unknowns of the problem. $z(t_{i+1}, t_i, z_i)$ is the solution of the Cauchy problem: $\dot{z} = \overrightarrow{H}(z)$, $z(t_i) = z_i$. b_f describes the final conditions *i.e.* $x(t_f) \in POM$ and $p_m(t_f) = 0$. Remember that in our case

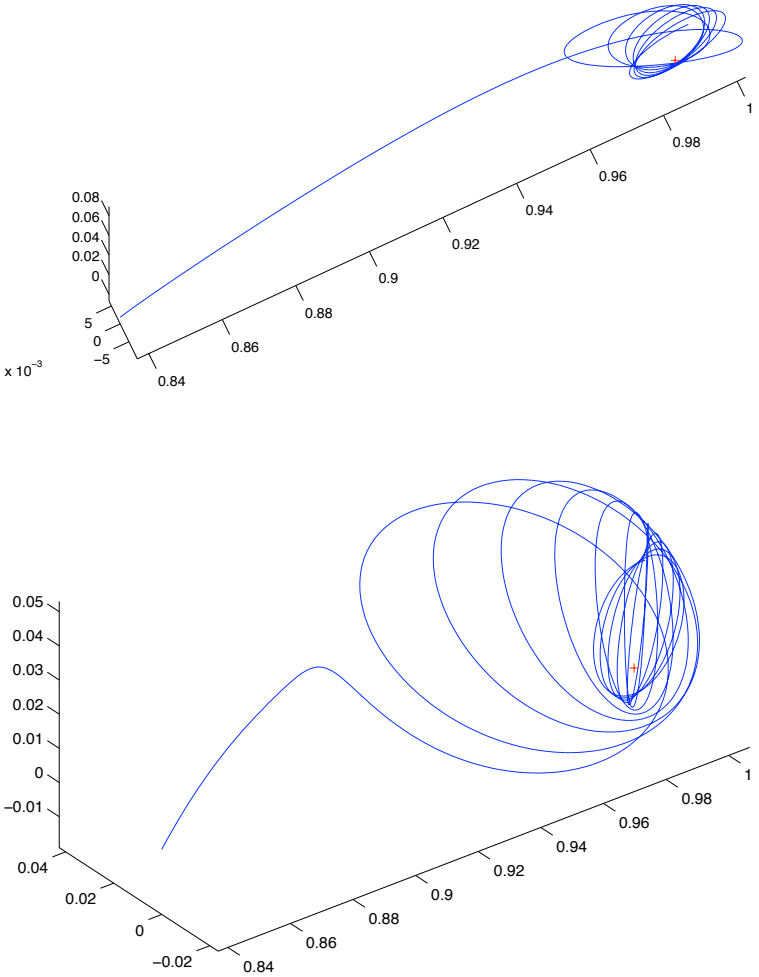

Figure 4.5: *Minimum time trajectory from L_2 to POM, $T_{\max} = 0.4$(left) and* 0.14N*(right), the 3D aspect of the transfer is appearing.*

$N = 2$, the multiple shooting function corresponding to (MBVP) is as thus:

$$S_t : \begin{pmatrix} (p_{x0}, p_{m0}) \\ t_1 \\ z_1 = (x_1, m_1, p_{x1}, p_{m1}) \\ t_f \end{pmatrix} \mapsto \begin{pmatrix} x(t_1, t_0, z_0) - x_1 \\ m(t_1, t_0, z_0) - m_1 \\ p_x(t_1, t_0, z_0) - p_{x1} \\ p_m(t_1, t_0, z_0) - p_{m1} \\ t_{f\min 1} - t_1 \\ x_1(t_f) - x_1^f \\ x_2(t_f) \\ x_3(t_f) - x_3^f \\ x_4(t_f) - x_4^f \\ x_5(t_f) \\ x_6(t_f) - x_6^f \\ p_m(t_f) \\ H(t_f) \end{pmatrix}$$

$t_{f_{\min 1}}$ denotes the minimum time which realizes the first branch transfer. Now one has to find a suitable guess to solve $S_t = 0$. The idea is to use the computed branches: From X_0 to L_2 and from L_2 to POM. In fact, the final condition on the state and costate and the Hamiltonian are verified. The condition $t_{f_{\min 1}} - t_1 = 0$ is satisfied if $t_1 = t_{f_{\min X_0 \to L_2}}$, the intermediate state (x_1, m_1) is already chosen such that equations $x(t_1, t_0, z_0) - x_1 = 0$ and $m(t_1, t_0, z_0) - m_1 = 0$ are satisfied. The problem lies in the equations $p_x(t_1, t_0, z_0) - p_{x1} = 0$ and $p_m(t_1, t_0, z_0) - p_{m1} = 0$, because the costate at the end of the transfer $X_0 \to L_2$ is not equal a priori at the initial costate of the transfer $L_2 \to POM$, which is true numerically. Hence, we introduce a continuation on those equations. Let $(p_{x^f_{X_0 \to L_2}}, p_{m^f_{X_0 \to L_2}})$ be the final costate vector of the transfer $X_0 \to L_2$ and $(p_{x^0_{L_2 \to POM}}, p_{m^0_{L_2 \to POM}})$ the initial costate vector of the transfer $L_2 \to POM$, we introduce the homotopic parameter λ in the shooting function as follows:

$$S_t^\lambda : \begin{pmatrix} (p_{x0}, p_{m0}) \\ t_1 \\ z_1 = (x_1, m_1, p_{x1}, p_{m1}) \\ t_f \end{pmatrix} \mapsto$$

$$\begin{pmatrix} x(t_1, t_0, z_0) - x_1 \\ m(t_1, t_0, z_0) - m_1 \\ p_x(t_1, t_0, z_0) - p_{x1} - \lambda(p_{x^f_{X_0 \to L_2}} - p_{x^0_{L_2 \to POM}}) \\ p_m(t_1, t_0, z_0) - p_{m1} - \lambda(p_{m^f_{X_0 \to L_2}} - p_{m^0_{L_2 \to POM}}) \\ t_{f_{\min 1}} - t_1 \\ x_1(t_f) - x_1^f \\ x_2(t_f) \\ x_3(t_f) - x_3^f \\ x_4(t_f) - x_4^f \\ x_5(t_f) \\ x_6(t_f) - x_6^f \\ p_m(t_f) \\ H(t_f) \end{pmatrix}.$$

It is then obvious that a solution of $S_t^{\lambda=0} = 0$ is given by the previously computed two transfers branches: From X_0 to L_2 and from L_2 to POM. To obtain the optimal solution for the whole transfer from X_0 to POM one only has to perform the homotopy on λ from 0 to 1. A discrete continuation on λ with homotopic step 0.1 is performed successfully for $T_{\max} = 0.7$N. The trajectory solution is shown in figure 4.2. Note that the final solution is a one phase transfer and the initialization solution is also a zero of the simple shooting function, corresponding to the transfer from X_0 to POM.

We test the same homotopy for lower thrusts for instance for $T_{\max} = 0.4$ and 0.14N. Neither the discrete nor the differential continuation methods is working. We think that it is due to the same reasons causing the failure of the homotopy on $T_{\max}$ for the transfer from L_2 to POM, *i.e.* the 3D aspect of this transfer and the null starting velocity for the transfer from L_2 to POM.

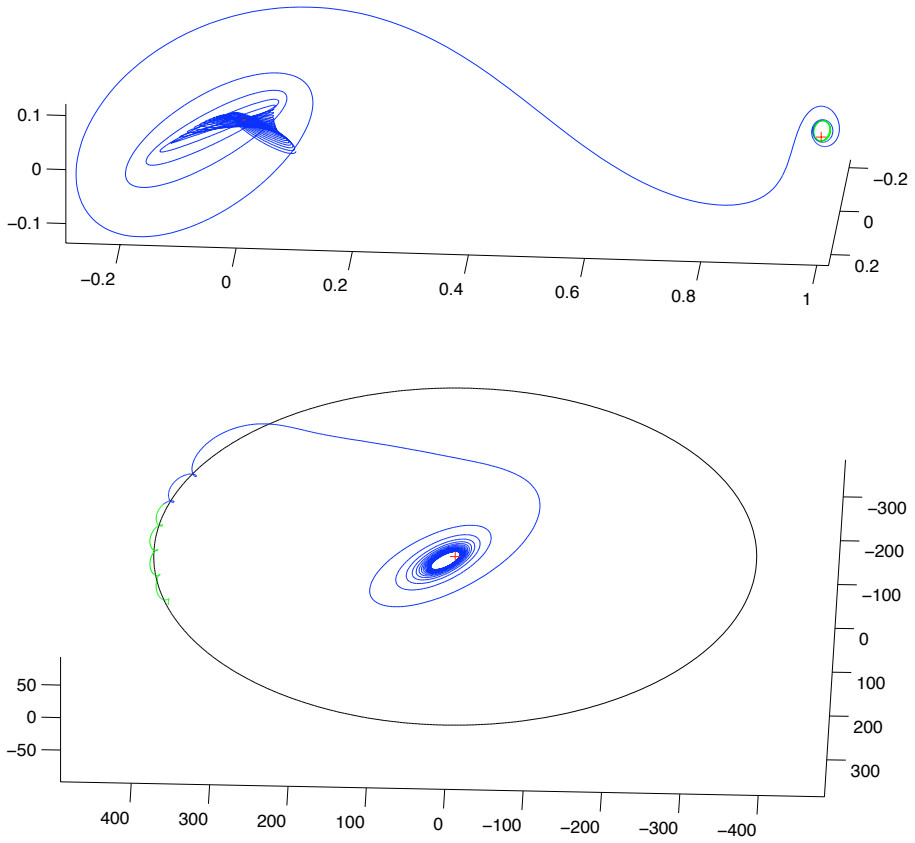

Figure 4.6: *Minimum time trajectory to POM. The figure at the top is in the CRTBP frame and figure at the bottom is in a fixed frame around the Earth. The black circle is the Moon's orbit, the blue curve is the extremal and the green curve is the free trajectory after the end of the transfer,* $T_{\max} = 0.7\text{N}$.

4.3 Minimum fuel consumption transfer

Consider the minimum fuel consumption problem.

$$(P)\begin{cases} \min \int_0^{t_f} |u| \mathrm{d}t \\ \dot{x} = F(x,u) = F_0(x) + \frac{T_{\max}}{m} \sum_{i=1}^{3} F_i(x) u_i \\ \dot{m} = -\beta T_{\max} |u| \\ |u| \leq 1 \\ x(0) \in GTO \\ x(t_f) \in POM \\ m(0) = 350\text{kg} \\ m(t_f) \text{ free} \end{cases}$$

We apply the Pontryagin Maximum Principle and we consider the normal case. Thus, if (x, m, u) is an optimal solution of (P) there exists a non identically zero

vector $(p_x, p_m) \in \mathbf{R}^6 \times \mathbf{R}$ such that:

$$\begin{aligned}
\dot{x} &= \frac{\partial H}{\partial p_x}(x, m, p_x, p_m, u) \\
\dot{m} &= \frac{\partial H}{\partial p_m}(x, m, p_x, p_m, u) \\
\dot{p}_x &= -\frac{\partial H}{\partial x}(x, m, p_x, p_m, u) \\
\dot{p}_m &= -\frac{\partial H}{\partial m}(x, m, p_x, p_m, u) \\
u &= argmax_{|v|\leq 1} H(x, m, p_x, p_m, v)
\end{aligned}$$

Where H is the Hamiltonian defined by:

$$\begin{aligned}
&H(x, m, p_x, p_m, u) = -|u| + p_x F(x, u) - p_m \beta T_{\max} |u| \\
&= -|u| + \underbrace{p_x F_0(x)}_{H_0} + \frac{T_{\max}}{m} \sum_{i=1}^{3} u_i \underbrace{p_x F_i(x)}_{H_i = p_{x\,i+3} = \varphi_i(p_x)} - p_m \beta T_{\max} |u|,\ \varphi(p_x) = (p_{x4}, p_{x5}, p_{x6}) \\
&= -|u| + H_0 + \frac{T_{\max}}{m} \langle \varphi(p_x), u \rangle - p_m \beta T_{\max} |u| \\
&\leq -|u| + H_0 + \frac{T_{\max}}{m} |\varphi(p_x)||u| - p_m \beta T_{\max} |u| \text{ (Cauchy-Schwartz)} \\
&\leq H_0 + \underbrace{(\frac{T_{\max}}{m} |\varphi(p_x)| - p_m \beta T_{\max} - 1)}_{\psi(x, m, p_x, p_m)} |u|
\end{aligned}$$

Equality happens when $u = \alpha \frac{\varphi(p_x)}{|\varphi(p_x)|}$, $0 \leq \alpha \leq 1$. The control u is expressed as below.

(i) $\psi(x, m, p_x, p_m) > 0 \Rightarrow |u| = 1 \Rightarrow u = \frac{\varphi(p_x)}{|\varphi(p_x)|}$,

(ii) $\psi(x, m, p_x, p_m) < 0 \Rightarrow |u| = 0 \Rightarrow u = 0$,

(iii) $\psi(x, m, p_x, p_m) = 0 \Rightarrow |u| \leq 1 \Rightarrow u = \alpha \frac{\varphi(p_x)}{|\varphi(p_x)|}$, $\alpha \in [0, 1]$.

The optimal control is bang-bang as in the previous chapter thus we introduce the same homotopic methods to solve the problem (P) *i.e.* the energy-consumption and the logarithmic barrier homotopies. We indicate in this section initial results to solve the minimum consumption problem. Those are the latest numerical simulation results in my PhD work. More time is needed to emphasize on this problem. In this section we deal with the transfer from the point X_0 on the *GTO* to the libration point L_2. We aim to apply the methods tested for the planar case in the previous chapter. Thus, one has first to find a suitable guess to solve the minimum energy transfer *i.e.* $(P_{\lambda=0})$ with (P_λ)

denoting the following problem

$$(P_\lambda)\begin{cases} \min \int_0^{t_f} (\lambda|u| + (1-\lambda)|u|^2)\mathrm{d}t \\ \dot{x} = F(x,u) = F_0(x) + \frac{T_{\max}}{m}\sum_{i=1}^{3} F_i(x)u_i \\ \dot{m} = -\beta T_{\max}|u| \\ |u| \leq 1 \\ x(0) \in GTO \\ x(t_f) = L_2 \\ m(0) = 350\text{kg} \\ m(t_f) \text{ free} \end{cases}$$

and then consider the energy-consumption or the logarithmic barrier homotopy to lead us to the minimum fuel consumption solution. To find a suitable guess to solve $S_0(z) = 0$ where S_λ is the shooting function relative to (P_λ) , we process as follows. We use the solutions of the minimum time transfer *i.e.* solution of $S_t^{L_2}$ as initializations, for different $T_{\max}$ values and for different final time values: $t_f = c_{t_f} t_{f_{\min}}$ c_{t_f} varaying from 1 to 2. The lowest maximal thrust reached with this technique is $T_{\max} = 0.8$N for final time transfer $t_f = 1.7 t_{f_{\min}}$. The energy-consumption homotopy is executed from $\lambda = 0.0$ until $\lambda = 0.97$. The optimal trajectory is given in figure 4.3. The corresponding optima control is almost bang-bang, *cf.* figure 4.3.

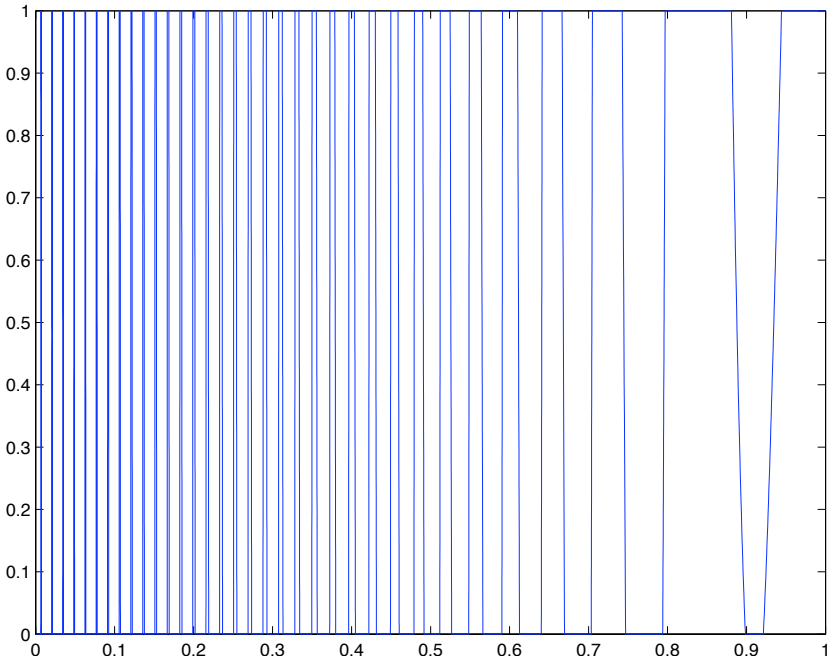

Figure 4.7: *Optimal control norm $|u_\lambda|$ versus time, energy-consumption homotopy $\lambda = 0.97$, $T_{\max} = 0.8$N, the control is almost bang-bang.*

In order to reach lower thrust, particularly 0.07N, we cosider an homotopy on the maximal thrust $T_{\max}$, we proceed as follows. The starting point is $T_{\max} = 0.8$N, a differential homotopic step is carried out until $T_{\max} = 0.7$N, then we execute a differential homotopy on the final time t_f to enlarge it since the

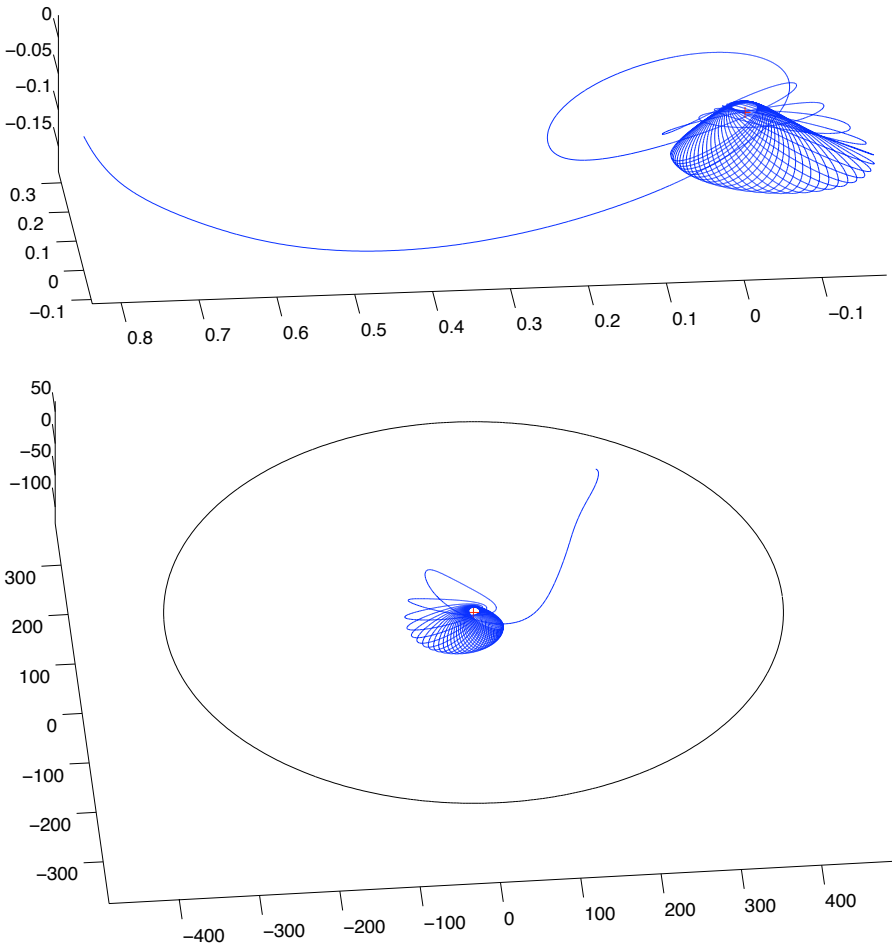

Figure 4.8: *Minimum fuel consumption trajectory to L_2, figure on the top is in the CRTBP frame and figure on the bottom is in a fixed frame around the Earth, black circle is the Moon orbit, energy-consumption homotopy $\lambda = 0.97$, $T_{\max} = 0.8$N.*

minimum final time increases when the thrust decreases. The homotopic step on t_f is performed from $t_f = 1.7 t_{f\,\min}(T_{\max} = 0.8\text{N})$ to $t_f = 1.7 t_{f\,\min}(T_{\max} = 0.7\text{N})$. We proceed in the same manner until we reach $T_{\max} = 0.3$N. This does not work above this maximal thrust. No lower $T_{\max}$ have been reached.

Conclusion

During this PhD thesis some results on the optimal control of the circular restricted three-body problem CRTBP have been given. Our main goal was to simulate the mission of the European Space Agency: SMART-1 using the CRTBP model and to achieve better transfer performances *i.e.* in terms of transfer time and fuel consumption using the optimal control theory. In the absence of previous numerical results on the controlled CR3BP using indirect methods, we first address simplified models: Planar case, constant spacecraft mass, medium maximal thrusts.

In this study, a general framework to solve optimal control problem in the CRTBP is provided for two optimization criteria: The minimum time transfer and the minimum fuel consumption transfer. However, we are unsatisfied with some points. First of all, we have not managed to reach low thrust for the transfers towards the orbit around the Moon LO, for both optimization criteria. This point needs more numerical investigation. A multiple shooting method could also be used, as in the last chapter. Secondly we do not succeeded to reach $T_{\max} = 0.07$N, for the minimum time transfer from the GTO to the POM. Only a solution for $T_{\max} = 0.7$N has been obtained by dividing the transfer into two parts: From GTO to L_2 and then from L_2 to POM. Changing the intermediate conditions *i.e.* the velocity of arrival and starting from the point L_2 might help to enable the connection between the two transfer parts for lower thrusts. Thirdly, more work is needed to initialize the minimum energy problem for low thrust for both transfers: GTO to L_2 and GTO to POM.

The minimum consumption solution is approximated using the energy-consumption homotopy (P_λ) when $\lambda \to 1$ or the logarithmic barrier homotopy (P_ε) when $\varepsilon \to 0$. Complementary work should be done to obtain the "exact" solution. Thus, a new component should be added: Take the solution of (P_λ) for λ close to 1 or (P_ε) for ε close to 0 and use it as an initial guess to solve the minimum consumption transfer problem (P). This numerical component has to take into account the bang-bang form of the control solution, thus a commutation detection should be included. In the same context, one can investigate the following question. From which value of λ close to 1 or ε close to 0, the corresponding solution is a suitable initial guess to solve (P)? So one has not to perform the continuation till a λ very close to 1 or an ε very close to 0, and deal with the possible numerical difficulties of these homotopies especially for low thrusts. Moreover, the second order condition tests are developed only for the smooth cases. Thus, one has to investigate how to implement those conditions for the bang-bang control case, and then test the local optimality of the solutions.

It is then recommended in future work to study the variations of the maximal

final mass solution of the minimum fuel consumption problem with respect to the final time transfer. This information is very helpful to choose the suitable time transfer for a mission and subsequently the suitable optimal command.

Bibliography

[1] A. Agrachev and Y. Sachkov. *Control theory from the geometric viewpoint*, volume 87. Springer, 2004.

[2] J. T. Betts and S. O. Erb. optimal low thrust tra jectories to the moon.. *J. Appl. Dyn. Syst.*, 2(2):144170, 2003.

[3] A. Bombrun, J. Chetboun, and J.-B. Pomet. transfert terre-lune en poussée faible par contrôle feedback – la mission smart-1 . *Rapport de recherche INRIA*, (5955):1–27, 2006.

[4] B. Bonnard, J.-B. Caillau, and G. Picot. Geometric and numerical techniques in optimal control of two and three-body problems. *communications in information and systems*, 10(4):239–278, 2010.

[5] B. Bonnard, J.-B. Caillau, and E. Trélat. Geometric optimal control of elliptic keplerian orbits. *Discrete and continuous Dynamical Systems-Series B*, 5(4):929–956, November 2005.

[6] B. Bonnard, J.-B. Caillau, and E. Trélat. Second order optimality conditions in the smooth case and applications in optimal control. *ESAIM: Control, Optimisation and Calculus of Variations*, 13(2):207–236, 2007.

[7] B. Bonnard and M. Chyba. *Singular trajectories and their role in control theory*. Springer, 2003.

[8] B. Bonnard, G. Launay, and M. Pelletier. classication générique de synthéses temps minimales avec cible de codimension un et applications.. *Ann. Inst. H. Poincaré section C*, 14(1):55102, 1997.

[9] J.-B. Caillau. *Contribution à l'étude du contrôle en temps minimal des transferts orbitaux*. Thèse de doctorat, Institut National Polytechnique de Toulouse, Toulouse, France, Novembre 2000.

[10] J.-B. Caillau, O. Cots, and J. Gergaud. Hampath package v1.0. User guide, ENSEEIHT-IRIT, UMR CNRS 5505, 2 rue Camichel, F-31071 Toulouse, December 2009. apo.enseeiht.fr/hampath.

[11] J.-B. Caillau, B. Daoud, and J. Gergaud. On some riemannian aspects of two and three-body controlled problems. *Recent Advances in Optimization and its Applications in Engineering (Proceedings of the 14th Belgian-French-German Conference on Optimization, Leuven, September 2009)*, pages 205–224, 2010.

[12] J.-B. Caillau, B. Daoud, and J. Gergaud. Discrete and differential homotopy in circular restricted three-body control. *Special number of Discrete and Continuous Dynamical Systems Journal*, To appear (Proceedings of 8th AIMS Conference on Dynamical Systems, Differential Equations and Applications, Dresden, May 2010.).

[13] J.-B. Caillau, J. Gergaud, and J. Noailles. 3d geosynchronous transfer of a satellite : Continuation on the thrust. *Journal of optimization theory and applications*, 118(3):541–565, September 2003.

[14] J.-B. Caillau and J. Noailles. Coplanar control of a satellite around the earth. *ESAIM: Control, Optimization and Calculus of Variations*, 6:239–258, February 2001.

[15] L. Cesari. *Optimization Theory and Applications.* Springer-Verlag, 1983.

[16] A. Chenciner. de l'espace des triangles au problème des trois corps. *Gazette French Math. Soc.*, 2004.

[17] B. Daoud. *Transfert orbital à faible poussée avec consommation minimale.* Rapport de master, Institut National Polytechnique de Toulouse, Toulouse, France, Septembre 2008.

[18] K. E. Davis, R. L. Anderson, D. J. Scheeres, and G. H. Born. the use of invariant manifolds for transfers between unstable periodic orbits of dierent energies. . *Celestial Mech. Dynam. Astronom.*, 107(4):471–485, 2010.

[19] M. P. do Carmo. *Riemannian geometry.* Birkhauser, 1992.

[20] C.B. Garcia and W.I. Zangwill. An approach to homotopy and degree theory. *Mathematics of operation research*, 4(4):390–405, 1979.

[21] J. Gergaud. *Sur la résolution numérique de problèmes de contrôle optimal à solution bang-bang via les méthodes homotopiques.* Hdr, Institut National Polytechnique de Toulouse, Toulouse, France, Février 2008.

[22] J. Gergaud and T. Haberkorn. homotopy method for minimum consumption orbit transfer problem. *ESAIM : Control, Optimisation and Calculus of Variations, EDP Sciences*, 12(2):294–310, 2006.

[23] V Jurdjevic. *Geometric control theory.* Cambridge University Press, 1996.

[24] J. E. Marsden and S. D. Ross. new methods in celestial mechanics and mission design.. *Amer. Math. Soc. (N.S.)*, 43(1):4373, 2006.

[25] G. Mingotti, F. Topputo, and F. Bernelli-Zazzera. low-energy, low-thrust transfers to the moon. *Celest. Mech. Dyn. Astr.*, 105:6174, 2009.

[26] M. T. Ozimek and K. C. Howell. low-thrust transfers in the earth moon system, including applications to libration point orbits.. *Journal of Guidance, Control, and Dynamics*, 33(2):4373, 2010.

[27] M.T. Ozimek. *A Low-Thrust Transfer Strategy to Earth-Moon Collinear Libration Point Orbits.* M.s.a.a. thesis, School of Aeronautics and Astronautics, Purdue University, West Lafayette, Indiana,USA, December 2006.

[28] M.T. Ozimek. *Low-Thrust Trajectory Design and Optimization of Lunar South Pole Coverage Missions*. Ph.d. dissertation, School of Aeronautics and Astronautics, Purdue University, West Lafayette, Indiana,USA, May 2010.

[29] H. Poincaré. on the three-body problem and the equations of dynamics (sur le probleme des trois corps et les équations de dynamique). *Acta mathematica*, (13):1–270, 1890.

[30] L. Pontryaguine, V. Boltianski, R. Gamkrelidze, and E. Michtchenko. *Théorie mathématiques des processus optimaux*. Éditions Mir, 1974.

[31] G. D. Racca and al. SMART-1: The first time of europe to the moon, wandering in the earth-moon space. *Earth, Moon and Planets*, (85–86):379–390, 2001.

[32] G. D. Racca and al. SMART-1 mission description and development status. *Planetary and space science*, (50):1323–1337, 2002.

[33] S. D. Ross and D. J. Scheeres. multiple gravity assists, capture, and escape in the restricted three-body problem. . *SIAM J. Appl. Dyn. Syst.*, 6(3):576–596, 2007.

[34] C. L. Siegel and J. K. Moser. *Lectures on celestial mechanics*. 1971.

[35] J. Stoer and R. Bulirsch. *Introduction to numerical analysis*. Springer, 2002.

[36] V. Szebehely. *Theory of orbits - The Restricted Problem of Three Bodies*. Academic Press, 1967.

Résumé. Le contexte de ce travail est la mécanique spatiale. Plus précisément, on se propose de réaliser des transferts à faible poussée dans le système Terre-Lune modélisé par le problème des trois corps restreint circulaire. Le but est de calculer la commande optimale de l'engin spatial pour deux critères d'optimisation: temps de transfer minimal et consommation de carburant minimale. Les contributions de cette thèse sont de deux ordres. Géométrique, tout d'abord, puisqu'on étudie la contrôlabilité du système ainsi que la géométrie des transferts (structure de la commande) à l'aide d'outils de contrôle géométrique. Numérique, ensuite, différentes méthodes homotopiques sont développées. En effet, une continuation deux-trois corps est considérée pour calculer des trajectoires temps minimales et puis une continuation sur la poussée maximale de l'engin pour atteindre des poussées faibles. Le problème de consommation minimale — minimisation de la norme L^1 du contrôle — est connecté par une continuation différentielle au probème de minimisation de la norme L^2 du contrôle. Les solutions trouvées sont comparées à celles calculées à l'aide d'une pénalisation par barrière logarithmique. Ces méthodes sont ensuite appliquées pour la mission SMART-1 de l'Agence Européenne Spatiale.

Mots-clés. transfert Terre-Lune, poussée faible, problème des trois corps circulaire restreint, contrôle optimal, trajectoires temps ou consommation minimales, méthode de tir, continuations discrète et différentielle

---

Abstract. The context of this work is space mechanics. More precisely, we aim at computing low thrust transfers in the Earth-Moon system modeled by the circular restricted three-body problem. The goal is to calculate the optimal steering of the spacecraft engine with respect to two optimization criteria: Final time and fuel consumption. The contributions of this thesis are of two kinds. Geometric, first, as we study the controllability of the system together with the geometry of the transfers (structure of the command) by means of geometric control tools. Numerical, then, different homotopic methods being developed. A two-three body continuation is used to compute minimum time trajectories, and then a continuation on the maximal thrust is considered to reach low thrusts. The minimum consumption problem—minimization of the L^1 norm of the control—is connected by a differential continuation to the minimization of the L^2 norm of the control. The trajectories computed are then compared to those obtained using a logarithmic interior penalty. Those methods are applied to simulate the SMART-1 mission of the European Space Agency.

Key words. Earth-Moon transfer, low thrust, circular restricted three-body problem, optimal control, minimum time or fuel consumption trajectories, shooting, discrete and differential continuation